The Hong Kong Polytechnic University

Department of Electronic & Information Engineering

Diversely Polarized Antenna-Array Signal Processing

YUAN Xin

A thesis submitted in partial fulfilment of the requirements

for the degree of Doctor of Philosophy

November 2011

CERTIFICATE OF ORIGINALITY

I hereby declare that this thesis is my own work and that, to the best of my knowledge and belief, it reproduces no material previously published or written, nor material that has been accepted for the award of any other degree or diploma, except where due acknowledgement has been made in the text.

_____ (Signed)

Yuan Xin (Name of Students)

Abstract

The dissertation is composed of three distinct but related components, which relate to direction finding and/or polarization estimation with diversely polarized antenna arrays. The three parts are briefly summarized below:

(1) "Vector cross-product direction-finding" with an electromagnetic vector-sensor of six orthogonally oriented but spatially *non*-collocating dipoles / loops

Direction-finding capability has recently been advanced by synergies between the customary approach of interferometry and the new approach of "vector cross product" based Poynting-vector estimator. The latter approach measures the incident electromagnetic wavefield for each of its six electromagnetic components, all at one point in space, to allow a vector cross-product between the measured electric-field vector and the measured magnetic-field vector. This would lead to the estimation of each incident source's Poynting-vector, which (after proper norm-normalization) would then reveal the corresponding Cartesian direction-cosines, and thus the azimuth-elevation arrival angles. Such a "vector cross product" algorithm has been predicated on the measurement of all six electromagnetic components at one same spatial location. This physically requires an electromagnetic vector-sensor, i.e., three identical but orthogonally oriented electrically short dipoles, plus three identical but orthogonally oriented magnetically small loops – all spatially *collocated* in a point-like geometry. Such a complicated "vector-antenna" would require exceptionally effective electromagnetic isolation among its six component-antennas. To minimize mutual coupling across these collocated antennas, considerable antennas-complexity and hardware cost could be required. Instead, Chapter 2 shows how to apply the "vector cross-product" direction-of-arrival estimator, even if the three dipoles and the three loops are located *separately* (instead of collocating in a point-like geometry). This new scheme has great practical value, in reducing mutual coupling, in simplifying the antennas hardware, and in extending the spatial aperture to refine the direction-finding accuracy by orders of magnitude.

(2) Various triad-compositions of collocated dipoles/loops, for direction finding & polarization estimation

To form a collocated triad of orthogonally oriented dipole(s) and/or loop(s), 20 different compositions are possible and these compositions are investigated in Chapter 3. For each such composition: (i) closed-form formulas are produced here to estimate the azimuth-elevation direction-of-arrival and the polarization-parameters, or (ii) reasoning is given why such estimation is inviable.

(3) Polarization estimation with a dipole-dipole pair, a dipole-loop pair, or a loop-loop pair of various orientations

Chapter 4 aims to estimate the polarization of fully polarized sources, given prior knowledge of the incident sources' azimuth-elevation directions-of-arrival, using a pair of diversely polarized antennas – two electrically small dipoles, or two small loops, or one each. The pair may be collocated, or spatially separated by a known displacement. Each antenna may orient along any Cartesian coordinate. Altogether, fifteen antenna/orientation configurations are thus possible. For each configuration, Chapter 4 derives (i) the closed-form polarization-estimation formulas, (ii) the associated Cramér-Rao bounds, and (iii) the associated computational numerical stability.

Acknowledgments

I would like to thank my beloved family for its support throughout my student career.

I would like to thank my supervisor, Dr. Kainam Thomas Wong, for his guidance and great help during the past 2.5 years.

I would like to thank Dr. Yue Ivan Wu, Yang Song, Bo Wang and many other research collaborators for their help to my work.

The exposition in this dissertation is taken from [161, 167, 168], which have been written jointly by myself and my co-authors, principally Dr. Wong, who has re-worked and re-written my exposition word-by-word from start to finish in [161, 167, 168].

I would like to thank Dr. Wong for sharing his high-level algorithmic development idea with me, leading to [161].

I would like to thank Yang Song for providing brainstorming ideas in my algorithmic development of [161].

I would like to thank Keshav Agrawal for re-checking and correcting my formulas in [167, 168].

I would like to thank Zixin Xu for re-checking and correcting my formulas in [167].

Contents

List of Figures

List of Tables

Chapter 1

Introduction

This dissertation presents 3 research projects of the candidate student's work during the the past two years and two months. All these 3 research projects have been published or accepted to publish in IEEE journals and all of them are about direction finding and/or polarization estimation with diversely polarized antenna arrays.

In radar and wireless communication systems, it is essential to consider the transmission, propagation and reception of electromagnetic waves, since they are inherent physical processes of the signal. Furthermore, they are polarization-sensitive processes. Polarimetry is the measurement and the interpretation of the polarization of transverse waves [8]. The polarization state of an incident wave could reveal attributes intrinsic to the emitter or the reflector, e.g. a star's photosphere asymmetry due to "limb polarization" [79]. Therefore, polarization-related considerations should be critical factors in the design and operation of any aforementioned system. Based on the polarization diversity among the receive-antennas, the incident sources can be separated on account of their polarization differences, in addition to their azimuth/elevation angular differences [32]. Commonly used for polarization-estimation are electrically short dipoles and small loops.[1] Such a dipole (loop), when oriented along a Cartesian coordinate, would measure the electric-field (magnetic-field) component of the incident transverse wavefield along that axis.

1.1 Review of the Electromagnetic Vector

Consider a far-field source S, depicted in Figure 1.1, emitting a completely polarized transverse electromagnetic wave, which can be characterized by the electric-field vector $\mathbf{e}$ and the magnetic-field vector $\mathbf{h}$. With (γ, η), defined in Table 1.1 [2], to denote the

[1] A dipole is considered "short", if it is much shorter than a wavelength. A loop is considered "small", if its circumference is below a quarter-wavelength [15].

[2] If the electromagnetic wave is linearly polarized, $\eta = 0$ [32]. If the electromagnetic wave is circularly polarized, $\gamma = 45^\circ$ and $\eta = \pm 90^\circ$ (+ for left circularly polarized and − for right circularly polarized) [32].

Table 1.1: Definitions of Symbols

Symbol	Definition
$\gamma \in [0, \pi/2]$	auxiliary polarization angle
$\eta \in [-\pi, \pi]$	polarization phase difference
$\theta \in [0, \pi]$	elevation angle
$\phi \in [0, 2\pi)$	azimuth angle

Table 1.2: List of Notations

Notation	Definition
^{T}	transposition operator
^{H}	Hermitian operator
*	complex conjugation
$\otimes$	Kronecker product
$\odot$	element-wise multiplication between two vectors
$\|\| \cdot \|\|$	Frobenius norm
$\angle$	the angle of the ensuring entity
$[\cdot]_\ell$	ℓth entity of the vector in [ ]

polarization state of the source, in spherical coordinates as shown in Figure 1.1, $\mathbf{e}$ and $\mathbf{h}$ can be expressed as [13, 20, 32]:

$$\mathbf{e} = \sin\gamma e^{j\eta}\vec{\mathbf{v}}_\phi + \cos\gamma\vec{\mathbf{v}}_\theta, \tag{1.1}$$

$$\mathbf{h} = \mathcal{Z}_o\left(\cos\gamma\vec{\mathbf{v}}_\phi + \sin\gamma e^{j\eta}\vec{\mathbf{v}}_\theta\right), \tag{1.2}$$

where $\mathcal{Z}_o$ is the intrinsic impedance of the transmission medium, $\vec{\mathbf{v}}_m$ is a unit vector along the direction of m (see Figure 1.1).

Equivalently, in Cartesian coordinates after normalization, $\mathbf{e}$ and $\mathbf{h}$ can be re-expressed as [13, 20, 32]

$$\begin{aligned}\mathbf{e} = {} & (\sin\gamma\cos\theta\cos\phi e^{j\eta} - \cos\gamma\sin\phi)\vec{\mathbf{v}}_x \\ & +(\sin\gamma\cos\theta\sin\phi e^{j\eta} + \cos\gamma\cos\phi)\vec{\mathbf{v}}_y \\ & -\sin\gamma\sin\theta e^{j\eta}\vec{\mathbf{v}}_z, \end{aligned} \tag{1.3}$$

$$\begin{aligned}\mathbf{h} = {} & -(\cos\gamma\cos\theta\cos\phi + \sin\gamma\sin\phi e^{j\eta})\vec{\mathbf{v}}_x \\ & -(\cos\gamma\cos\theta\sin\phi - \sin\gamma\cos\phi e^{j\eta})\vec{\mathbf{v}}_y \\ & +\cos\gamma\sin\theta\vec{\mathbf{v}}_z, \end{aligned} \tag{1.4}$$

where (θ, ϕ) symbolize the direction-of-arrival of the source and they are defined in Table

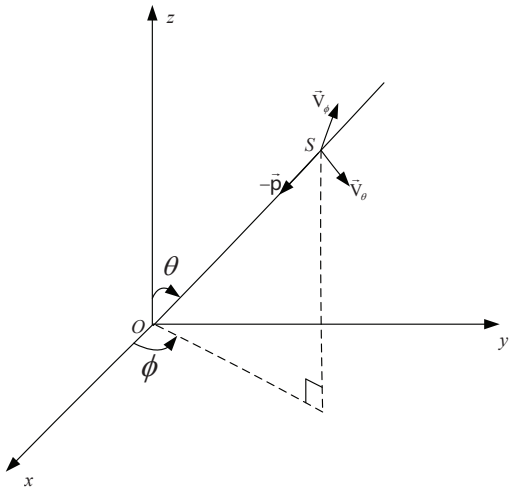

Figure 1.1: Electromagnetic vector.

1.1. Re-express the above **e** and **h** in matrix form as [15, 20, 32]:

$$\mathbf{a} \overset{\text{def}}{=} \begin{bmatrix} e_x(\theta,\phi,\gamma,\eta) \\ e_y(\theta,\phi,\gamma,\eta) \\ e_z(\theta,\gamma,\eta) \\ h_x(\theta,\phi,\gamma,\eta) \\ h_y(\theta,\phi,\gamma,\eta) \\ h_z(\theta,\gamma) \end{bmatrix} \overset{\text{def}}{=} \begin{bmatrix} \sin\gamma\cos\theta\cos\phi e^{j\eta} - \cos\gamma\sin\phi \\ \sin\gamma\cos\theta\sin\phi e^{j\eta} + \cos\gamma\cos\phi \\ -\sin\gamma\sin\theta e^{j\eta} \\ -\cos\gamma\cos\theta\cos\phi - \sin\gamma\sin\phi e^{j\eta} \\ -\cos\gamma\cos\theta\sin\phi + \sin\gamma\cos\phi e^{j\eta} \\ \cos\gamma\sin\theta \end{bmatrix} \tag{1.5}$$

$$= \underbrace{\begin{bmatrix} \cos\theta\cos\phi & -\sin\phi \\ \cos\theta\sin\phi & \cos\phi \\ -\sin\theta & 0 \\ -\sin\phi & -\cos\theta\cos\phi \\ \cos\phi & -\cos\theta\sin\phi \\ 0 & \sin\theta \end{bmatrix}}_{\overset{\text{def}}{=}\boldsymbol{\Theta}(\theta,\phi)} \underbrace{\begin{bmatrix} \sin\gamma e^{j\eta} \\ \cos\gamma \end{bmatrix}}_{\overset{\text{def}}{=}\mathbf{g}(\gamma,\eta)}. \tag{1.6}$$

Table 1.2 lists the notations used in this dissertation and they will not be defined again in the later chapters.

1.2 Literature Review of Diversely Polarized Antennas Investigated for Direction Finding and Polarization Estimation

Direction-of-arrival estimation is an important functional requirement in various systems and practical applications, such as: the smart antennas, radar, mobile communication,

imaging, biomedical systems and target tracking applications. A variety of algorithms have been investigated for direction-of-arrival estimation with antenna arrays [30, 41], for example: the Capon [1] algorithm, the subspace fitting algorithm [10], MUSIC [4] like algorithms [7, 14, 57, 58, 80, 93], ESPRIT [6] like algorithms [5, 24, 141, 151], and the maximum likelihood (ML) method [9], etc.

Since polarized antennas can provide additional information of the incident source, *diversely* polarized antenna arrays have received considerable attentions during the past two decades and they have been exploited extensively for direction-finding by adopting various algorithms mentioned above [13, 17, 20, 21, 23, 110]. Widely used polarized antennas in the literature include: a) the six-component *collocated* electromagnetic vector sensor, b)*collocated* antenna triads, and c)*collocated* antenna pairs. The spatial collocation of an array of receive-antennas would mean no *spatial* phase delay in the array manifold. Hence, the array manifold would be independent of the incident sources' frequency-spectrum.

1.2.1 The Six-Component Collocated Electromagnetic Vector Sensor

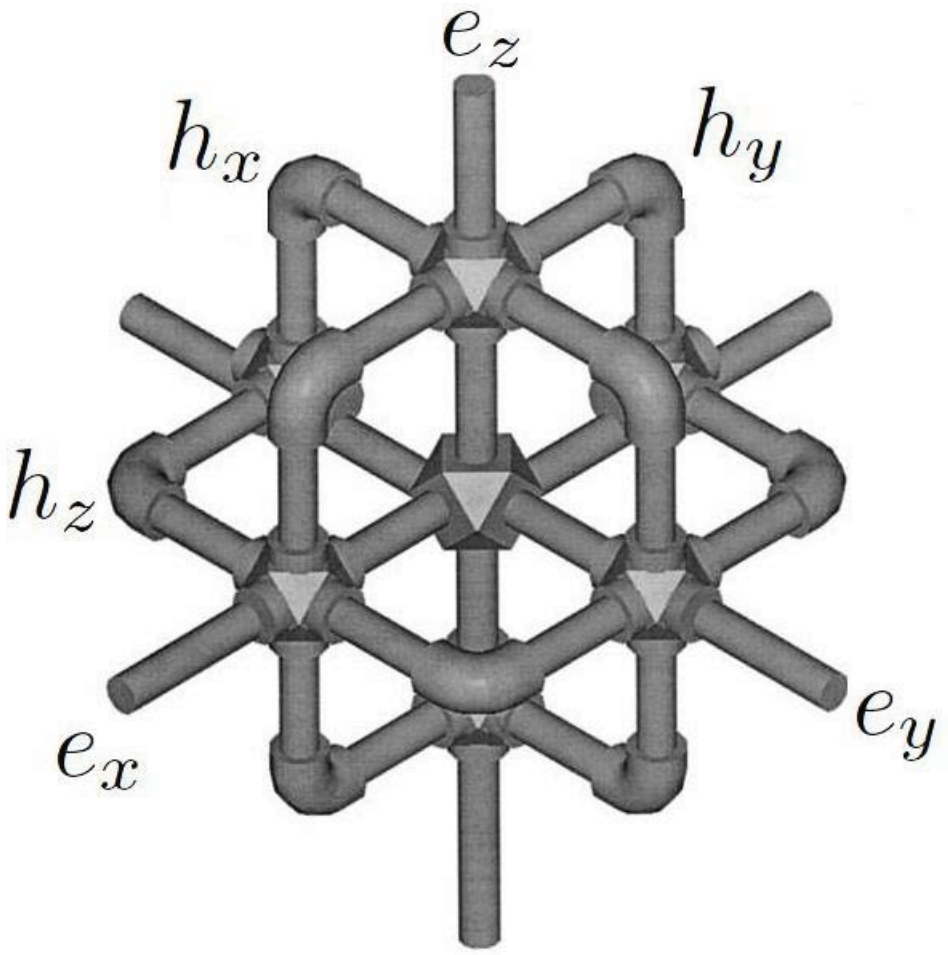

Figure 1.2: Electromagnetic vector sensor. [101]

A six-component electromagnetic vector-sensor consists of three identical, but orthogonally oriented, electrically short *dipoles* ($\{e_x, e_y, e_z\}$ in Figure 1.2), plus three identical but orthogonally oriented magnetically small *loops* ($\{h_x, h_y, h_z\}$ in Figure 1.2) – all **spatially collocated** in a point-like geometry (see Figure 1.2) [32]. This electromagnetic vector-sensor aims to distinctly measure all three Cartesian components of the incident electric field and all three Cartesian components of the incident magnetic field, as a 6×1 vector, **at one spatial location** and at one time-instant.

Such an electromagnetic vector-sensor's array manifold may be idealized, by overlooking all mutual coupling among its six **collocated** constituent antennas. This idealized array manifold would be a concatenation of the 3×1 electric-field vector $\mathbf{e}$ with the 3×1 magnetic-field vector $\mathbf{h}$, to be (1.5) in Section 1.1 [13, 20, 32].

The unique array-manifold in (1.5) has been much exploited by various eigenstructure-based direction-finding schemes [15, 27, 32, 33, 37, 43, 46, 47, 50–53, 56, 63, 71, 73–76, 86, 87, 89, 94, 97–100, 102, 105, 109, 116, 119, 131–135, 137, 138, 150].

{a} "Vector-cross-product" approach of direction-finding with an electromagnetic vector sensor was proposed in [20] and this method was used for source tracking in [47]. This "vector-cross-product" approach was advanced in [50–53] for direction-finding and polarization estimation with electromagnetic vector sensor arrays. The direction-finding and polarization estimation of multiple sources with a *single* electromagnetic vector sensor were investigated in [32, 56, 76, 87, 97, 98, 133, 134]. The separation and tracking of multiple sources were studied in [63] with one electromagnetic vector sensor.

{b} The ESPRIT [6] algorithm was investigated in [15] for direction-of-arrival and polarization estimation with electromagnetic vector sensors and a simplified algorithm was developed in [50] by adopting the above "vector-cross-product" approach. [46] advanced the ESPRIT algorithm for direction finding with electromagnetic vector sensors in a scenario with both completely and incompletely polarized signals.

{c} MUSIC-based algorithms were developed in [53, 75, 133, 134] and quaternion-based direction-finding algorithms were studied in [73, 89, 109, 131] with electromagnetic vector sensors. The propagator method was adopted in [137] for direction-of-arrival estimation with electromagnetic vector sensors and a twofold mode-projection based direction-finding algorithm was proposed in [138].

{d} Direction-finding of coherent sources with electromagnetic vector sensors were investigated in [71, 74, 105, 150].

1.2.2 Various Triad-Compositions of Collocated Dipoles/Loops

For simultaneous estimation of the azimuth/elevation arrival angles (ϕ, θ) and polarization parameters (γ, η), a minimum of three diversely polarized antennas are needed, because at least three *complex*-value equations (based on three antennas' measurements) are needed to be solved for the four unknown *real*-value source-parameters (i.e. $\theta, \phi, \gamma, \eta$) and for the one unknown complex-value multiplicative coefficient α, which arises from the eigen-based estimation of the source's steering vector.

To select three out of the six electromagnetic components, the number of different choices amount to $\left(\begin{array}{c} 6 \\ 3 \end{array} \right) = 20$. Among these 20 possible configurations,

1) The *dipole* triad (a.k.a. a tripole) has been used for direction-of-arrival estimation in [40, 42, 48, 49, 59, 68, 77, 91, 95, 96, 107, 111, 120, 128–130, 137, 138, 144, 146, 163], with closed-form estimation formulas available in [59, 137, 146]. The dipole triad has also been used for polarization estimation in [59, 137], with closed-form estimation formulas available therein. For closed-form Cramér-Rao bound expressions, please refer to [136]. For antenna-electromagnetic implementation of this tripole, please see [111].

2) The *loop* triad has been used for direction-of-arrival estimation in [59, 61, 129, 137], with closed-form estimation formulas available in [59, 137]. The dipole triad has also been used for polarization estimation in [59, 137], with closed-form estimation formulas available therein. For closed-form Cramér-Rao bound expressions, please refer to [136]. For antenna-electromagnetic implementation of this loop triad, please see [61].

3) The $\{e_x, e_y, h_z\}$ triad has been investigated in [129]; however, no closed-form formula is available in this reference.

4) The $\{e_z, h_x, h_y\}$ triad has been investigated in [34, 81, 85, 101, 103], with closed-form estimation formula available for the azimuth arrival angle in [81], but no closed-form estimation formula is available for the elevation arrival angle nor for the polarization parameters in any of these references. For closed-form Cramér-Rao bound expressions, please refer to [136].

5) The $\{e_x, e_y, h_x\}$ triad has been investigated in [129]; however, no closed-form formula is available therein.

1.2.3 Antennas Pairs of of Various Orientations

Polarization is bivariate; hence, a minimum of two diversely polarized antennas are needed for polarimetry of a fully polarized wavefield. If limiting the choice of antennas to linearly polarized antennas (i.e. dipole(s) or/and loop(s)) aligned along some Cartesian axes, there exist $\begin{pmatrix} 6 \\ 2 \end{pmatrix} = 15$ possible antenna/orientation configurations, because two components are here chosen, out of a total of six electromagnetic components.

Such dipole/dipole, loop/loop, or dipole/loop antenna-pairs have been much investigated in the open literature:

(a) **One dipole and one loop**, collocated and *identically oriented*, are labeled a "Co-centered Orthogonal Loop and Dipole" (COLD) array. Its physical implementation and electromagnetics are discussed in [44, 60, 104, 114, 123, 124]. It is used to estimate the arrival-angles and/or the polarization in [29, 88, 113, 127, 145, 147, 153, 162, 165].

(i) Specifically the *vertical* oriented COLD array is studied in [29, 88, 127, 147, 153] (with the corresponding Cramér-Rao bounds available in [145]).

(ii) Specifically the *horizontal* oriented COLD array is investigated in [129].

[3]

(b) **Two identical dipoles**:

(i) When *both horizontally but orthogonally* oriented in spatial collocation, they have been used as a unit for the estimation of the arrival-angles and/or the polarization in [11–13, 18, 25, 26, 28, 31, 38, 45, 64, 66, 78, 108, 122, 125, 126, 129, 138, 142, 152, 157, 159].

(ii) With *one vertical and one horizontal*, they are similarly used in [35, 54, 55, 70, 115, 130, 158].

(iii) *Other orthogonally oriented* dipole-pairs are similarly studied in [16, 19, 22, 39, 67, 70, 92, 148, 166].

Physical implementations of a dipole-pair are presented in [84, 90, 121, 139, 140, 149, 160].

(c) **Two identical loops**:

[3] An orthogonally (not identically) oriented dipole/loop pair has its electromagnetics investigated in [36, 82, 112].

(i) When *horizontally and orthogonally* oriented in spatial collocation, they have been used as a unit for the estimation of the arrival-angles and/or the polarization in [81, 85, 101, 106, 155].

(ii) *Other orthogonally oriented* loop-pairs are similarly studied in [92, 156].

Hardware implementations and electromagnetics are discussed in [3, 65, 72, 83, 154, 164].

1.3 Contributions of This Work

The main contributions presented in this thesis are listed below:

{Ch-2} In Chapter 2, a new scheme is proposed to reduce the mutual coupling across the six **collocated** antennas that constitute the electromagnetic vector-sensor. Unrealistically presumed by the algorithms cited in Section 1.2.1, however, is *negligible* mutual coupling across the six **collocated** antennas. Mutual coupling could be reduced but never entirely avoided, and only by intricate electromagnetic isolation, that would categorically complicate the antenna implementation and would thus sky-rocket the hardware cost [143]. Instead, Chapter 2 will propose a new scheme to by-pass this mutual coupling problem, by spatially **displacing** the six component-antennas and showing how to modify the "vector-cross-product" Poynting-vector estimator accordingly. That is, the proposed method will retain all advantages of *collocated* vector-sensor direction-finding, despite spatially *separating* the six component-antennas here. Furthermore, *additional* advantages will be available, such as reducing the mutual coupling and extending the spatial aperture to improve the azimuth-elevation spatial resolution. Much of this contribution has been published in [161].

{Ch-3} Chapter 3 will investigate various triad-compositions of collocated dipoles/loops for direction finding and polarization estimation. An electrically short dipole measures one Cartesian component of the electric-field vector, along the Cartesian axis on which the dipole is aligned. Similarly, a magnetically small loop measures one Cartesian component of the magnetic-field vector, along which the loop-axis is aligned. Hence, with a collocated triad of three such diversely polarized antennas, three components of the six-element electromagnetic-field vector can be measured, at one point in space. As reviewed in Section 1.2.2, only 2 out of 20 possible compositions have closed-form formulas available in the open literature for the estimation of the arrival angles or the polarization. Overlooked, in the open literature, are the other 18 compositions. Chapter 3 aims to fill this literature gap. Closed-form estimation

formulas for θ, ϕ, γ, and η (and their associated validity regions) are advanced for 14 of the overlooked configurations. For the remaining 4 configurations, they will be shown to be inadequate for such closed-form estimation. Much of this contribution appears in [167].

{Ch-4} Chapter 4 aims to estimate the polarization of fully polarized sources, given prior knowledge of the incident sources' azimuth-elevation directions-of-arrival, using a pair of diversely polarized antennas – two electrically small dipoles, or two small loops, or one each. There exist 15 possible antenna/orientation configurations for a pair of polarized antennas to measure any 2 of the 6 components of the electromagnetic-field vector. The effectiveness of polarimetry depends critically on what and how the antennas are employed. As reviewed in Section 1.2.3, the open literature presently offers no comprehensive comparison among these 15 configurations. This literature gap is filled by Chapter 4. The 15 antenna pairs investigated in Chapter 4 may be collocated, or spatially separated by a known displacement. Each antenna may orient along any Cartesian coordinate. For each configuration, Chapter 4 derives (i) the closed-form polarization-estimation formulas, (ii) the associated Cramér-Rao bounds, and (iii) the associated computational numerical stability. Much of this contribution appears in [168].

Chapter 2

"Vector Cross-Product Direction-Finding" with an Electromagnetic Vector-Sensor of Six Orthogonally Oriented but Spatially *Non*-Collocating Dipoles / Loops

This chapter will propose a class of array-configurations to spatially space the six constituent antennas of the now-spread electromagnetic vector-sensor, such that the vector cross-product estimator would still work – and would work better, indeed. The proposed scheme is utilized to by-pass the mutual coupling among the six constituent antennas of the electromagnetic vector-sensor, by spatially **displacing** the six component-antennas and showing how to modify the "vector-cross-product" Poynting-vector estimator accordingly. The proposed method will retain all advantages of *collocated* vector-sensor direction-finding, despite spatially *separating* the six component-antennas, and also provide additional advantages. [1]

[1] Much of this chapter has been published in [161].

2.1 "Vector Cross-Product Direction-Finding" with a *Collocated* Electromagnetic Vector Sensor

By measuring the incident electromagnetic wavefield explicitly in terms of its six individual electromagnetic components, the electromagnetic vector-sensor physically gathers the full data necessary to estimate the Poynting-vector $\mathbf{p}$, via a simple vector-cross-product between the measured electric-field vector and the measured magnetic-field vector. This estimated Poynting-vector, when normalized with respect to its Frobenius norm $\|\cdot\|$, gives the incident source's Cartesian direction-cosines (and hence the incident source's elevation-angle and azimuth-angle). Mathematically [20],

$$\mathbf{p} \overset{\text{def}}{=} \begin{bmatrix} p_x \\ p_y \\ p_z \end{bmatrix} = \frac{\mathbf{e} \times \mathbf{h}^*}{\|\mathbf{e}\| \cdot \|\mathbf{h}^*\|} = \begin{bmatrix} u \\ v \\ w \end{bmatrix} \overset{\text{def}}{=} \begin{bmatrix} \sin\theta \cos\phi \\ \sin\theta \sin\phi \\ \cos\theta \end{bmatrix}, \tag{2.1}$$

where $\times$ symbolizes the vector cross-product operator, with u, v, and w representing the impinging source's direction-cosines respectively along the x-axis, the y-axis, and the z-axis.

Many are the advantages offered by this six-component electromagnetic vector-sensor to arrival-angle estimation:

{1} In a multi-source scenario, each source's three Cartesian direction-cosine estimates (and thus each source's azimuth-angle estimate and elevation-angle estimate) can be automatically paired without further post-processing.

{2} Like other diversely polarized antenna-arrays, the electromagnetic vector-sensor can resolve incident sources on account of the sources' polarization-difference, in addition to their azimuth/elevation angular differences.

{3} The "vector-cross-product" approach of direction-finding in (2.1) can complement the customary interferometry approach of DOA-estimation, which is based on the spatial phase-delay across displaced antennas. Creative synergy between these two approaches has produced several novel capabilities:

(a) The direction-of-arrival estimation accuracy can be improved by orders of magnitude, by extending the spatial aperture, with*out* incurring ambiguity in the direction-of-arrival estimates and with*out* requiring additional antennas. [51], [52].

(b) The directions-of-arrival may be estimated with*out* prior knowledge/estimation of the nominal/actual geometric array-grid and with*out* any calibration-source, thereby easing "real-world" deployment. [50]

(c) No prior coarse estimate is needed to initiate the MUSIC (MUltiple SIgnal Classification) iterative parameter-estimation routine. Instead, MUSIC can now "self-initiate" its iteration. [53]

(d) Blind geolocation, beamforming, and interference-rejection are possible for frequency-hopping sources of unknown and arbitrary hop-sequences and directions-of-arrival. [56]

2.2 An Electromagnetic Vector-Sensor of Spatially Non-Collocating Component-Antennas

Unrealistically presumed by the algorithms cited in Section 1.2.1, however, is *negligible* mutual coupling across the six **collocated** antennas that constitute the electromagnetic vector-sensor. Mutual coupling could be reduced but never entirely avoided, and only by intricate electromagnetic isolation, that would categorically complicate the antenna implementation and would thus sky-rocket the hardware cost [143]. Instead, this proposed scheme by-passes this mutual coupling problem, by spatially **displacing** the six component-antennas and showing how to modify the "vector-cross-product" Poynting-vector estimator accordingly. That is, this proposed method will retain all advantages mentioned in Section 2.1 of *collocated* vector-sensor direction-finding, despite spatially *separating* the six component-antennas here. Furthermore, *additional* advantages become available, as explained below:

{4} As the six constituent antennas now span an extended spatial aperture (instead of collocating at one point), the resulting antennas have improved azimuth-elevation spatial resolution. That is, the present scheme spatially extends the geometric aperture, with*out* additional antenna.

{5} As already mentioned, spatially separation of the six component-antennas reduces their mutual coupling, thereby saving the cost to implement electromagnetic isolation.

The key question now is: Across the **spatially displaced** component-antennas, spatial phase shifts exist, invalidating the array manifold of (1.5) and nullifying the vector cross-product Poynting-vector estimation in (2.1). To these problems, this chapter will advance a class of array-configurations to spatially space the six constituent antennas of the now-spread electromagnetic vector-sensor, such that the vector cross-product estimator would

still work – and would work better, indeed. [2] [3]

2.3 Array Manifold for the New Electromagnetic Vector-Sensor with Non-Collocated Component-Antennas

The following notation will be used: The symbol E_x refers to the dipole oriented along the x-axis, similarly for E_y and E_z. The symbol H_x corresponds to the loop oriented along the x-axis, analogously for H_y and H_z. The symbols $\tilde{\theta}, \tilde{\phi}, \Delta_{x,y}$ signify, respectively, the elevation-angle, the azimuth-angle, and the distance of E_y relative to E_x. Similarly, $\Delta_{y,z}$ defines the distance of E_z from E_y.

This work will show the following:

The "vector-cross-product" estimator remains applicable for an electromagnetic vector-sensor of spatially *non*-collocated component-antennas, if [a]

{A} The $x-$, $y-$, and $z-$axis oriented **dipoles** are all placed on a straight line, with a spacing $\Delta_{x,y}$ between the first two dipoles, and a spacing $\Delta_{y,z}$ between the last two dipoles.

{B} The $x-$, $y-$, and $z-$axis oriented **loops** are placed in an order opposite to that in {A}, on another straight line in parallel to the first straight line, [b] with a spacing $\Delta_{x,y}$ between the first two loops, and a spacing $\Delta_{y,z}$ between the last two loops.

[a] These constitute a sufficient condition, maybe not a necessary condition.

[b] If $\tilde{\theta} = \frac{\pi}{2}$, the aforementioned two array-axes will be parallel to the x-y Cartesian plane. If $\tilde{\phi} = \frac{\pi}{2}$ additionally, the two lines are parallel to the y-axis; if $\tilde{\phi} = 0$ instead, the two lines lie in parallel to x-axis.

For the spatially *non*-collocating electromagnetic vector-sensor mentioned above, the

[2] [59] has previously shown how the vector-cross-product DOA-estimator remains fully applicable, for a dipole-triad that is displaced from a loop-triad. However, the three dipoles there remain spatially *co*llocated among themselves; and so do the three loops among themselves. Hence, mutual coupling, though reduced in [59], remains very substantial. In contrast, the present scheme allows each of six constituent antennas to occupy its distinct location, away from all other five component-antennas.

[3] Estimation accuracy bounds are derived in [69] for a spatially extended electromagnetic vector-sensor under certain specific array-configurations; however, *no algorithm* is presented therein. [117, 118] advance hardware implementations of a spatially extended electromagnetic vector-sensor, but again no algorithm. Original to the present work is the modification of the vector cross-product estimator to adopt to a spatially extended electromagnetic vector-sensor.

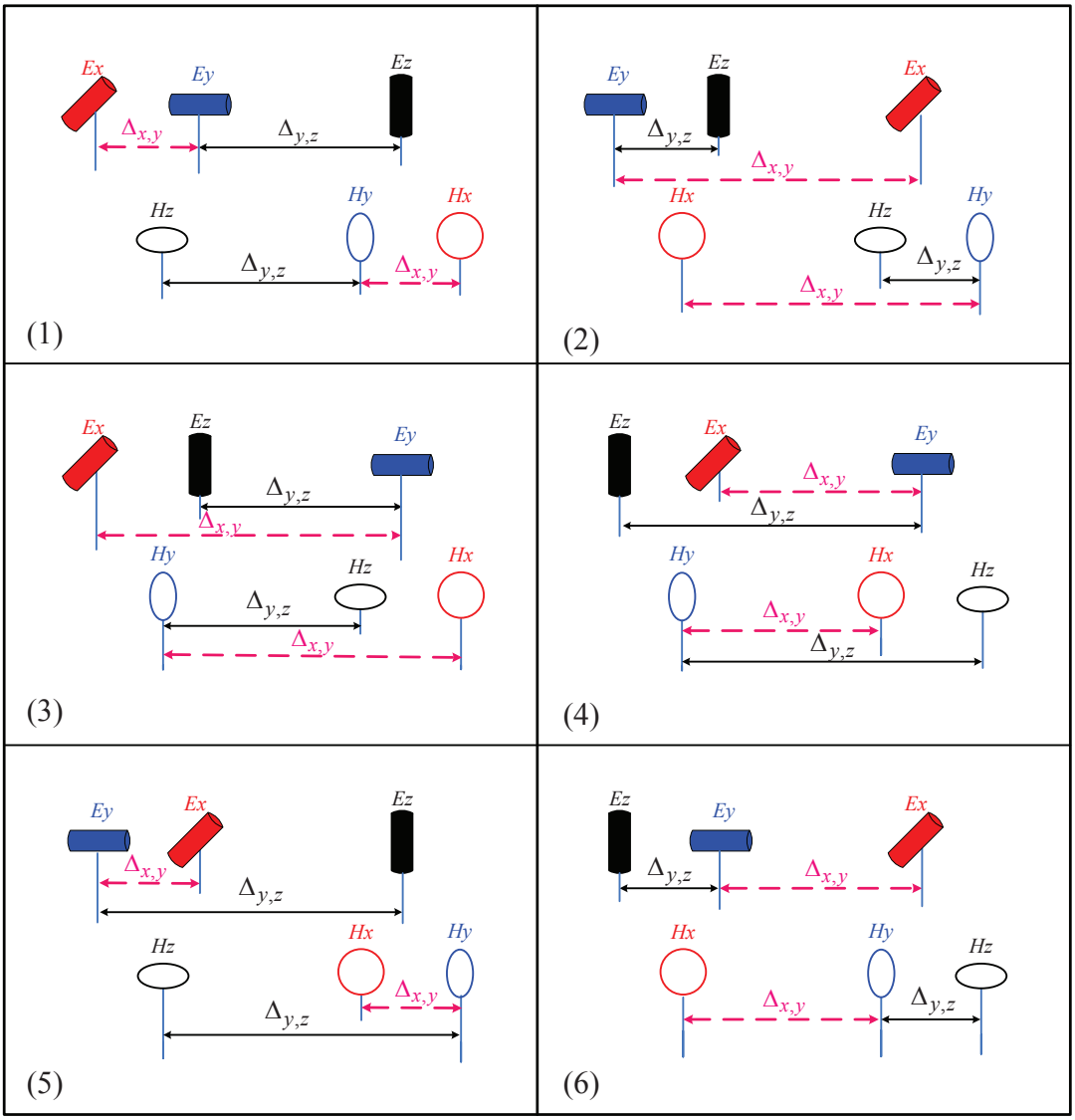

Figure 2.1: Six permutations to place the six orthogonally dipoles / triads on two parallel lines, which may lie arbitrarily in three dimensional space as shown in Figure 2.2.

array manifold is no longer (1.5), but

$$\tilde{\mathbf{a}} \stackrel{\text{def}}{=} \begin{bmatrix} \tilde{\mathbf{e}} \\ \tilde{\mathbf{h}} \end{bmatrix} \stackrel{\text{def}}{=} \underbrace{\begin{bmatrix} 1 \\ e^{-j\frac{2\pi}{\lambda}\Delta_{x,y}(\tilde{u}u+\tilde{v}v+\tilde{w}w)} \\ e^{-j\frac{2\pi}{\lambda}[\Delta_{x,y}(\tilde{u}u+\tilde{v}v+\tilde{w}w)+\Delta_{y,z}(\tilde{u}u+\tilde{v}v+\tilde{w}w)]} \\ e^{-j\frac{2\pi}{\lambda}(x_h u+y_h v+z_h w)} \\ e^{-j\frac{2\pi}{\lambda}(x_h u+y_h v+z_h w)} e^{j\frac{2\pi}{\lambda}\Delta_{x,y}(\tilde{u}u+\tilde{v}v+\tilde{w}w)} \\ e^{-j\frac{2\pi}{\lambda}(x_h u+y_h v+z_h w)} e^{j\frac{2\pi}{\lambda}[\Delta_{x,y}(\tilde{u}u+\tilde{v}v+\tilde{w}w)+\Delta_{y,z}(\tilde{u}u+\tilde{v}v+\tilde{w}w)]} \end{bmatrix}}_{\stackrel{\text{def}}{=}\mathbf{d}(\theta,\phi)} \odot \underbrace{\begin{bmatrix} e_x \\ e_y \\ e_z \\ h_x \\ h_y \\ h_z \end{bmatrix}}_{\mathbf{a}}, \tag{2.2}$$

where $\tilde{u} = \sin(\tilde{\theta})\cos(\tilde{\phi})$, $\tilde{v} = \sin(\tilde{\theta})\sin(\tilde{\phi})$, $\tilde{w} = \cos(\tilde{\theta})$, (x_h, y_h, z_h) is the coordinate of the loop H_x, and $\odot$ symbolizes the element-wise multiplication between two vectors. The spatial support-region is hemispherical, with the hemispherical base perpendicular to the two array-axes, as in Figure 2.2. [4] In (2.2), the ℓth element of $\mathbf{d}(\theta, \phi)$ represents the ℓth component-antenna's spatial phase-factor, whereas the ℓth element of $\mathbf{a}$ gives the ℓth component-antenna's gain / phase /polarization response. Note the anti-symmetry in the exponents of E_y and E_z, versus the exponents of H_y and H_z. This will be critical to the success of the proposed scheme.

2.4 A New "Vector-Cross-Product" Direction-Finding Algorithm

In all eigen-based "vector-cross-product" direction-finding schemes cited in Section 2.3, an intermediate algorithmic step would estimate each incident source's steering vector, but correct to only within an *un*known complex-value scalar c. [5] That is, available (in each algorithm for each incident emitter)[6] is the estimate $\hat{\mathbf{a}} \approx c\mathbf{a}$, from which θ and ϕ are to be estimated. (This approximation becomes an equality in noiseless or asymptotic cases.) The question now is whether $\hat{\tilde{\mathbf{a}}} \approx c\tilde{\mathbf{a}}$ suffices to estimate θ and ϕ unambiguously, where $\tilde{\mathbf{a}}$ denotes the spatially extended (2.2), instead of the collocated (1.5).

[4] In the special case of the two parallel lines parallel to the x-axis, the spatial support-region for the estimates would be either the right or the left hemisphere. If the two parallel lines are parallel to the y-axis, the spatial support-region would be either the front or the back hemisphere. If parallel to the z-axis, the spatial support-region for the estimates would be either the upper or the lower hemisphere.

[5] For example, see step {2c.} in Section 2.5.1, which reviews the key algorithmic steps in the *Uni-Vector-Sensor ESPRIT* method of [32].

[6] This does NOT presume only a single incident source. Multiple, possibly cross-correlated / broadband / time-varying sources can be handled. For details, please refer to those references directly.

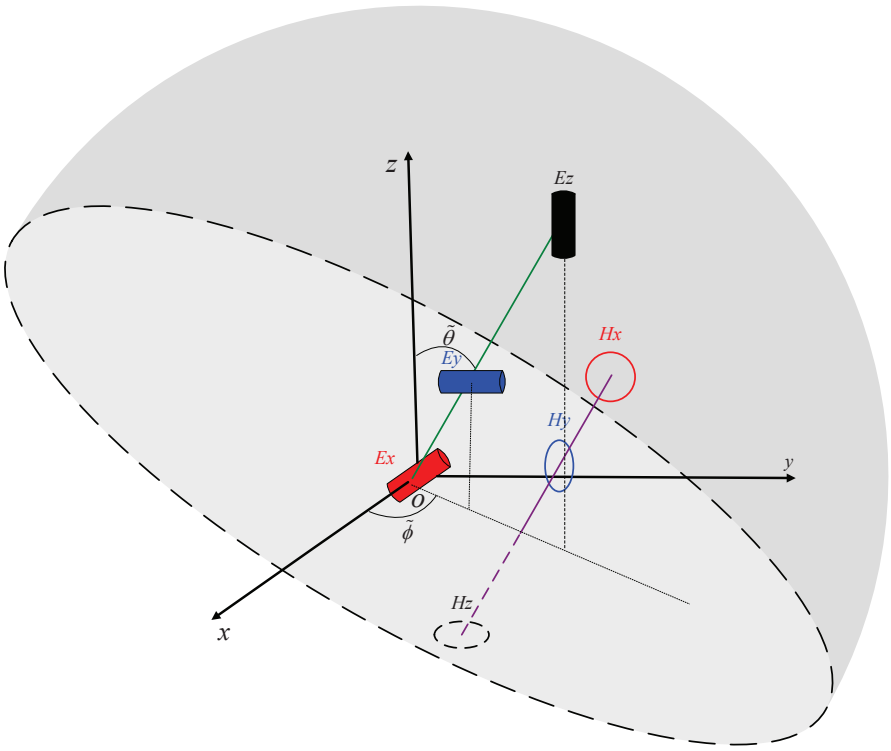

Figure 2.2: Spatial geometry, showing for the dipoles/loops permutation case (1) in Figure 2.1.

The answer is "yes"; and the following shows why and how. Cross-multiply $c\tilde{\mathbf{e}}$ and $c\tilde{\mathbf{h}}$ to give

$$c\tilde{\mathbf{e}} \times \left(c\tilde{\mathbf{h}}\right)^* = |c|^2 e^{j\frac{2\pi}{\lambda}(x_h u + y_h v + z_h w)} \begin{bmatrix} u\ e^{-j\frac{2\pi}{\lambda}[(2\Delta_{x,y}+\Delta_{y,z})(\tilde{u}u+\tilde{v}v+\tilde{w}w)]} \\ v\ e^{-j\frac{2\pi}{\lambda}[(\Delta_{x,y}+\Delta_{y,z})(\tilde{u}u+\tilde{v}v+\tilde{w}w)]} \\ w\ e^{-j\frac{2\pi}{\lambda}\Delta_{x,y}(\tilde{u}u+\tilde{v}v+\tilde{w}w)} \end{bmatrix}. \quad (2.3)$$

Next, normalize (2.3) according to its Frobenius norm,

$$\frac{(c\tilde{\mathbf{e}}) \times (c\tilde{\mathbf{h}})^*}{\left\|(c\tilde{\mathbf{e}}) \times (c\tilde{\mathbf{h}})^*\right\|} = e^{j\frac{2\pi}{\lambda}(x_h u + y_h v + z_h w)} \begin{bmatrix} u\ e^{-j\frac{2\pi}{\lambda}[(2\Delta_{x,y}+\Delta_{y,z})(\tilde{u}u+\tilde{v}v+\tilde{w}w)]} \\ v\ e^{-j\frac{2\pi}{\lambda}[(\Delta_{x,y}+\Delta_{y,z})(\tilde{u}u+\tilde{v}v+\tilde{w}w)]} \\ w\ e^{-j\frac{2\pi}{\lambda}\Delta_{x,y}(\tilde{u}u+\tilde{v}v+\tilde{w}w)} \end{bmatrix} \stackrel{\text{def}}{=} \mathbf{q}.$$

To ease subsequent exposition, assume *momentarily* that the two array-axes are parallel to one of the Cartesian axis.

2.4.1 If the Two Array-Axes are Parallel to the x-Axis

This special case has $\tilde{\theta} = \pi/2$ and $\tilde{\phi} = 0$; hence, $\mathbf{q}$ degrades to:

$$\mathbf{q}_x \stackrel{\text{def}}{=} e^{j\frac{2\pi}{\lambda}(x_h u + y_h v + z_h w)} \begin{bmatrix} u\ e^{-j\frac{2\pi}{\lambda}(2\Delta_{x,y}+\Delta_{y,z})u} \\ v\ e^{-j\frac{2\pi}{\lambda}(\Delta_{x,y}+\Delta_{y,z})u} \\ w\ e^{-j\frac{2\pi}{\lambda}\Delta_{x,y}u} \end{bmatrix}.$$

Consider the following two disjoint cases, separately.

Suppose $\phi \in [-\pi/2, \pi/2]$

Consequentially, the x-axis direction-cosine $u \geq 0, \forall \theta \in [0, \pi]$. Hence,

$$\mathbf{q}_x e^{-j\angle[\mathbf{q}_x]_1} = \begin{bmatrix} u & \\ v & e^{j\frac{2\pi}{\lambda}\Delta_{x,y}u} \\ w & e^{j\frac{2\pi}{\lambda}(\Delta_{x,y}+\Delta_{y,z})u} \end{bmatrix} \stackrel{\text{def}}{=} \acute{\mathbf{q}}_x. \tag{2.4}$$

The above equation leads to these estimates of the three Cartesian direction-cosines,

$$\begin{aligned} \hat{u}_{\text{coarse}} &= [\acute{\mathbf{q}}_x]_1, \\ \hat{v} &= \text{Re}\left\{ [\acute{\mathbf{q}}_x]_2 \; e^{-j\frac{2\pi}{\lambda}\Delta_{x,y}\hat{u}_{\text{coarse}}} \right\}, \\ \hat{w} &= \text{Re}\left\{ [\acute{\mathbf{q}}_x]_3 \; e^{-j\frac{2\pi}{\lambda}(\Delta_{x,y}+\Delta_{y,z})\hat{u}_{\text{coarse}}} \right\}, \end{aligned} \tag{2.5}$$

In the above, $\hat{u}_{\text{coarse}}$ is set to $[\acute{\mathbf{q}}_x]_1$, not to $|[\acute{\mathbf{q}}_x]_1|$, to retain the sign of $[\acute{\mathbf{q}}_x]_1$. Similar considerations apply for $\hat{v}$ and $\hat{w}$. The operand, under noiseless or asymptotic conditions, would necessarily be real-value for each inverse-trigonometric operator above. These operands could become complex-value with noise, hence the real-value operators above.

However, the complex-phases in (2.4) can afford also *fine* estimates of the x-axis direction-cosine:

$$\hat{u}_{\text{fine},1} = \frac{\lambda}{2\pi}\frac{1}{\Delta_{x,y}} \angle \left\{ \frac{[\acute{\mathbf{q}}_x]_2}{\hat{v}} \right\}, \tag{2.6}$$

$$\hat{u}_{\text{fine},2} = \frac{\lambda}{2\pi}\frac{1}{(\Delta_{x,y}+\Delta_{y,z})} \angle \left\{ \frac{[\acute{\mathbf{q}}_x]_3}{\hat{w}} \right\}. \tag{2.7}$$

These finer-resolution estimates are obtainable, due to the non-zero inter-antenna spacings of $\Delta_{x,y}$ and $\Delta_{y,z}$, on account of the sparse array-spacing principle.

These more accurate estimates are available here for only the x-axis direction-cosine, because both $\Delta_{x,y}$ and $\Delta_{y,z}$ are aligned along the x-axis. Therefore, the inter-antenna spacings are sparse along only the x-axis, but not along the y-axis nor along the z-axis.

As $\Delta_{x,y}$ lengthens beyond $\frac{\lambda}{2}$, more than one value may exist of $\hat{u}_{\text{fine},1}$ that satisfy (2.6). Hence, this more accurate $\hat{u}_{\text{fine},1}$ could be cyclically ambiguous, in contrast to $\hat{u}_{\text{coarse}}$, which is *un*ambiguous but coarser in estimation accuracy. Similar considerations hold for $\hat{u}_{\text{fine},2}$. These several complementary estimates of u in (2.5), (2.6), (2.7)), could be synergized by using $\hat{u}_{\text{coarse}}$ to disambiguate $\hat{u}_{\text{fine},1}$ and $\hat{u}_{\text{fine},2}$, to produce an estimate that is both fine in estimation resolution and unambiguous:

$$\hat{u} = \frac{1}{2}\left\{ \hat{u}_{\text{fine},1} + m^{\circ}_{x,y}\frac{\lambda}{\Delta_{x,y}} \right\} + \frac{1}{2}\left\{ \hat{u}_{\text{fine},2} + m^{\circ}_{x,z}\frac{\lambda}{\Delta_{x,y}+\Delta_{y,z}} \right\}, \tag{2.8}$$

where

$$\begin{aligned} m^{\circ}_{x,y} &= \overset{\arg\min}{m_{x,y}} \left| \hat{u}_{\text{coarse}} - \hat{u}_{\text{fine},1} - m_{x,y} \frac{\lambda}{\Delta_{x,y}} \right| \\ m^{\circ}_{x,z} &= \overset{\arg\min}{m_{x,z}} \left| \hat{u}_{\text{coarse}} - \hat{u}_{\text{fine},2} - m_{x,z} \frac{\lambda}{\Delta_{x,y}+\Delta_{y,z}} \right| \end{aligned}$$

for

$$\begin{aligned} m_{x,y} &\in \left\{ \left\lceil \frac{\Delta_{x,y}}{\lambda}(-1-\hat{u}_{\text{coarse}}) \right\rceil, \left\lfloor \frac{\Delta_{x,y}}{\lambda}(1-\hat{u}_{\text{coarse}}) \right\rfloor \right\}, \\ m_{x,z} &\in \left\{ \left\lceil \frac{\Delta_{x,y}+\Delta_{y,z}}{\lambda}(-1-\hat{u}_{\text{coarse}}) \right\rceil, \left\lfloor \frac{\Delta_{x,y}+\Delta_{y,z}}{\lambda}(1-\hat{u}_{\text{coarse}}) \right\rfloor \right\}, \end{aligned}$$

where $\lceil \alpha \rceil$ refers to the smallest integer not less than α, and $\lfloor \alpha \rfloor$ refers to the largest integer not exceeding α.

However, for $\Delta_{x,y} < \lambda$, the spatial aperture is not much extended; hence, simply set $\hat{u} = \hat{u}_{\text{coarse}}$.

Lastly,

$$\begin{aligned} \hat{\phi} &= \arctan\left\{ \frac{\hat{v}}{\hat{u}} \right\} \\ \hat{\theta} &= \arccos\{\hat{w}\}. \end{aligned}$$

Suppose $\phi \in [\pi/2, 3\pi/2]$

Consequentially, $u \leq 0, \forall \theta \in [0, \pi]$. This gives

$$\begin{aligned} \mathbf{q}_x e^{-j\angle[\mathbf{q}_x]_1} &= \begin{bmatrix} -u & \\ -v & e^{j\frac{2\pi}{\lambda}\Delta_{x,y}u} \\ -w & e^{j\frac{2\pi}{\lambda}(\Delta_{x,y}+\Delta_{y,z})u} \end{bmatrix} \overset{\text{def}}{=} \acute{\mathbf{q}}_x, \\ \hat{u}_{\text{coarse}} &= -[\acute{\mathbf{q}}_x]_1 \\ \hat{v} &= \text{Re}\left\{ -[\acute{\mathbf{q}}_x]_2 \, e^{-j\frac{2\pi}{\lambda}\Delta_{x,y}\hat{u}_{\text{coarse}}} \right\} \\ \hat{w} &= \text{Re}\left\{ -[\acute{\mathbf{q}}_x]_3 \, e^{-j\frac{2\pi}{\lambda}(\Delta_{x,y}+\Delta_{y,z})\hat{u}_{\text{coarse}}} \right\} \\ \hat{\phi} &= \arctan\left\{ \frac{\hat{v}}{\hat{u}} \right\} + \pi \\ \hat{\theta} &= \arccos\{\hat{w}\} \ , \end{aligned}$$

with $\hat{u}_{\text{fine},1}$ remains as in (2.6), $\hat{u}_{\text{fine},2}$ as in (2.7), and $\hat{u}$ as in (2.8).

2.4.2 If the Two Array-Axes are Parallel to the y-Axis

This special case has $\tilde{\theta} = \pi/2$ and $\tilde{\phi} = \pi/2$; therefore, $\mathbf{q}$ degrades to

$$\mathbf{q}_y \overset{\text{def}}{=} e^{j\frac{2\pi}{\lambda}(x_h u + y_h v + z_h w)} \begin{bmatrix} u \, e^{-j\frac{2\pi}{\lambda}(2\Delta_{x,y}+\Delta_{y,z})v} \\ v \, e^{-j\frac{2\pi}{\lambda}(\Delta_{x,y}+\Delta_{y,z})v} \\ w \, e^{-j\frac{2\pi}{\lambda}\Delta_{x,y}v} \end{bmatrix}.$$

Separately consider the following two disjoint cases:

Suppose $\phi \in [0, \pi]$

Hence the y-axis direction-cosine $v \geq 0, \forall \theta \in [0, \pi]$. Hence,

$$\begin{aligned}
\mathbf{q}_y e^{-j\angle[\mathbf{q}_y]_2} &= \begin{bmatrix} u & e^{-j\frac{2\pi}{\lambda}\Delta_{x,y}v} \\ v & \\ w & e^{j\frac{2\pi}{\lambda}\Delta_{y,z}v} \end{bmatrix} \stackrel{\text{def}}{=} \acute{\mathbf{q}}_y, && (2.9) \\
\hat{v}_{\text{coarse}} &= [\acute{\mathbf{q}}_y]_2 \\
\hat{v}_{\text{fine},1} &= -\frac{\lambda}{2\pi}\frac{1}{\Delta_{x,y}}\angle\left\{\frac{[\acute{\mathbf{q}}_y]_1}{\hat{u}}\right\}, && (2.10) \\
\hat{v}_{\text{fine},2} &= \frac{\lambda}{2\pi}\frac{1}{\Delta_{y,z}}\angle\left\{\frac{[\acute{\mathbf{q}}_y]_3}{\hat{w}}\right\}, && (2.11) \\
\hat{v} &= \frac{1}{2}\left\{\hat{v}_{\text{fine},1} + m^{\circ}_{x,y}\frac{\lambda}{\Delta_{x,y}}\right\} + \frac{1}{2}\left\{\hat{v}_{\text{fine},2} + m^{\circ}_{x,z}\frac{\lambda}{\Delta_{x,y}+\Delta_{y,z}}\right\}, && (2.12)
\end{aligned}$$

if $\Delta_{x,y} \geq \lambda$, where

$$\begin{aligned}
m^{\circ}_{x,y} &= \stackrel{\arg\min}{m_{x,y}} \left|\hat{v}_{\text{coarse}} - \hat{v}_{\text{fine},1} - m_{x,y}\frac{\lambda}{\Delta_{x,y}}\right| \\
m^{\circ}_{x,z} &= \stackrel{\arg\min}{m_{x,z}} \left|\hat{v}_{\text{coarse}} - \hat{v}_{\text{fine},2} - m_{x,z}\frac{\lambda}{\Delta_{x,y}+\Delta_{y,z}}\right|
\end{aligned}$$

for

$$\begin{aligned}
m_{x,y} &\in \left\{\left\lceil\frac{\Delta_{x,y}}{\lambda}(-1-\hat{v}_{\text{coarse}})\right\rceil, \left\lfloor\frac{\Delta_{x,y}}{\lambda}(1-\hat{v}_{\text{coarse}})\right\rfloor\right\}, \\
m_{x,z} &\in \left\{\left\lceil\frac{\Delta_{x,y}+\Delta_{y,z}}{\lambda}(-1-\hat{v}_{\text{coarse}})\right\rceil, \left\lfloor\frac{\Delta_{x,y}+\Delta_{y,z}}{\lambda}(1-\hat{v}_{\text{coarse}})\right\rfloor\right\}.
\end{aligned}$$

However, for $\Delta_{x,y} < \lambda$, simply set $\hat{v} = \hat{v}_{\text{coarse}}$.

Also from (2.9),

$$\begin{aligned}
\hat{u} &= \text{Re}\left\{[\acute{\mathbf{q}}_y]_1\, e^{j\frac{2\pi}{\lambda}\Delta_{x,y}\hat{v}_{\text{coarse}}}\right\} \\
\hat{w} &= \text{Re}\left\{[\acute{\mathbf{q}}_y]_3\, e^{-j\frac{2\pi}{\lambda}\Delta_{y,z}\hat{v}_{\text{coarse}}}\right\} \\
\hat{\phi} &= \begin{cases} \arctan\left\{\frac{\hat{v}}{\hat{u}}\right\}, & \text{if} \quad \hat{u} \geq 0 \\ \arctan\left\{\frac{\hat{v}}{\hat{u}}\right\} + \pi, & \text{if} \quad \hat{u} < 0 \end{cases} \\
\hat{\theta} &= \arccos\{\hat{w}\}.
\end{aligned}$$

Suppose $\phi \in [\pi, 2\pi]$

This implies that the y-axis direction-cosine $v \leq 0, \forall \theta \in [0, \pi]$. Therefore,

$$\mathbf{q}_y e^{-j\angle[\mathbf{q}_y]_2} = \begin{bmatrix} -u & e^{-j\frac{2\pi}{\lambda}\Delta_{x,y}v} \\ -v & \\ -w & e^{j\frac{2\pi}{\lambda}\Delta_{y,z}v} \end{bmatrix} \stackrel{\text{def}}{=} \acute{\mathbf{q}}_y.$$

$$
\begin{aligned}
\hat{v}_{\text{coarse}} &= -[\acute{\mathbf{q}}_y]_2 \\
\hat{u} &= \text{Re}\left\{-[\acute{\mathbf{q}}_y]_1\, e^{j\frac{2\pi}{\lambda}\Delta_{x,y}\hat{v}_{\text{coarse}}}\right\} \\
\hat{w} &= \text{Re}\left\{-[\acute{\mathbf{q}}_y]_3\, e^{-j\frac{2\pi}{\lambda}\Delta_{y,z}\hat{v}_{\text{coarse}}}\right\} \\
\hat{\phi} &= \begin{cases} \arctan\left\{\frac{\hat{v}}{\hat{u}}\right\}, & \text{if} \quad \hat{u} \geq 0 \\ \arctan\left\{\frac{\hat{v}}{\hat{u}}\right\} + \pi, & \text{if} \quad \hat{u} < 0 \end{cases} \\
\hat{\theta} &= \arccos\{\hat{w}\},
\end{aligned}
$$

with $\hat{v}_{\text{fine},1}$ remains as in (2.10), $\hat{v}_{\text{fine},2}$ as in (2.11), and $\hat{v}$ as in (2.12).

2.4.3 If the Two Array-Axes are Parallel to the z-Axis

This particular case has $\tilde{\theta} = 0$. $\mathbf{q}$ degrades to:

$$
\mathbf{q}_z \stackrel{\text{def}}{=} e^{j\frac{2\pi}{\lambda}(x_h u + y_h v + z_h w)} \begin{bmatrix} u\; e^{-j\frac{2\pi}{\lambda}(2\Delta_{x,y}+\Delta_{y,z})w} \\ v\; e^{-j\frac{2\pi}{\lambda}(\Delta_{x,y}+\Delta_{y,z})w} \\ w\; e^{-j\frac{2\pi}{\lambda}\Delta_{x,y}w} \end{bmatrix}. \tag{2.13}
$$

Separately consider the following two disjoint cases:

Suppose $\theta \in [0, \pi/2]$

This would imply that the z-axis direction-cosine $w \geq 0$. Therefore,

$$
\mathbf{q}_z e^{-j\angle[\mathbf{q}_z]_3} = \begin{bmatrix} u & e^{-j\frac{2\pi}{\lambda}(\Delta_{y,z}+\Delta_{x,y})w} \\ v & e^{-j\frac{2\pi}{\lambda}\Delta_{y,z}w} \\ w & \end{bmatrix} \stackrel{\text{def}}{=} \acute{\mathbf{q}}_z.
$$

From the above equation,

$$
\begin{aligned}
\hat{w}_{\text{coarse}} &= [\acute{\mathbf{q}}_z]_3, \\
\hat{w}_{\text{fine},1} &= -\frac{\lambda}{2\pi}\frac{1}{(\Delta_{x,y}+\Delta_{y,z})}\angle\left\{\frac{[\acute{\mathbf{q}}_z]_1}{\hat{u}}\right\}, && (2.14) \\
\hat{w}_{\text{fine},2} &= -\frac{\lambda}{2\pi}\frac{1}{\Delta_{y,z}}\angle\left\{\frac{[\acute{\mathbf{q}}_z]_2}{\hat{v}}\right\}, && (2.15) \\
\hat{w} &= \frac{1}{2}\left\{\hat{w}_{\text{fine},1} + m^{\circ}_{x,z}\frac{\lambda}{\Delta_{x,y}+\Delta_{y,z}}\right\} + \frac{1}{2}\left\{\hat{w}_{\text{fine},2} + m^{\circ}_{y,z}\frac{\lambda}{\Delta_{y,z}}\right\}, && (2.16)
\end{aligned}
$$

for $\Delta_{y,z} \geq \lambda$, where

$$
\begin{aligned}
m^{\circ}_{x,z} &= \stackrel{\arg\min}{m_{x,z}} \left|\hat{w}_{\text{coarse}} - \hat{w}_{\text{fine},1} - m_{x,z}\frac{\lambda}{\Delta_{x,y}+\Delta_{y,z}}\right| \\
m^{\circ}_{y,z} &= \stackrel{\arg\min}{m_{y,z}} \left|\hat{w}_{\text{coarse}} - \hat{w}_{\text{fine},2} - m_{y,z}\frac{\lambda}{\Delta_{y,z}}\right|
\end{aligned}
$$

for

$$
\begin{aligned}
m_{x,z} &\in \left\{\left\lceil\frac{\Delta_{x,y}+\Delta_{y,z}}{\lambda}(-1-\hat{w}_{\text{coarse}})\right\rceil, \left\lfloor\frac{\Delta_{x,y}+\Delta_{y,z}}{\lambda}(1-\hat{w}_{\text{coarse}})\right\rfloor\right\}, \\
m_{y,z} &\in \left\{\left\lceil\frac{\Delta_{y,z}}{\lambda}(-1-\hat{w}_{\text{coarse}})\right\rceil, \left\lfloor\frac{\Delta_{y,z}}{\lambda}(1-\hat{w}_{\text{coarse}})\right\rfloor\right\}.
\end{aligned}
$$

However, for $\Delta_{y,z} < \lambda$, simply set $\hat{w} = \hat{w}_{\text{coarse}}$.

Also from (2.13),

$$\begin{aligned}
\hat{u} &= \text{Re}\left\{[\acute{\mathbf{q}}_z]_1 \, e^{j\frac{2\pi}{\lambda}(\Delta_{x,y}+\Delta_{y,z})\hat{w}_{\text{coarse}}}\right\} \\
\hat{v} &= \text{Re}\left\{[\acute{\mathbf{q}}_z]_2 \, e^{j\frac{2\pi}{\lambda}\Delta_{y,z}\hat{w}_{\text{coarse}}}\right\} \\
\hat{\phi} &= \begin{cases} \arctan\left\{\frac{\hat{v}}{\hat{u}}\right\}, & \text{if} \quad \hat{u} \geq 0 \\ \arctan\left\{\frac{\hat{v}}{\hat{u}}\right\} + \pi, & \text{if} \quad \hat{u} < 0 \end{cases} \\
\hat{\theta} &= \arccos\{\hat{w}\}.
\end{aligned}$$

Suppose $\theta \in [\pi/2, \pi]$

This implies that $w \leq 0$. Therefore,

$$\mathbf{q}_z e^{-j\angle[\mathbf{q}_z]_3} = \begin{bmatrix} -u & e^{-j\frac{2\pi}{\lambda}(\Delta_{y,z}+\Delta_{x,y})w} \\ -v & e^{-j\frac{2\pi}{\lambda}\Delta_{y,z}w} \\ -w & \end{bmatrix} \stackrel{\text{def}}{=} \acute{\mathbf{q}}_z.$$

As a result,

$$\begin{aligned}
\hat{u} &= \text{Re}\left\{-[\acute{\mathbf{q}}_z]_1 \, e^{j\frac{2\pi}{\lambda}(\Delta_{x,y}+\Delta_{y,z})\hat{w}}\right\} \\
\hat{v} &= \text{Re}\left\{-[\acute{\mathbf{q}}_z]_2 \, e^{j\frac{2\pi}{\lambda}\Delta_{y,z}\hat{w}}\right\} \\
\hat{w}_{\text{coarse}} &= -[\acute{\mathbf{q}}_z]_3 \\
\hat{\phi} &= \begin{cases} \arctan\left\{\frac{\hat{v}}{\hat{u}}\right\}, & \text{if} \quad \hat{u} \geq 0 \\ \arctan\left\{\frac{\hat{v}}{\hat{u}}\right\} + \pi, & \text{if} \quad \hat{u} < 0 \end{cases} \\
\hat{\theta} &= \arccos\{\hat{w}\},
\end{aligned}$$

with $\hat{w}_{\text{fine},1}$ remains as in (2.14), $\hat{w}_{\text{fine},2}$ as in (2.15), and $\hat{w}$ as in (2.16).

2.4.4 If the Two Array-Axes are Arbitrarily Oriented

In the general case that the two parallel array-axes are arbitrarily oriented, a new coordinate (x', y', z') could be defined such that the two array-axes would fit with one of the special cases in Sections 2.4.1-2.4.3. With reference to these (x', y', z'), the directional cosines (u', v', w') are estimated. Then the following rotational transformation through the Euler angles (α, β, τ) (see Figure 2.3 and p. 147 of [2]) would give the Cartesian directional cosines $(\hat{u}, \hat{v}, \hat{w})$ in the Cartesian coordinates (x, y, z).

$$\begin{bmatrix} u \\ v \\ w \end{bmatrix} = \begin{bmatrix} \cos\tau & \sin\tau & 0 \\ -\sin\tau & \cos\tau & 0 \\ 0 & 0 & 1 \end{bmatrix} \begin{bmatrix} 1 & 0 & 0 \\ 0 & \cos\beta & \sin\beta \\ 0 & -\sin\beta & \cos\beta \end{bmatrix} \begin{bmatrix} \cos\alpha & \sin\alpha & 0 \\ -\sin\alpha & \cos\alpha & 0 \\ 0 & 0 & 1 \end{bmatrix} \begin{bmatrix} u' \\ v' \\ w' \end{bmatrix}.$$

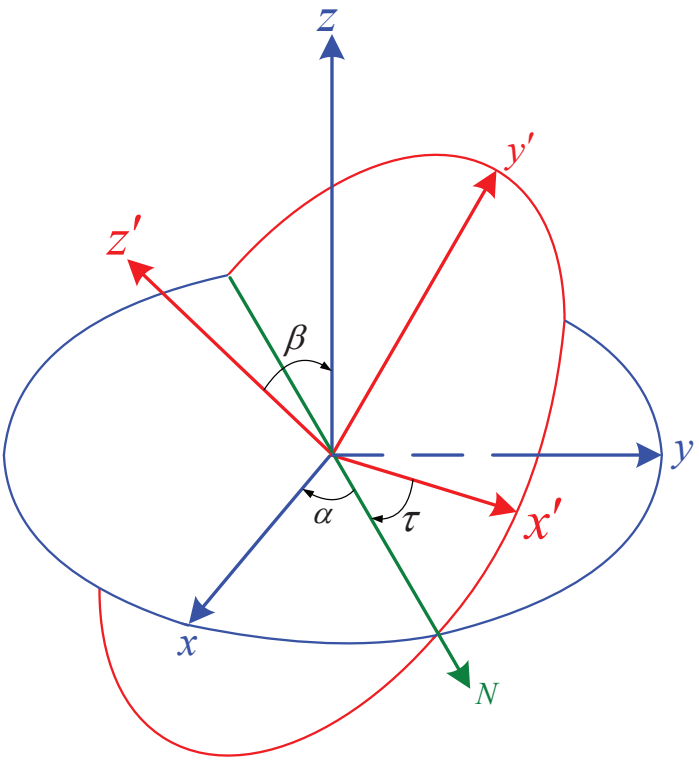

Figure 2.3: The Cartesian coordinates (x', y', z') are rotated through the Euler angles (α, β, τ), to give a second set of Cartesian coordinates (x, y, z). (This diagram is based on a similar diagram in Wikipedia's entry on "Euler angles".)

2.5 A Full Algorithm to Illustrate How to Apply the New Technique in Section 2.4

The new "vector-cross-product" direction-finding technique proposed in Section 2.4 may be applied to *any* eigen-based parameter-estimation algorithm that can estimate a source's steering vector (to at least within a possibly unknown complex-value scalar).

To illustrate how so, this section will consider the "uni-vector-sensor ESPRIT" algorithm of [32], which is originally developed for an electromagnetic vector-sensor of *collocated* component-antennas. This section will instead show how the technique in Section 2.4 can modify [32] for a *spatially spread* vector-sensor as defined in the boxed description in Section 2.3.

2.5.1 Review of Data Model & Algorithm of [32] for a *Collocated* Electromagnetic Vector-Sensor

Multiple completely polarized transverse electromagnetic waves, having traveled through an homogeneous isotropic medium, impinge upon a single electromagnetic vector-sensor, with spatially *collocated* component-antennas, all at the origin of the Cartesian coordinates. The kth such wavefront is associated with the steering vector $\mathbf{a}_k$, defined analogously as in (1.5). Let the kth incoming signal $s_k(t)$ have power $\mathcal{P}_k$, but to be temporally monochromatic at a frequency f_k (distinct from all other incident sources' frequencies) with an initial phase of ϵ_k. With K such incident sources, the 6×1 data-vector collected at time t equals $\mathbf{z}(t) = \sum_{k=1}^{K} \sqrt{\mathcal{P}_k}\mathbf{a}_k e^{j2\pi f_k t + \epsilon_k} + \mathbf{n}(t)$, where $\mathbf{n}(t)$ symbolizes the additive noise at the electromagnetic vector-sensor. [7]

The *Uni-Vector-Sensor ESPRIT* algorithm [32] would form these two time-delayed data-subsets out of the aforementioned collected data: $\{\mathbf{z}(t_n),\ \forall n = 1, \ldots, N\}$ and $\{\mathbf{z}(t_n + \Delta_T), \forall\ n = 1, \ldots, N\}$, where Δ_T represents a constant time-delay between the two sets of time samples.

The following will summarize the algorithmic steps of the *Uni-Vector-Sensor ESPRIT* algorithm. For the motivations underlying these algorithmic steps, please refer to the lengthy exposition in [32] itself.

$\{1.\}$ Form the $6 \times N$ data-matrices $\mathbf{Z}_1 = [\mathbf{z}(t_1), \mathbf{z}(t_2), \cdots, \mathbf{z}(t_N)]$ and $\mathbf{Z}_2 = [\mathbf{z}(t_1 + \Delta_T), \mathbf{z}(t_2 + \Delta_T), \cdots, \mathbf{z}(t_N + \Delta_T)]$. [8] Then, form the 6×6 data-correlation

[7] The technique proposed in Section 2.4 may be readily applied to other data models, and not restricted to the one reviewed here of [32]. This present data model serves only as an illustrative example.

[8] The two datasets $\mathbf{Z}_1$ and $\mathbf{Z}_2$ are inter-related by the temporal "invariances" of $\left\{e^{j(2\pi f_k \Delta_T),\ k=1,2,\cdots,K}\right\}$, thereby allowing the use of the parameter-estimation method of *ESPRIT* ("Estimation of Signal Parameters

matrices $\mathbf{R}_1 = \mathbf{Z}_1\mathbf{Z}_1^H$ and $\mathbf{R}_2 = \mathbf{Z}_2\mathbf{Z}_2^H$.

{2.} Apply ESPRIT to the matrix-pencil $\{\mathbf{R}_1, \mathbf{R}_2\}$, as follows, to estimate all K impinging sources' steering-vectors:

{2a.} Let $\mathbf{E}_1$ denote the $6 \times K$ signal-subspace eigenvector matrix whose K columns are the 6×1 signal-subspace eigenvectors associated with the K largest eigenvalues of $\mathbf{R}_1$. Let $\mathbf{E}_2$ denote the corresponding signal-subspace eigenvector matrix for $\mathbf{R}_2$.

{2b.} Define the $K \times K$ matrix,

$$\mathbf{\Psi} \;=\; \left(\mathbf{E}_1^H\mathbf{E}_1\right)^{-1}\left(\mathbf{E}_1^H\mathbf{E}_2\right) \;=\; \mathbf{T}^{-1}\mathbf{\Phi}\mathbf{T},$$

where the jth eigenvalue of $\mathbf{\Psi}$ equals $\{[\mathbf{\Phi}]_{j,j} = e^{j2\pi f_j \triangle_T},\;\; j = 1, \ldots, K\}$ and the corresponding right-eigenvector constitutes the jth column of $\mathbf{T}$.

{2c.} The K impinging sources' steering-vectors of (1.5) may be estimated, to within a complex-value multiplicative scalar, as

$$[\hat{\mathbf{a}}_1, \cdots, \hat{\mathbf{a}}_K] \;=\; \frac{1}{2}\{\mathbf{E}_1\mathbf{T}^{-1} + \mathbf{E}_2\mathbf{T}^{-1}\mathbf{\Phi}^{-1}\}.$$

These K *unknown* complex-value multiplicative scalars arise from the eigen-decomposition of $\mathbf{\Psi}$.

{3.} Apply the vector-cross-product of (2.1) to the kth source's above-estimated steering-vectors, as follows, to obtain the three corresponding Cartesian direction-cosine estimates:

$$\begin{bmatrix} \hat{u}_k \\ \hat{v}_k \\ \hat{w}_k \end{bmatrix} \;=\; \frac{\hat{\mathbf{e}}_k}{\|\hat{\mathbf{e}}_k\|} \times \frac{\hat{\mathbf{h}}_k^*}{\|\hat{\mathbf{h}}_k\|}.$$

The kth source's azimuth-elevation direction-of-arrival can then be estimated as:

$$\begin{aligned} \hat{\theta}_k \;&=\; \arcsin(\sqrt{\hat{u}_k^2 + \hat{v}_k^2}) \;=\; \arccos(\hat{w}_k), \\ \hat{\phi}_k \;&=\; \arctan(\hat{v}_k/\hat{u}_k), \end{aligned}$$

and the corresponding polarization parameters can then be estimated as:

$$\hat{\gamma}_k \;=\; \arctan\left|\frac{\hat{g}_{k,1}}{\hat{g}_{k,2}}\right|, \tag{2.17}$$

$$\hat{\eta}_k \;=\; \angle\left(\hat{g}_{k,1}/\hat{g}_{k,2}\right) \tag{2.18}$$

$$\text{where} \quad \hat{\mathbf{g}}_k = \begin{bmatrix} \hat{g}_{k,1} \\ \hat{g}_{k,2} \end{bmatrix} \;=\; \left[\mathbf{\Theta}^H(\hat{\theta}_k, \hat{\phi}_k)\mathbf{\Theta}(\hat{\theta}_k, \hat{\phi}_k)\right]^{-1}\mathbf{\Theta}^H(\hat{\theta}_k, \hat{\phi}_k)\hat{\mathbf{a}}_k \tag{2.19}$$

Via Rotational Invariance Techniques") [6].

2.5.2 Applying Section 2.4's Proposed Method, to the *Uni-Vector-Sensor ESPRIT* Algorithm of [32], but Now with the Component-Antennas *Spatially Spread* as in Section 2.3

Suppose now the *spatially spread* electromagnetic vector-sensor of Section 2.3 is now deployed, instead of a *spatially collocated* electromagnetic vector-sensor.

The 6×1 data-vector collected at time t would now equal $\tilde{\mathbf{z}}(t) = \sum_{k=1}^{K} \sqrt{\mathcal{P}_k}\tilde{\mathbf{a}}_k e^{j2\pi f_k t+\epsilon_k} + \mathbf{n}(t)$, instead. From this, Section 2.5.1's algorithmic steps {1.}, {2a.}, {2b.}, and {2c.} can still follow here, but now with a tilde atop all symbols.

However, as for $\hat{u}_k, \hat{v}_k, \hat{w}_k, \hat{\phi}_k, \hat{\theta}_k$ of the preceding Section 2.5.1, replace them by their counterpart estimation-formulas newly defined in Sections 2.4.1, 2.4.1, 2.4.2, 2.4.2, 2.4.3,or 2.4.3. [9]

2.6 Monte Carlo Simulation for the Algorithm Obtained from Modifying [32] by the Technique Proposed in Section 2.4

The proposed scheme's direction-finding efficacy and extended-aperture capability are demonstrated by Monte Carlo simulations.

Figures 2.4-2.6 show a three-source scenario simulation results of direction-cosines estimation with three different array configurations. [10] The array geometry in each figure is set with the two array-axes paralleling to one of the three Cartesian coordinate axes ($x/y/z$-axis). Each graph plots the mean-square-error of each incident source's Cartesian direction-cosine estimate along the array-axes, versus the inter-antenna spacing parameter $\frac{\Delta}{\lambda} = \ell$. Each data-point on each graph consists of 1000 statistically independent Monte Carlo trials. These estimates use 400 temporal snapshots. All sources have unity power. Each source's signal-to-noise ratio equals 30dB. The "spatially spread" electromagnetic vector-sensor conforms to a rectangular grid. Specifically, referring to the array geometric symbols defined in Figure 2.2: $(x_h, y_h, z_h) = \ell\lambda(2, 1, \sqrt{2})$, $\frac{\Delta}{\lambda} = \frac{\Delta_{x,y}}{\lambda} = \frac{\Delta_{y,z}}{\lambda} = \ell$, with λ defined to equal the minimum of $\lambda_1, \cdots, \lambda_K$.

Figures 2.4-2.6 clearly demonstrate the proposed scheme's success in resolving the incident sources, even if the electromagnetic vector-sensor's six component-antennas are spaced very far apart. In fact, this spatial *non*-collocation leads to orders-of-magnitude improvement in estimation accuracy, even as mutual coupling is reduced. Moreover, the

[9] For polarization estimation, (2.17)-(2.19) remain applicable, except that (2.19) needs to have its $\hat{\mathbf{a}}_k$ replaced by $\hat{\tilde{\mathbf{a}}}_k$, and to have its $\mathbf{\Theta}(\hat{\theta}_k, \hat{\phi}_k)$ replaced by $\mathbf{d}(\hat{\theta}_k, \hat{\phi}_k) \odot \mathbf{\Theta}(\hat{\theta}_k, \hat{\phi}_k)$.

[10] The estimation bias is about an order-of-magnitude smaller than the corresponding estimation MSE.

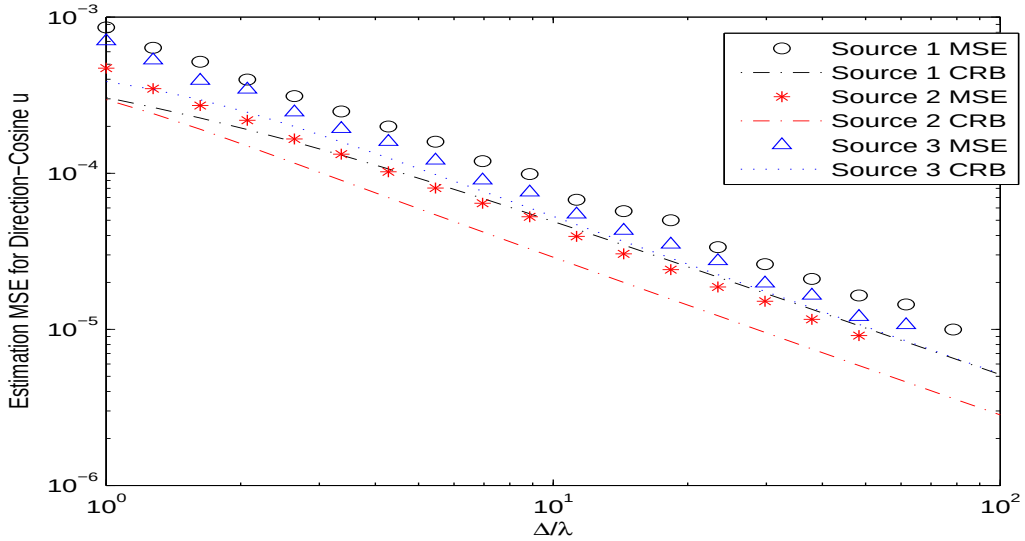

Figure 2.4: The mean-square-error (MSE) of the Cartesian direction-cosine estimate $\hat{u}$, for *three* incident sources, at digital frequencies $f_1' = 0.0985$, $f_2' = 0.1765$, and $f_3' = 0.1165$, respectively with $(\theta_1, \phi_1, \gamma_1, \eta_1) = (33^\circ, 42^\circ, 45^\circ, -90^\circ)$, $(\theta_2, \phi_2, \gamma_2, \eta_2) = (38^\circ, 35^\circ, 45^\circ, 90^\circ)$, and $(\theta_3, \phi_3, \gamma_3, \eta_3) = (52^\circ, 51^\circ, 45^\circ, -90^\circ)$. The same "spatially spread" electromagnetic vector-sensor configuration is set as $(\tilde{\theta}, \tilde{\phi}) = (90^\circ, 0^\circ)$, with the two array-axes paralleling to x-axis in the Cartesian coordinate system.

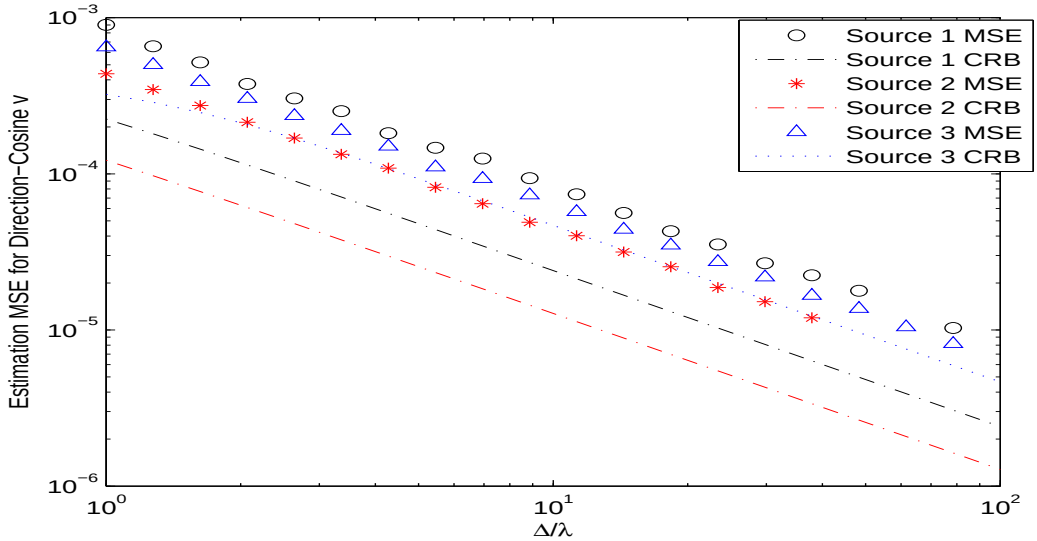

Figure 2.5: The mean-square-error of the Cartesian direction-cosine estimate $\hat{v}$, for the *three* same incident sources as in Figure 2.4. The "spatially spread" electromagnetic vector-sensor configuration is set as $(\tilde{\theta}, \tilde{\phi}) = (90^\circ, 90^\circ)$, with the two array-axes paralleling to y-axis in the Cartesian coordinate system.

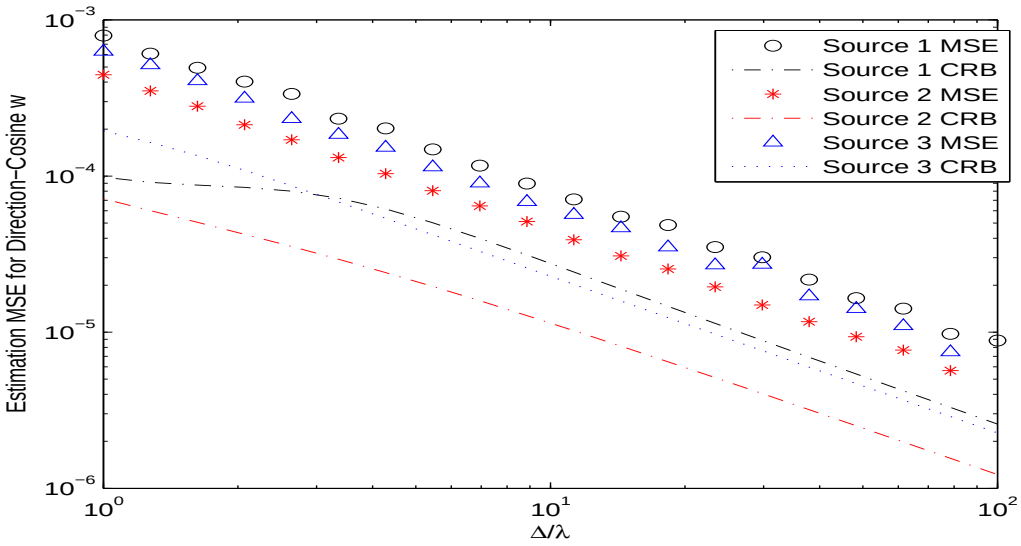

Figure 2.6: The mean-square-error of the Cartesian direction-cosine estimate $\hat{w}$, for the *three* same incident sources as in Figure 2.4. The "spatially spread" electromagnetic vector-sensor configuration is set as $(\tilde{\theta}, \tilde{\phi}) = (0°, 90°)$, with the two array-axes paralleling to z-axis in the Cartesian coordinate system.

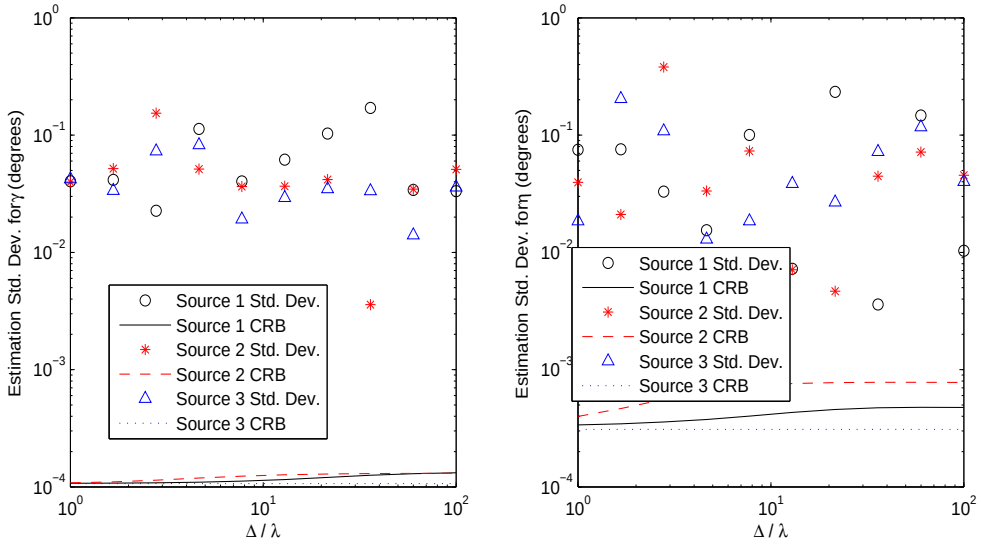

Figure 2.7: The standard derivations of the estimates for the polarization parameters $\{\gamma_k, \eta_k\}$, for the *three* same incident sources as in Figure 2.4.

estimation is very close to the Cramér-Rao lower bound (derived in the Appendix) as the inter-antenna spacing increases above a few wavelengths.

On the other hand, the non-collocating configuration of the vector sensor studied in this work assumes the polarization is the same as the collocating case. Hence, the investigated algorithm for the non-collocating scheme will not affect the polarization estimation. Figure 2.7 plots the standard derivations of the estimates for the polarization parameters $\{\gamma_k, \eta_k\}$ in the scenario corresponding to Figure 2.4. Figure 2.7 shows that the standard derivations of the estimates for the polarization parameters remain in a very small region in different inter-antenna spacings and this verifies the assumption that the polarization of the non-collocating vector sensor remains the same as the collocating electromagnetic vector sensor.

2.7 Summary

Many direction-finding advantages are offered by the recent synergy between interferometry and "vector cross-product" Poynting-vector estimation. However, the practicality of this synergy is limited by the mutual coupling across the six component-antennas comprising the electromagnetic vector-sensor. To alleviate this mutual-coupling problem, and thus to simplify the antenna implementation and to reduce hardware cost, this chapter shows a method how to achieve "vector cross-product" Poynting-vector estimation while spacing the six component-antennas far from each other. This spatial non-collocation extends the spatial aperture, to improve direction-finding accuracy by *orders of magnitude*, at *lower* hardware cost.

2.8 To Follow-Up the Non-Collocating Electromagnetic Vector-Sensor

The following problems can be investigated to follow-up the non-collocating electromagnetic vector-sensor proposed in this chapter:

1) coherent sources direction finding and polarization estimation with non-collocating electromagnetic vector-sensors,

2) wideband sources direction finding and polarization estimation with the non-collocating electromagnetic vector-sensor,

3) linear dependence of steering vectors of sources with the non-collocating electromagnetic vector-sensor,

4) more generalized array configurations of the non-collocating electromagnetic vector-sensor:

The previous results require a very specific array geometry, namely, two parallel lines, one with only dipoles, the other one with only loops and in specific permutation. The future work will further explore more generalized array configurations.

Assume that the three dipoles and three loops are arbitrarily located in the space with: e_x at $(0,0,0)$, e_y at (x_{ey}, y_{ey}, z_{ey}), e_z at (x_{ez}, y_{ez}, z_{ez}), h_x at (x_{hx}, y_{hx}, z_{hx}), h_y at (x_{hy}, y_{hy}, z_{hy}) and h_z at (x_{hz}, y_{hz}, z_{hz}), the "vector-cross-product" will then be

$$\mathbf{e}\times\mathbf{h}^* = \begin{bmatrix} 0 & -e_z & e_y \\ e_z & 0 & -e_x \\ -e_y & e_x & 0 \end{bmatrix} \begin{bmatrix} h_x^* \\ h_y^* \\ h_z^* \end{bmatrix} = \begin{bmatrix} -e_z h_y^* + e_y h_z^* \\ e_z h_x^* - e_x h_z^* \\ -e_y h_x^* + e_x h_y^* \end{bmatrix}$$

$$= \begin{bmatrix} (\sin\theta\cos\phi\sin^2\gamma - \sin\theta\cos\theta\sin\phi\sin\gamma\cos\gamma e^{j\eta}) \\ \times e^{j\frac{2\pi}{\lambda}[(x_{hy}-x_{ez})u+(y_{hy}-y_{ez})v+(z_{hy}-z_{ez})w]} \\ +(\sin\theta\cos\phi\cos^2\gamma + \sin\theta\cos\theta\sin\phi\sin\gamma\cos\gamma e^{j\eta}) \\ \times e^{j\frac{2\pi}{\lambda}[(x_{hz}-x_{ey})u+(y_{hz}-y_{ey})v+(z_{hz}-z_{ey})w]} \\ (\sin\theta\sin\phi\sin^2\gamma + \sin\theta\cos\theta\cos\phi\sin\gamma\cos\gamma e^{j\eta}) \\ \times e^{j\frac{2\pi}{\lambda}[(x_{hx}-x_{ez})u+(y_{hx}-y_{ez})v+(z_{hx}-z_{ez})w]} \\ -(\sin\theta\cos\theta\sin\phi\sin\gamma\cos\gamma e^{j\eta} - \sin\theta\sin\phi\cos^2\gamma) \\ \times e^{j\frac{2\pi}{\lambda}[x_{hz}u+y_{hz}v+z_{hz}w]} \\ [\cos\theta(\sin^2\phi\sin^2\gamma + \cos^2\phi\cos^2\gamma)] \\ \times e^{j\frac{2\pi}{\lambda}[(x_{hx}-x_{ey})u+(y_{hx}-y_{ey})v+(z_{hx}-z_{ey})w]} \\ +[\cos\theta(\cos^2\phi\sin^2\gamma + \sin^2\phi\cos^2\gamma)]e^{j\frac{2\pi}{\lambda}[x_{hy}u+y_{hy}v+z_{hy}w]} \\ +[\sin\phi\cos\phi\sin\gamma\cos\gamma(e^{-j\eta} + \cos^2\theta e^{j\eta})] \\ \times e^{j\frac{2\pi}{\lambda}[(x_{hx}-x_{ey})u+(y_{hx}-y_{ey})v+(z_{hx}-z_{ey})w]} \\ -[\sin\phi\cos\phi\sin\gamma\cos\gamma(e^{-j\eta} + \cos^2\theta e^{j\eta})]e^{j\frac{2\pi}{\lambda}[x_{hy}u+y_{hy}v+z_{hy}w]} \end{bmatrix}. \quad (2.20)$$

This notation will facilitate the subsequent exposition: Define $(\theta_y, \phi_y, \Delta_y)$ as the elevation-angle, azimuth-angle, and distance of the location of E_y **relative to** the location of E_x. Similarly, define $(\theta_z, \phi_z, \Delta_z)$ as the elevation-angle, azimuth-angle, and distance of the location of E_z **relative to** the location of E_y.

The basic insight is as follows: Suppose the three dipoles and the three loops are displaced to satisfy:

$$\overrightarrow{E_x E_y} = -\overrightarrow{H_x H_y} \quad (2.21)$$

$$\overrightarrow{E_y E_z} = -\overrightarrow{H_y H_z}, \quad (2.22)$$

where $\overrightarrow{AB}$ represents the vector specifying the location of antenna B relative to the location of antenna A. Then the "vector-cross-product" result in (2.20) would be simplified to

$$\mathbf{q} = e^{j\beta_h} \begin{bmatrix} u\ e^{-j2\alpha_y} e^{-j\alpha_z} \\ v\ e^{-j\alpha_y} e^{-j\alpha_z} \\ w\ e^{-j\alpha_y} \end{bmatrix}, \tag{2.23}$$

where

$$\begin{aligned} \beta_h &= \frac{2\pi}{\lambda}(x_h u + y_h v + z_h w), \\ \alpha_y &= \frac{2\pi}{\lambda}\Delta_y(\tilde{u}_y u + \tilde{v}_y v + \tilde{w}_y w), \\ \alpha_z &= \frac{2\pi}{\lambda}\Delta_z(\tilde{u}_z u + \tilde{v}_z v + \tilde{w}_z w), \\ \tilde{u}_y &= \sin\theta_y \cos\phi_y, \\ \tilde{v}_y &= \sin\theta_y \sin\phi_y, \\ \tilde{w}_y &= \cos\theta_y, \\ \tilde{u}_z &= \sin\theta_z \cos\phi_z, \\ \tilde{v}_z &= \sin\theta_z \sin\phi_z, \\ \tilde{w}_z &= \cos\theta_z. \end{aligned}$$

Some specific array configurations are depicted in Figure 2.8:

(a) All six component-antennas lie on the same plane, but not necessarily parallel to any Cartesian axis.

(b) A special case (a), with the plane equal to the x-y Cartesian plane at $z = 0$. Then, $\theta_y = \theta_z = \pi/2$. This is portrayed in Figure 2.8b.

(c) A special case (a), the six component-antennas lie on a circle, e.g., if the circle is on the xoy plane, with $\Delta_y = \Delta_z$, $\phi_y = 0$, and $\phi_z = -2\pi/3$; or with $\Delta_y = \Delta_z$, $\phi_y = \pi/2$, and $\phi_z = \pi/3$. See Figure 2.8c. [11]

For each candidate array configuration, a corresponding estimation algorithm for the direction-of-arrival and polarization will be investigated. In addition, the corresponding estimation accuracy and the estimation region of each parameter will be analyzed.

2.9 Appendix: Derivation of the Cramér-Rao Bound

To avoid unnecessary distraction, simple assumptions will be made of the signal statistical model in Section 2.5.1: One single pure-tone's frequency and known initial phase are presumed as known constants. The data sampling instants occur at $t = nT_s$, where T_s refers

[11] The right circular configuration in Figure 2.8c was named "DEMCA" in [102].

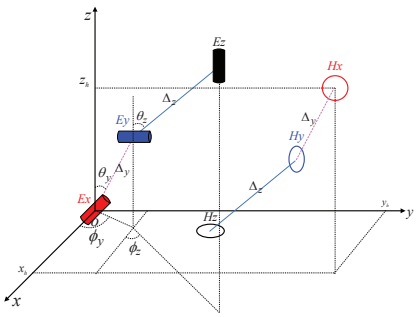

Figure 2.8a: One permutation to place the six orthogonally dipoles / triads, which may lie arbitrarily in the three dimensional space.

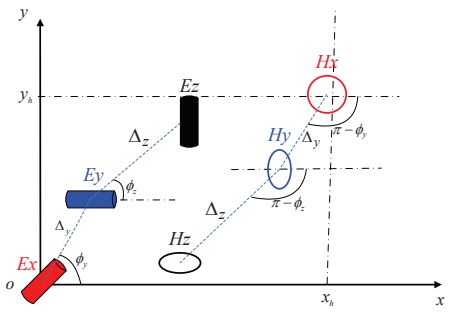

Figure 2.8b: One composition on the xoy plane.

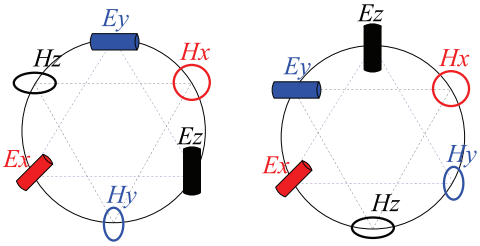

Figure 2.8c: Two circular configurations.

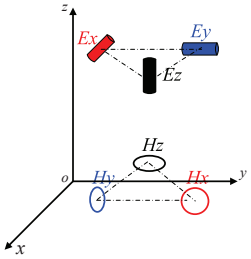

Figure 2.8d: Dual-triad configuration.

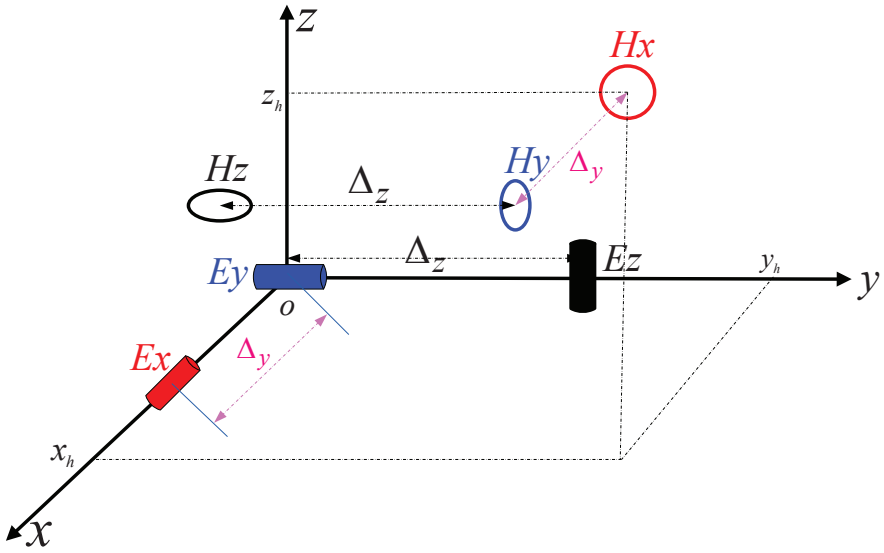

Figure 2.8e: A special array configuration in which the dipoles/loops are oriented along the x/y-axis.

to the time-sampling period, and $\mathbf{n}(t)$ denotes a 6×1 vector of additive zero-mean spatio-temporally uncorrelated complex Gaussian noise, with an unknown covariance-matrix of $\mathbf{\Gamma}_0$, which is deterministic, 6×6, diagonal with all diagonal elements equal to σ^2, which represents the known noise-variance at each component-antenna.

With N number of time-samples, the data-set is $6N \times 1$ and equals

$$\boldsymbol{\zeta} \;=\; \left[(\mathbf{z}(T_s))^T, \cdots, (\mathbf{z}(NT_s))^T\right]^T \;=\; \underbrace{\sum_{k=1}^{K} (\mathbf{s}_k \otimes \tilde{\mathbf{a}}_k)}_{=\boldsymbol{\mu}} + \underbrace{\left[(\mathbf{n}(T_s))^T, \cdots, (\mathbf{n}(NT_s))^T\right]^T}_{=\boldsymbol{\nu}},$$

where $\mathbf{s}_k = e^{j\epsilon}\left[e^{j2\pi f_k T_s}, e^{j4\pi f_k T_s}, \cdots, e^{j2N\pi f_k T_s}\right]^T$, $\boldsymbol{\nu}$ represents a $6N \times 1$ noise vector with a spatio-temporal covariance matrix of $\boldsymbol{\Gamma} = \mathbf{I}_N \otimes \boldsymbol{\Gamma}_0$, and $\mathbf{I}_N$ denotes an $N \times N$ identity matrix. Therefore, $\boldsymbol{\zeta} \sim \mathcal{N}(\boldsymbol{\mu}, \boldsymbol{\Gamma})$, i.e., a Gaussian vector with mean $\boldsymbol{\mu}$ and covariance $\boldsymbol{\Gamma}$.

Collect all deterministic unknown entities into a $4K \times 1$ vector,
$\boldsymbol{\psi} = [\theta_1, \phi_1, \gamma_1, \eta_1, \cdots, \theta_K, \phi_K, \gamma_K, \eta_K]^T$. The resulting $4K \times 4K$ Fisher Information Matrix (FIM), $\mathbf{J}$, would have its (i,j)th entry equal to (equation (8.34) in [62])

$$[\mathbf{J}]_{i,j} \;=\; 2\mathrm{Re}\left[\left(\frac{\partial \boldsymbol{\mu}}{\partial [\boldsymbol{\psi}]_i}\right)^H \boldsymbol{\Gamma}^{-1} \left(\frac{\partial \boldsymbol{\mu}}{\partial [\boldsymbol{\psi}]_j}\right)\right] + \mathrm{Tr}\left[\boldsymbol{\Gamma}^{-1}\frac{\partial \boldsymbol{\Gamma}}{\partial [\boldsymbol{\psi}]_i}\boldsymbol{\Gamma}^{-1}\frac{\partial \boldsymbol{\Gamma}}{\partial [\boldsymbol{\psi}]_j}\right],$$

where Re[.] denotes the real-value part of the entity inside [.], and Tr[.] represents the trace operator.

Any unbiased estimation of the directions-of-arrival would have these Cramér-Rao lower bounds:

$$\begin{aligned} \mathrm{CRB}(\theta_k) &= \left[\mathbf{J}^{-1}\right]_{4k-3,4k-3}, \\ \mathrm{CRB}(\phi_k) &= \left[\mathbf{J}^{-1}\right]_{4k-2,4k-2}. \end{aligned}$$

These equations may be easily evaluated by MATLAB's symbolic toolbox, to obtain the Cramér-Rao bound curves in Figures 2.4-2.6.

For a general K-source scenario, the Fisher Information Matrix would be $4K \times 4K$ in size, to be specified by $8K^2 + 2K$ number of distinct scalar equations (after accounting for symmetry in the matrix). As illustration the following equations present the 10 equations for the Fisher Information Matrix's 16 elements in the single-source case, for the specific case of $\Delta_{x,y} = \Delta_{y,z} = k\lambda$. The equations would become excessively lengthy to state here for the general array manifold of (2.2). Define the elements of the single-source Fisher Information Matrix as follows:

$$\mathbf{J} \;=\; \begin{bmatrix} J_{\theta,\theta} & J_{\theta,\phi} & J_{\theta,\gamma} & J_{\theta,\eta} \\ J_{\phi,\theta} & J_{\phi,\phi} & J_{\phi,\gamma} & J_{\phi,\eta} \\ J_{\gamma,\theta} & J_{\gamma,\phi} & J_{\gamma,\gamma} & J_{\gamma,\eta} \\ J_{\eta,\theta} & J_{\eta,\phi} & J_{\eta,\gamma} & J_{\eta,\eta} \end{bmatrix}$$

Using symbolic programming by MATLAB and Mathematica,

$$
\begin{aligned}
J_{\theta,\theta} \;=\; & \frac{2N}{\sigma^2\lambda^2}\{\lambda^2+4\pi^2z_h^2-8k\lambda\pi^2z_h(\cos\phi)c_1+16k^2\lambda^2\pi^2(\cos\tilde{\theta})^2+4k^2\lambda^2\pi^2c_1^2 \\
& +8k\lambda\pi^2(\cos\gamma)^2[(\cos\tilde{\theta})(-2z_h+z_h(\cos\phi)^2+x_h(\cos\phi)\sin(2\gamma)+y_h(\sin\phi)\sin(2\gamma)) \\
& +z_h\cos(\phi-\tilde{\phi})\sin(2\gamma)(\sin\tilde{\theta})]+4k\lambda\pi^2(\cos\theta)^4[-3k\lambda\sin(2\phi)c_3c_2 \\
& +(\cos\gamma)^2(-2z_h(\cos\tilde{\theta})+(y_h(\cos\tilde{\phi})\sin(2\phi)+(2y_h+x_h\sin(2\phi))(\sin\tilde{\phi}))(\sin\tilde{\theta})) \\
& +3k\lambda(-1+2(\cos\tilde{\theta})^2+c_2^2)+(\cos\phi)^3(\sin\phi)(k\lambda(\cos\tilde{\theta})^2\sin(2\tilde{\phi})+2x_h(\cos\gamma)^2c_3 \\
& +(\cos\tilde{\phi})(-2k\lambda(\sin\tilde{\phi})+2y_h(\cos\gamma)^2(\sin\tilde{\theta}))) \\
& +(\cos\phi)^4(-k\lambda(\cos\tilde{\theta})^2+2(\cos\gamma)^2(x_h(\cos\tilde{\phi})-y_h(\sin\tilde{\phi}))(\sin\tilde{\theta}) \\
& +k\lambda(1-2c_2^2))-(\cos\phi)^2(2(\cos\gamma)^2(z_h(\cos\tilde{\theta})-x_hc_2)+k\lambda(-2+(\cos\tilde{\theta})^2 \\
& +5c_2^2))]-4\pi^2\cos\theta[-2c_{10}k\lambda z_h(\cos\tilde{\theta})\sin(2\phi)+2(\sin\theta)(x_hz_h(\cos\phi)+y_hz_h(\sin\phi) \\
& +k\lambda(\cos\phi)^3(-z_hc_2(\sin\gamma)^2+(\cos\tilde{\theta})(-x_h(\sin\gamma)^2+k\lambda c_2)) \\
& +k\lambda(\cos\phi)^2\sin\phi(-z_h(\sin\gamma)^2c_3+(\cos\tilde{\theta})(-y_h(\sin\gamma)^2+k\lambda c_3)))] \\
& -4\pi^2\cos\theta^2[-4k^2\lambda^2-y_h^2+z_h^2+11k^2\lambda^2(\cos\tilde{\theta})^2 \\
& -2k^2\lambda^2\sin(2\phi)\sin(2\tilde{\phi})+2k^2\lambda^2(\cos\tilde{\theta})^2\sin(2\phi)\sin(2\tilde{\phi}) \\
& +4k^2\lambda^2c_2^2+2k\lambda\cos\gamma^2(-3z_h(\cos\tilde{\theta})+(y_h(\cos\tilde{\phi})\sin(2\phi) \\
& +(2y_h+x_h\sin(2\phi))(\sin\tilde{\phi}))(\sin\tilde{\theta}))+(\cos\phi)^2(3k^2\lambda^2-x_h^2+y_h^2 \\
& -k^2\lambda^2(\cos\tilde{\theta})^2-2k\lambda(\cos\tilde{\theta})(z_h-2x_hc_{10}c_4)+4k\lambda z_hc_{10}c_2c_4 \\
& +2k\lambda y_hc_3+2k\lambda\cos\gamma^2(2x_h(\cos\tilde{\phi})-3y_h(\sin\tilde{\phi}))(\sin\tilde{\theta})-7k^2\lambda^2c_2^2) \\
& +k\lambda(\cos\phi)^4(\sin\tilde{\theta})(2x_h(\cos\tilde{\phi})(\sin\gamma)^2-k\lambda(\cos\tilde{\phi})c_2 \\
& +(\sin\tilde{\phi})(-2y_h(\sin\gamma)^2+k\lambda c_3))+(\cos\phi)(-2x_hy_h(\sin\phi)+4k\lambda c_{10}(\sin\theta)(y_h(\cos\tilde{\theta}) \\
& +z_hc_3))-2k\lambda(\cos\phi)^3(2c_{10}\sin\theta(y_h(\cos\tilde{\theta})+z_hc_3)+(\sin\phi)(\sin\tilde{\theta})(-x_h(\sin\gamma)^2(\sin\tilde{\phi}) \\
& +(\cos\tilde{\phi})(-y_h(\sin\gamma)^2+k\lambda c_3)))]-8k^2\lambda^2\pi^2(\cos\phi)(\cos\tilde{\phi})\sin(2\gamma)[\sin(2\tilde{\theta})] \\
& -8k^2\lambda^2\pi^2(\sin\phi)\sin(2\gamma)(\sin\tilde{\phi})[\sin(2\tilde{\theta})]+4k\lambda\pi^2(\cos\theta)^3[c_{10}\sin(2\phi)(-2z_h(\cos\tilde{\theta}) \\
& +2\cos(\phi-\tilde{\phi})(x_h(\cos\phi)+y_h(\sin\phi))(\sin\tilde{\theta})) \\
& -(\sin\theta)((\cos\gamma)^2(3+\cos(2\phi))(\cos\phi(x_h(\cos\tilde{\theta})+z_hc_2) \\
& +(\sin\phi)(y_h(\cos\tilde{\theta})+z_hc_3))-0.5k\lambda(7+\cos(2\phi))\cos(\phi-\tilde{\phi})(\sin(2\tilde{\theta})))]\}
\end{aligned}
$$

$$
\begin{aligned}
J_{\theta,\phi} \;=\; & J_{\phi,\theta} = \frac{N}{2\sigma^2\lambda^2}\pi\{16k\lambda\pi(\cos\phi)^4\sin(2\theta)(\sin\tilde{\theta})[(-x_h + x_h(\cos\gamma)^2(1+(\cos\theta)^2) \\
& -2c_{10}y_h(\cos\theta))(\sin\tilde{\phi}) + (\cos\tilde{\phi})(-y_h + y_h(\cos\gamma)^2(1+(\cos\theta)^2) \\
& +2c_{10}x_h(\cos\theta) + k\lambda(\sin\theta)^2c_3)] + 8k\lambda\pi(\cos\phi)^3[2k\lambda(\cos\theta)\cos(2\tilde{\phi})(\cos\tilde{\theta})^2(\sin\phi)(\sin\theta)^3 \\
& +k\lambda(\sin\phi)\sin(2\theta) + 2x_h(\sin\phi)\sin(2\theta)c_2 + 2z_hc_3 - 2z_h(\cos\gamma)^2c_3 \\
& +(\cos\theta)^4(z_h + z_h\cos(2\gamma) - 2k\lambda(\cos\tilde{\theta}))c_3 + 2y_h(\cos\gamma)^2(\sin\phi)\sin(2\theta)c_3 \\
& +2(\cos\theta)^2(-z_h(\sin\tilde{\phi}) + 4c_{10}c_4(y_h(\cos\tilde{\phi}) + x_h(\sin\tilde{\phi})))(\sin\tilde{\theta}) \\
& -4(\cos\theta)(k\lambda(\cos\tilde{\phi})^2(\sin\phi)(\sin\theta) + (\cos\gamma)(\cos\tilde{\phi})(z_h(\cos\eta)(\sin\gamma) \\
& +x_h(\cos\gamma)c_4)(\sin\tilde{\theta}) + y_hc_4c_3) + 2(\cos\tilde{\theta})(y_h + y_h(\cos\gamma)^2(-1+(\cos\theta)^4) \\
& -2c_{10}x_h(\cos\theta) + 2c_{10}x_h(\cos\theta)^3 - (\cos\theta)^2(y_h - 2k\lambda c_3)) + 2(\cos\theta)^3(2z_h2c_{10}c_2 \\
& +c_4(-k\lambda + 2k\lambda(\cos\tilde{\phi})^2 - 2x_h(\cos\gamma)^2c_2 + 2y_h(\cos\gamma)^2c_2)) - k\lambda c_6] \\
& +8(\cos\phi)[-2k\lambda\pi(\cos\theta)^3(2x_h(\cos\gamma)^2c_2c_4 + 2c_{10}(x_h(\cos\tilde{\theta}) + z_hc_2)) \\
& +2k\lambda\pi(\cos\theta)^4(-3k\lambda(\cos\tilde{\theta})c_3 + (\cos\gamma)^2(y_h(\cos\tilde{\theta}) + z_hc_3)) - 2\pi(y_hz_h \\
& +4k^2\lambda^2(\cos\tilde{\theta})c_3 - 2k\lambda(\cos\gamma)^2(y_h(\cos\tilde{\theta}) + z_hc_3)) + 2k\lambda\pi(\cos\theta)(2c_{10}(x_h(\cos\tilde{\theta}) + z_hc_3) \\
& -4c_4(k\lambda(\cos\tilde{\theta})^2 + y_h(\cos\gamma)^2c_3)) + (\cos\theta)^2(2\pi y_hz_h - \lambda x_hc_{11} - 6k\lambda\pi(\cos\gamma)^2(y_h(\cos\tilde{\theta}) \\
& +z_hc_3) + 7k^2\lambda^2\pi c_6)] - 4[2k\lambda\pi(\cos\theta)^2(\sin\theta)(\sin\tilde{\theta})(2c_{10}\sin(2\phi)(y_h(\cos\tilde{\phi}) + x_h(\sin\tilde{\phi})) \\
& +2(\cos\gamma)^2(\cos\theta)(y_h(\cos\tilde{\phi}) + (x_h - y_h\sin(2\phi))(\sin\tilde{\phi})) - 3k\lambda(\cos\theta)(\cos(2\tilde{\phi})\sin(2\phi) \\
& +\sin(2\tilde{\phi}))(\sin\tilde{\theta})) + \sin(2\theta)(-\lambda z_hc_{11} + \pi(2x_hy_h - 4k\lambda(\cos\gamma)^2(y_h(\cos\tilde{\phi}) \\
& +x_h(\sin\tilde{\phi}))(\sin\tilde{\theta}) + 4k^2\lambda^2\sin(2\tilde{\phi})(\sin\tilde{\theta})^2 + \sin(2\phi)(-4k^2\lambda^2 + x_h^2 - y_h^2 - 4k\lambda x_h(\cos\gamma)^2c_2 \\
& +8k^2\lambda^2c_2^2))) + 2(\sin\phi)(k\lambda\pi(\cos\theta)^4(2(\cos\gamma)^2(x_h(\cos\tilde{\theta}) + z_hc_2) - 3k\lambda c_5) \\
& -2\pi(x_hz_h - 2k\lambda(\cos\gamma)^2(x_h(\cos\tilde{\theta}) + z_hc_2) + 2k^2\lambda^2c_5) \\
& +(\cos\theta)^2(2\pi x_hz_h + \lambda y_hc_{11} - 6k\lambda\pi(\cos\gamma)^2(x_h(\cos\tilde{\theta}) + z_hc_2) + 7k^2\lambda^2\pi c_5))] \\
& +\pi(\cos\phi)^2[-16k\lambda z_h(\cos\gamma)^2(\cos\theta)^4(\sin\phi)c_2 + 32(\cos\theta)(x_hy_h(\sin\theta) \\
& -k\lambda y_h(\cos\tilde{\theta})c_{10}c_4(\sin\theta) - k\lambda z_hc_{10}(\sin\phi)c_3) + 16k\lambda(\cos\theta)^2(x_h(\cos\gamma)^2(\cos\tilde{\theta})c_4(\sin\theta) \\
& +z_h(\sin\phi)c_2 - 4c_{10}(\sin\theta)(x_h(\cos\tilde{\phi}) - y_h(\sin\tilde{\phi}))(\sin\tilde{\theta})) - 8k\lambda(\cos\theta)^3(-4z_h4c_{10}(\sin\phi)c_3 \\
& +(\sin\theta)(5k\lambda\sin(2\tilde{\phi}) - 2(\cos\gamma)^2(y_h(\cos\tilde{\phi}) + x_h(\sin\tilde{\phi}))(\sin\tilde{\theta}))) \\
& -k\lambda(16x_h(\cos\tilde{\theta})(\sin\gamma)^2c_4(\sin\theta) + k\lambda(\cos\tilde{\theta})^2(18\sin(2\theta) - 5\sin(4\theta))\sin(2\tilde{\phi}) \\
& +4(\sin(2\theta)(-7k\lambda\sin(2\tilde{\phi}) + (3+5\cos(2\gamma))(y_h(\cos\tilde{\phi}) + x_h(\sin\tilde{\phi}))(\sin\tilde{\theta})) \\
& +2(\cos\tilde{\phi})(\sin\phi)(2z_h(\sin\gamma)^2(\sin\tilde{\theta}) - k\lambda(\sin\theta)^4\sin(2\tilde{\theta})))]\}
\end{aligned}
$$

$$
\begin{aligned}
J_{\theta,\gamma} &= J_{\gamma,\theta} = \frac{N}{2\sigma^2} k\pi[(-6+6\cos(2\phi)+\cos(2(\phi-\theta))+6\cos(2\theta)+\cos(2(\phi+\theta)))\sin(2\gamma) \\
&\quad -8(\cos\theta)(\sin\eta)\sin(2\phi)][-(\cos\tilde{\theta})(\sin\theta)+(\cos\theta)\cos(\phi-\tilde{\phi})(\sin\tilde{\theta})], \\
J_{\theta,\eta} &= J_{\eta,\theta} = \frac{2N}{\sigma^2\lambda} 2\pi(\sin\gamma)\{k\lambda(\cos\phi)^3(\cos\theta)[(1+(\cos\theta)^2)(\cos\tilde{\phi})(\sin\gamma)+2c_7(\sin\tilde{\phi})](\sin\tilde{\theta}) \\
&\quad +k\lambda(\cos\phi)^2[-(1/4)(\cos\tilde{\theta})(\sin\gamma)(5(\sin\theta)+\sin(3\theta))+(\cos\theta)(\sin\phi)(-2c_7(\cos\tilde{\phi}) \\
&\quad +(1+(\cos\theta)^2)(\sin\gamma)c_3]+(\sin\gamma)[-k\lambda(\cos\theta)^2(\cos\tilde{\theta})(\sin\theta)+(z_h+2k\lambda(\cos\tilde{\theta}))(\sin\theta) \\
&\quad +k\lambda(\cos\theta)^3(\sin\phi)(\sin\tilde{\phi})(\sin\tilde{\theta})-(\cos\theta)(\sin\phi)(y_h+2k\lambda c_3)]+(\cos\phi)(\cos\theta)[-(\sin\gamma)(x_h \\
&\quad -0.5k\lambda(-3+\cos(2\theta))c_2)+2k\lambda(\cos\eta)(\cos\gamma)((\cos\tilde{\theta})c_4-(\cos\theta)c_3)]\}, \\
J_{\phi,\phi} &= \frac{2N}{\sigma^2\lambda^2}\{\lambda^2+4\pi^2x_h^2+16k^2\lambda^2\pi^2(\cos\tilde{\phi})^2-16k^2\lambda^2\pi^2(\cos\tilde{\phi})^2(\cos\tilde{\theta})^2-8k^2\lambda^2\pi^2\sin(2\phi)\sin(2\tilde{\phi}) \\
&\quad +8k^2\lambda^2\pi^2(\cos\tilde{\theta})^2\sin(2\phi)\sin(2\tilde{\phi})-16k\lambda\pi^2x_h(\cos\gamma)^2(\cos\tilde{\phi})(\sin\tilde{\theta}) \\
&\quad +8k\lambda\pi^2y_h(\cos\gamma)^2(\cos\tilde{\phi})c_8-8k\lambda\pi^2x_h(\cos\theta)^3(\cos\tilde{\phi})c_{10}c_8 \\
&\quad +8k\lambda\pi^2x_h(\cos\gamma)^2(\sin\tilde{\phi})c_8+4\lambda\pi x_h(\cos\theta)\sin(2\gamma)[(\sin\eta)(\sin\phi)(\sin\theta) \\
&\quad +k\pi(\cos\eta)(\cos\tilde{\phi})\sin(2\phi)(\sin\tilde{\theta})]-2k\lambda\pi^2(\cos\theta)^4(\sin\tilde{\theta})(4x_h(\cos\gamma)^2(\cos\tilde{\phi}) \\
&\quad +3k\lambda(-2(\cos\tilde{\phi})^2+\sin(2\phi)\sin(2\tilde{\phi}))(\sin\tilde{\theta}))+(\cos\theta)^2(\lambda^2-4\pi^2x_h^2 \\
&\quad +24k\lambda\pi^2x_h(\cos\gamma)^2c_2-28k^2\lambda^2\pi^2c_2^2)+k\lambda\pi^2(\cos\phi)^3(\sin\phi)(\sin\tilde{\theta})[8x_h(\cos\gamma)^2(\cos\theta)^4(\sin\tilde{\phi}) \\
&\quad +8x_h(\sin\gamma)^2(\sin\tilde{\phi})-16c_{10}y_h(\cos\theta)^3(\sin\tilde{\phi})+16c_{10}(\cos\theta)(-x_hc_9 \\
&\quad +y_h(\sin\tilde{\phi}))-(\cos\tilde{\phi})(-8y_h(\sin\gamma)^2(\sin\theta)^2+k\lambda(11+4\cos(2\theta)+\cos(4\theta))c_3) \\
&\quad -8(\cos\theta)^2(y_h(\cos\gamma)^2c_9+(\sin\tilde{\phi})(x_h-2k\lambda c_2))] \\
&\quad -4k\lambda\pi^2(\cos\phi)^4(\sin\theta)^2[-k\lambda+k\lambda(\cos\tilde{\theta})^2-2x_h(\sin\gamma)^2c_2+2y_hc_3-2y_h(\cos\gamma)^2c_3 \\
&\quad -4c_{10}(\cos\theta)(y_h(\cos\tilde{\phi})+x_h(\sin\tilde{\phi}))(\sin\tilde{\theta})+2k\lambda c_2^2+(\cos\theta)^2(-k\lambda(\cos\tilde{\theta})^2 \\
&\quad +2(\cos\gamma)^2(x_hc_2-y_hc_3)+k\lambda(1-2c_2^2))] \\
&\quad -4\pi^2(\cos\phi)^2(\sin\theta)^2[-4k^2\lambda^2+x_h^2-y_h^2+4k^2\lambda^2(\cos\tilde{\theta})^2-k\lambda x_h(1+3\cos(2\gamma))c_2 \\
&\quad +4k\lambda y_h(\cos\gamma)^2c_3+4c_{10}k\lambda(\cos\theta)(y_hc_2+x_hc_3)+7k^2\lambda^2c_2^2 \\
&\quad -k\lambda(\cos\theta)^2(3k\lambda(\cos\tilde{\theta})^2+2y_h(\cos\gamma)^2c_3+k\lambda(-3+5c_2^2))] \\
&\quad +8\pi(\cos\phi)[-0.5c_{11}\lambda y_h(\cos\theta)(\sin\theta)+\pi(\sin\phi)(-x_hy_h+k\lambda(\cos\gamma)^2(\cos\theta)^4(y_h(\cos\tilde{\phi}) \\
&\quad +x_h(\sin\tilde{\phi}))(\sin\tilde{\theta})+(\cos\theta)^2(x_hy_h-3k\lambda(\cos\gamma)^2(y_h(\cos\tilde{\phi}) \\
&\quad +x_h(\sin\tilde{\phi}))(\sin\tilde{\theta})+7k^2\lambda^2(\cos\tilde{\phi})(\sin\tilde{\theta})c_3))]\}, \\
J_{\phi,\gamma} &= J_{\gamma,\phi} = \frac{-4N}{\sigma^2}(\cos\theta)\{\cos\eta-k\pi(\sin\eta)[\sin(2\phi)](\sin\theta)[\sin(\phi-\tilde{\phi})](\sin\tilde{\theta})\}, \\
J_{\phi,\eta} &= J_{\eta,\phi} = \frac{2N}{\sigma^2\lambda}\pi(\sin\gamma)(\sin\theta)\{-2k\lambda(\cos\phi)^2(\sin\phi)[(1+(\cos\theta)^2)(\cos\tilde{\phi})(\sin\gamma) \\
&\quad +2c_7(\sin\tilde{\phi})](\sin\tilde{\theta})+2k\lambda(\cos\phi)^3[-2c_7(\cos\tilde{\phi})+(1+(\cos\theta)^2)(\sin\gamma)(\sin\tilde{\phi})](\sin\tilde{\theta}) \\
&\quad +(\sin\gamma)(\sin\phi)[2x_h-k\lambda(-3+\cos(2\theta))c_2]+(\cos\phi)[4k\lambda c_7c_2+(\sin\gamma)(-2y_h \\
&\quad +k\lambda(-3+\cos(2\theta))c_3)]\},
\end{aligned}
$$

$$
\begin{aligned}
J_{\gamma,\gamma} &= \frac{4N}{\sigma^2}, \\
J_{\gamma,\eta} &= J_{\eta,\gamma} = 0, \\
J_{\eta,\eta} &= \frac{4N(\sin\gamma)^2}{\sigma^2},
\end{aligned}
$$

where $c_1 = (\cos\phi)(\cos\tilde{\theta})$, $c_2 = (\cos\tilde{\phi})(\sin\tilde{\theta})$, $c_3 = (\sin\tilde{\phi})(\sin\tilde{\theta})$, $c_4 = (\sin\phi)(\sin\theta)$, $c_5 = (\cos\tilde{\phi})\sin(2\tilde{\theta})$, $c_6 = (\sin\tilde{\phi})\sin(2\tilde{\theta})$, $c_7 = (\cos\eta)(\cos\gamma)(\cos\theta)$, $c_8 = \sin(2\phi)(\sin\tilde{\theta})$, $c_9 = (\cos\tilde{\phi})(\sin\theta)^2$, $c_{10} = (\cos\eta)(\cos\gamma)(\sin\gamma)$, $c_{11} = (\sin\eta)\sin(2\gamma)$.

The Cramér-Rao bounds would be excessively lengthy to state here for the spatially spread electromagnetic vector-sensor, even for the single-source case. These expressions are very long, because the Fisher Information matrix needs be inverted to produce the Cramér-Rao bounds. However, for $\ell = 0$ (i.e. the six component-antennas are spatially collocated), the Cramér-Rao bounds equal:

$$
\begin{aligned}
\mathrm{CRB}_c(\theta) &= \frac{\sigma^2}{2N}, \\
\mathrm{CRB}_c(\phi) &= \frac{\sigma^2}{2N} \frac{1}{\{1 + (\cos\theta)^2[1 - 2(\cos\eta)^2 - 2(\cos\gamma)^2(\sin\eta)^2]\}}, \\
\mathrm{CRB}_c(\gamma) &= \frac{\sigma^2}{4N} \frac{\left[1 + (\cos\theta)^2 - 2(\cos\theta)^2(\cos\gamma)^2(\sin\eta)^2\right]}{\{1 + (\cos\theta)^2[1 - 2(\cos\eta)^2 - 2(\cos\gamma)^2(\sin\eta)^2]\}}, \\
\mathrm{CRB}_c(\eta) &= \frac{\sigma^2}{4N} \frac{1}{(\sin\gamma)^2} \frac{[1 + (\cos\theta)^2 - 2(\cos\theta)^2(\cos\eta)^2]}{\{1 + (\cos\theta)^2[1 - 2(\cos\eta)^2 - 2(\cos\gamma)^2(\sin\eta)^2]\}}.
\end{aligned}
$$

Chapter 3

Various Triads of Collocated Dipoles/Loops, for Direction Finding & Polarization Estimation

For simultaneous estimation of the azimuth/elevation arrival angles (ϕ, θ) and polarization parameters (γ, η), a minimum of three diversely polarized antennas are needed, because at least three *complex*-value equations (based on three antennas' measurements) are needed to solved for the four unknown *real*-value source-parameters (i.e. $\theta, \phi, \gamma, \eta$) and for the one unknown complex-value multiplicative coefficient α, which arises from the eigen-based estimation of the source's steering vector. Because at least three antennas are needed, this chapter will focus on diversely polarized antennas in a *triad*.

For antennas spatially *collocated* in a point-like geometry, no *spatial* phase-factor will exist among them. These collocated antennas' resulting array manifold will thus enjoy the following advantages: (i) The array manifold is independent from the spectrum of the incident signal. This includes independence from the signal's center-frequency and bandwidth.[1] (ii) The array manifold is less sensitive to the source's distance from the antenna-array. (iii) In a K-source scenario, the K azimuth-angle estimates, the K elevation-angle estimates, and the K polarizations can all be intrinsically associated to the proper sources, even without any further post-estimation processing. [32] (iv) The antenna-triad is physically more compact.

This chapter will investigate a collocated triad of dipole(s) and/or loop(s). An electrically short dipole measures one Cartesian component of the electric-field vector, along the Cartesian axis on which the dipole is aligned. Similarly, a magnetically small loop

[1] Real antenna patterns depend on frequency. The array manifold would not depend on frequency if all antennas have the same frequency-dependence.

measures one Cartesian component of the magnetic-field vector, along which the loop-axis is aligned. Hence, with a collocated triad of three such diversely polarized antennas, three components of the six-element electromagnetic-field vector can be measured, at one point in space. To select three out of the six electromagnetic components, there exist 20 different configurations. Among these 20 possible configurations, only 2 out of 20 possible compositions have closed-form formulas available in the open literature for the estimation of the arrival. This chapter aims to fill this literature gap. Closed-form estimation formulas for θ, ϕ, γ, and η (and their associated support regions) are herein advanced for 14 of the 18 overlooked configurations. For the remaining 4 configurations, they will be shown to be inadequate for such closed-form estimation. [2]

3.1 A Triad's Directional & Polarizational Responses

A unit-power, completely polarized, transverse electromagnetic wave may be characterized by its six-component electromagnetic-field vector, expressible in the Cartesian coordinates as [20]

$$\begin{bmatrix} \mathbf{e} \\ \mathbf{h} \end{bmatrix} \overset{\text{def}}{=} \begin{bmatrix} e_x \\ e_y \\ e_z \\ h_x \\ h_y \\ h_z \end{bmatrix} \overset{\text{def}}{=} \underbrace{\begin{bmatrix} \cos\phi\cos\theta & -\sin\phi \\ \sin\phi\cos\theta & \cos\phi \\ -\sin\theta & 0 \\ -\sin\phi & -\cos\phi\cos\theta \\ \cos\phi & -\sin\phi\cos\theta \\ 0 & \sin\theta \end{bmatrix}}_{\overset{\text{def}}{=}\boldsymbol{\Theta}} \underbrace{\begin{bmatrix} \sin\gamma\, e^{j\eta} \\ \cos\gamma \end{bmatrix}}_{\overset{\text{def}}{=}\mathbf{g}} \tag{3.1}$$

$$= \begin{bmatrix} \cos\phi\cos\theta\sin\gamma\cos\eta - \sin\phi\cos\gamma \\ \sin\phi\cos\theta\sin\gamma\cos\eta + \cos\phi\cos\gamma \\ -\sin\theta\sin\gamma\cos\eta \\ -\sin\phi\sin\gamma\cos\eta - \cos\phi\cos\theta\cos\gamma \\ \cos\phi\sin\gamma\cos\eta - \sin\phi\cos\theta\cos\gamma \\ \sin\theta\cos\gamma \end{bmatrix} + j \begin{bmatrix} \cos\phi\cos\theta\sin\gamma\sin\eta \\ \sin\phi\cos\theta\sin\gamma\sin\eta \\ -\sin\theta\sin\gamma\sin\eta \\ -\sin\phi\sin\gamma\sin\eta \\ \cos\phi\sin\gamma\sin\eta \\ 0 \end{bmatrix} \tag{3.2}$$

where $\theta \in [0, \pi]$ signifies the emitter's elevation-angle measured from the positive z-axis, $\phi \in [0, 2\pi)$ denotes the corresponding azimuth-angle measured from the positive x-axis, $\gamma \in [0, \pi/2)$ refers to the auxiliary polarization angle, and $\eta \in [-\pi, \pi)$ symbolizes the polarization phase difference. Note that $\boldsymbol{\Theta}$ depends on only the source's direction-of-arrival, whereas $\mathbf{g}$ depends on only the incident source's polarization state.

[2] Much of this chapter appears in [167].

Any three of the six elements in (3.1) may be measured, at a point in space, by a triad of collocated dipoles and/or loops oriented along the corresponding Cartesian axes. Such a triad's 3×1 array manifold would be

$$\mathbf{a} \;=\; \mathbf{S} \begin{bmatrix} \mathbf{e} \\ \\ \mathbf{h} \end{bmatrix}, \tag{3.3}$$

where $\mathbf{S}$ symbolizes a 3×6 selection-matrix of all zeroes, except one entry of a "1" at a different position on each row. For example, a dipole-triad has

$$\mathbf{S} \;=\; \begin{bmatrix} 1 & 0 & 0 & 0 & 0 & 0 \\ 0 & 1 & 0 & 0 & 0 & 0 \\ 0 & 0 & 1 & 0 & 0 & 0 \end{bmatrix}.$$

3.2 Closed-Form Formulas to Estimate the Azimuth-Elevation Arrival Angles & the Polarization-Parameters

In most eigen-based sensor-array parameter-estimation algorithms, an intermediate step estimates each incident source's steering vector, but correct to only within an *un*known complex-value scalar α. That is, available (in each algorithm for each incident emitter)[3] is the estimate $\hat{\mathbf{a}} \approx \alpha \mathbf{a}$, [4]from which θ, ϕ, γ, and η are to be estimated. (This approximation becomes equality in noiseless or asymptotic cases.) The question is whether $\hat{\mathbf{a}} \approx \alpha \mathbf{a}$ suffices to estimate θ, ϕ, γ, and η. The following five tables shows what, how, and why.

Tables 3.1 [5] to 3.5 list the closed-form estimation-formulas for $\hat{\theta}, \hat{\phi}, \hat{\gamma}, \hat{\eta}$. These estimation-formulas are new to the open literature, except as noted earlier in Section 1.2.2, to the

[3]This does NOT presume only a single incident source. Multiple, possibly cross-correlated / broadband / time-varying sources can be handled. For details, please refer to those references directly.

[4] The following simple data-model demonstrates how eigen-based parameter-estimation algorithms would lead to $\hat{\mathbf{a}} \approx \alpha \mathbf{a}$.

Suppose the emitted signal arrives at the triad as $s(t)$, but corrupted additively by the triad's thermal noise-vector $\mathbf{n}(t)$. The triad's measured data thus equals a 3×1 vector $\mathbf{z}(t) = s(t)\mathbf{a} + \mathbf{n}(t)$, at each $t = t_m$. From M such time-samples, an eigen-based parameter-estimation algorithm can form a 3×3 data covariance matrix $\hat{\mathbf{C}} = \frac{1}{M} \sum_{m=1}^{M} \mathbf{z}(t_m) \left[\mathbf{z}(t_m)\right]^H$, where the superscript ^{H} symbolizes the hermitian operator. Suppose further that $\{s(t), \forall t\}$ and $\{\mathbf{n}(t), \forall t\}$ are each temporally white, each temporally stationary, and not cross-correlated. Then, $\hat{\mathbf{C}} \approx \mathbf{C} = P_s \mathbf{a}\mathbf{a}^H + P_n \mathbf{I}$, where P_s denotes the power of the incident signal, P_n refers to the thermal noise power at each antenna, and $\mathbf{I}$ signifies a 3×3 identity matrix. This 3×3 matrix $\hat{\mathbf{C}}$ is Hermitian, and asymptotically approaches $\mathbf{C}$, as $M \to \infty$. The asymptotic $\mathbf{C}$ has a principal eigenvector equal to $\alpha \mathbf{a}$, where α can be any complex-value number that has a magnitude of $1/\|\mathbf{a}\|$ and that is algebraically independent of $\mathbf{a}$. Hence, the principal eigenvector of the sampled data-covariance matrix $\hat{\mathbf{C}}$ is approximately $\alpha \mathbf{a}$.

This $\hat{\mathbf{a}} \approx \alpha \mathbf{a}$ arises also for more complex data-models involving multiple incident sources, more complicated channels, and more complicated noises.

[5]For compositions 1.1 and 1.2 in Table 3.1, the $\hat{\phi}$ formula in [59] is erroneous.

best knowledge of the present authors. These formulas are valid, except at a finite number of discrete values, which occur with probability zero, anyway. Some estimation-formulas may require some prior information as specified in the far-right column in those tables. These formulas are obtained by algebraic and trigonometric manipulations of the three complex-value equations (i.e. six real-value equations) from the three component-antenna consisting of the triad, to solve for the six real-value unknown scalars of θ, ϕ, γ, η, $\mathrm{Re}\{\alpha\}$, and $\mathrm{Im}\{\alpha\}$. The Appendix shows such detailed algebraic and trigonometric manipulations for the composition of $\{e_x, e_y, h_z\}$. The derivation would be similar for the other cases. In these estimation-formulas, $\mathrm{Re}\{\cdot\}$ refers to the real-value part of the entity inside the curly brackets, $\mathrm{Im}\{\cdot\}$ denotes to the imaginary-value part of the entity inside the curly brackets.

Table 3.1: Formulas for Direction Finding & Polarization Estimation, Already Available in the Literature.

Composition	Antennas	Estimation Formulas	Intermediate Variables	Prior Info. Required
1.1 [59, 137]	$\{e_x, e_y, e_z\}$	$\hat{\theta} = \begin{cases} \tan^{-1}\left\{\frac{-[\mathbf{d}]_3}{\mathrm{Re}\{[\mathbf{d}]_1\}\cos\hat{\phi}+\mathrm{Re}\{[\mathbf{d}]_2\}\sin\hat{\phi}}\right\}, & \text{if } (\mathrm{Re}\{[\mathbf{d}]_1\}\cos\hat{\phi}+\mathrm{Re}\{[\mathbf{d}]_2\}\sin\hat{\phi}) \le 0 \\ \tan^{-1}\left\{\frac{-[\mathbf{d}]_3}{\mathrm{Re}\{[\mathbf{d}]_1\}\cos\hat{\phi}+\mathrm{Re}\{[\mathbf{d}]_2\}\sin\hat{\phi}}\right\}+\pi, & \text{if } (\mathrm{Re}\{[\mathbf{d}]_1\}\cos\hat{\phi}+\mathrm{Re}\{[\mathbf{d}]_2\}\sin\hat{\phi}) > 0 \end{cases}$ $\hat{\phi} = \begin{cases} \tan^{-1}\left\{\frac{-\mathrm{Im}\{[\mathbf{d}]_1\}}{\mathrm{Im}\{[\mathbf{d}]_2\}}\right\}, & \text{if } (\sin\eta\cdot\mathrm{Im}\{[\mathbf{d}]_2\}) \ge 0 \\ \tan^{-1}\left\{\frac{-\mathrm{Im}\{[\mathbf{d}]_1\}}{\mathrm{Im}\{[\mathbf{d}]_2\}}\right\}+\pi, & \text{if } (\sin\eta\cdot\mathrm{Im}\{[\mathbf{d}]_2\}) < 0 \end{cases}$ $\hat{\gamma} = \sin^{-1}\left\{\frac{\lvert[\mathbf{d}]_3\rvert}{\sin\hat{\theta}}\right\}$ $\hat{\eta} = -\angle\left\{[\mathbf{d}]_1\sin\hat{\phi}-[\mathbf{d}]_2\cos\hat{\phi}\right\}$	$\mathbf{d} \stackrel{\text{def}}{=} \frac{\hat{\mathbf{a}}e^{-j\angle[\hat{\mathbf{a}}]_3}}{\lVert\hat{\mathbf{a}}\rVert}$	$\eta \in [0,\pi)$ or $\eta \in [-\pi, 0)$
1.2 [59, 137]	$\{h_x, h_y, h_z\}$	$\hat{\theta} = \begin{cases} \tan^{-1}\left\{\frac{-[\mathbf{d}]_3}{\mathrm{Re}\{[\mathbf{d}]_1\}\cos\hat{\phi}+\mathrm{Re}\{[\mathbf{d}]_2\}\sin\hat{\phi}}\right\}, & \text{if } (\mathrm{Re}\{[\mathbf{d}]_1\}\cos\hat{\phi}+\mathrm{Re}\{[\mathbf{d}]_2\}\sin\hat{\phi}) \le 0 \\ \tan^{-1}\left\{\frac{-[\mathbf{d}]_3}{\mathrm{Re}\{[\mathbf{d}]_1\}\cos\hat{\phi}+\mathrm{Re}\{[\mathbf{d}]_2\}\sin\hat{\phi}}\right\}+\pi, & \text{if } (\mathrm{Re}\{[\mathbf{d}]_1\}\cos\hat{\phi}+\mathrm{Re}\{[\mathbf{d}]_2\}\sin\hat{\phi}) > 0 \end{cases}$ $\hat{\phi} = \begin{cases} \tan^{-1}\left\{\frac{-\mathrm{Im}\{[\mathbf{d}]_1\}}{\mathrm{Im}\{[\mathbf{d}]_2\}}\right\}, & \text{if } (\sin\eta\cdot\mathrm{Im}\{[\mathbf{d}]_2\}) \ge 0 \\ \tan^{-1}\left\{\frac{-\mathrm{Im}\{[\mathbf{d}]_1\}}{\mathrm{Im}\{[\mathbf{d}]_2\}}\right\}+\pi, & \text{if } (\sin\eta\cdot\mathrm{Im}\{[\mathbf{d}]_2\}) < 0 \end{cases}$ $\hat{\gamma} = \cos^{-1}\left\{\frac{\lvert[\mathbf{d}]_3\rvert}{\sin\hat{\theta}}\right\}$ $\hat{\eta} = \angle\left\{[\mathbf{d}]_2\cos\hat{\phi}-[\mathbf{d}]_1\sin\hat{\phi}\right\}$	$\mathbf{d} \stackrel{\text{def}}{=} \frac{\hat{\mathbf{a}}e^{-j\angle[\hat{\mathbf{a}}]_3}}{\lVert\hat{\mathbf{a}}\rVert}$	$\eta \in [0,\pi)$ or $\eta \in [-\pi, 0)$
1.3	$\{e_x, e_y, h_z\}$	$\hat{\theta} = \begin{cases} \sin^{-1}\left\{\left\lvert\frac{\mathrm{Re}\{[\mathbf{b}]_3\}}{\mathrm{Re}\{[\mathbf{b}]_2\}\cos\hat{\phi}-\mathrm{Re}\{[\mathbf{b}]_1\}\sin\hat{\phi}}\right\rvert\right\}, & \text{if}\theta \in [0,\pi/2] \\ \pi-\sin^{-1}\left\{\left\lvert\frac{\mathrm{Re}\{[\mathbf{b}]_3\}}{\mathrm{Re}\{[\mathbf{b}]_2\}\cos\hat{\phi}-\mathrm{Re}\{[\mathbf{b}]_1\}\sin\hat{\phi}}\right\rvert\right\}, & \text{if}\theta \in (\pi/2,\pi] \end{cases}$ $\hat{\phi} = \begin{cases} \tan^{-1}\frac{\mathrm{Im}\{[\mathbf{b}]_2\}}{\mathrm{Im}\{[\mathbf{b}]_1\}}, & \text{if } (\cos\theta\sin\eta\cdot\mathrm{Im}\{[\mathbf{b}]_1\}) \ge 0 \\ \tan^{-1}\frac{\mathrm{Im}\{[\mathbf{b}]_2\}}{\mathrm{Im}\{[\mathbf{b}]_1\}}+\pi, & \text{if } (\cos\theta\sin\eta\cdot\mathrm{Im}\{[\mathbf{b}]_1\}) < 0 \end{cases}$ $\hat{\gamma} = \tan^{-1}\left\{\left\lvert\frac{\mathrm{Im}\{[\mathbf{b}]_1\}\tan\hat{\theta}}{\mathrm{Re}\{[\mathbf{b}]_3\}\cos\hat{\phi}\sin\hat{\eta}}\right\rvert\right\}$ $\hat{\eta} = \angle\left\{\frac{[\mathbf{b}]_1\cos\hat{\phi}+[\mathbf{b}]_2\sin\hat{\phi}}{\cos\hat{\theta}}\right\}$	$\mathbf{b} \stackrel{\text{def}}{=} \hat{\mathbf{a}}e^{-j\angle[\hat{\mathbf{a}}]_3}$	$\theta \in [0, \frac{\pi}{2}]$ or $\theta \in (\frac{\pi}{2}, \pi]$ $\eta \in [0,\pi)$ or $\eta \in [-\pi, 0)$
1.4 [81, 101]	$\{e_z, h_x, h_y\}$	$\hat{\theta} = \begin{cases} \sin^{-1}\left\{\left\lvert\frac{\mathrm{Re}\{[\mathbf{e}]_1\}}{\mathrm{Re}\{[\mathbf{e}]_2\}\sin\hat{\phi}-\mathrm{Re}\{[\mathbf{b}]_3\}\cos\hat{\phi}}\right\rvert\right\}, & \text{if} \quad \theta \in [0,\pi/2]. \\ \pi-\sin^{-1}\left\{\left\lvert\frac{\mathrm{Re}\{[\mathbf{e}]_1\}}{\mathrm{Re}\{[\mathbf{e}]_2\}\sin\hat{\phi}-\mathrm{Re}\{[\mathbf{b}]_3\}\cos\hat{\phi}}\right\rvert\right\}, & \text{if} \quad \theta \in (\pi/2,\pi]. \end{cases}$ $\hat{\phi} = \begin{cases} \tan^{-1}\left\{\frac{\mathrm{Im}\{[\mathbf{e}]_3\}}{\mathrm{Im}\{[\mathbf{e}]_2\}}\right\}, & \text{if } (\cos\theta\sin\eta\cdot\mathrm{Im}\{[\mathbf{e}]_2\}) \le 0 \\ \tan^{-1}\left\{\frac{\mathrm{Im}\{[\mathbf{e}]_3\}}{\mathrm{Im}\{[\mathbf{e}]_2\}}\right\}+\pi, & \text{if } (\cos\theta\sin\eta\cdot\mathrm{Im}\{[\mathbf{e}]_2\}) > 0 \end{cases}$ $\hat{\gamma} = \tan^{-1}\left\{\left\lvert\frac{\mathrm{Re}\{[\mathbf{e}]_1\}\sin\hat{\phi}\sin\hat{\eta}}{\mathrm{Im}\{[\mathbf{e}]_3\}\tan\hat{\theta}}\right\rvert\right\}$ $\hat{\eta} = -\angle\left\{\frac{[\mathbf{e}]_2\cos\hat{\phi}+[\mathbf{e}]_3\sin\hat{\phi}}{\cos\hat{\theta}}\right\}$	$\mathbf{e} \stackrel{\text{def}}{=} \hat{\mathbf{a}}e^{-j\angle[\hat{\mathbf{a}}]_1}$	$\theta \in [0, \frac{\pi}{2}]$ or $\theta \in (\frac{\pi}{2}, \pi]$ $\eta \in [0,\pi)$ or $\eta \in [-\pi, 0)$

Table 3.2: Formulas for Direction Finding & Polarization Estimation, for Triads with Both the z-Dipole and the z-Loop.

Composition	Antennas	Estimation Formulas	Intermediate Variables	Prior Info. Required
2.1	$\{e_x, e_z, h_z\}$	$\hat{\theta} = \begin{cases} \tan^{-1}\left\{\frac{\sqrt{1-D_1^2-D_2^2+\sqrt{D_1^4+(D_2^2-1)^2+2D_1^2(1+D_2^2)}}}{\sqrt{2}\lvert D_1\rvert}\right\}, & \text{if } \theta \in [0,\pi/2]. \\ \pi - \tan^{-1}\left\{\frac{\sqrt{1-D_1^2-D_2^2+\sqrt{D_1^4+(D_2^2-1)^2+2D_1^2(1+D_2^2)}}}{\sqrt{2}\lvert D_1\rvert}\right\}, & \text{if } \theta \in (\pi/2,\pi]. \end{cases}$ $\hat{\phi} = \begin{cases} \tan^{-1}\left\{\frac{D_2\cos\hat{\theta}}{-D_1}\right\}, & \text{if } D_1\tan\hat{\theta} < 0, \\ \tan^{-1}\left\{\frac{D_2\cos\hat{\theta}}{-D_1}\right\}+\pi, & \text{if } D_1\tan\hat{\theta} \geq 0. \end{cases}$ $\hat{\gamma} = \arctan\left\lvert\frac{[\hat{\mathbf{a}}]_2}{[\hat{\mathbf{a}}]_3}\right\rvert$ $\hat{\eta} = \angle\left\{\frac{[\hat{\mathbf{a}}]_2}{[\hat{\mathbf{a}}]_3}\right\} - \pi$	$\mathbf{b} \stackrel{\text{def}}{=} \hat{\mathbf{a}}e^{-j\angle[\hat{\mathbf{a}}]_3}$ $D_1 = \frac{\text{Im}\{[\mathbf{b}]_1\}}{\text{Im}\{[\mathbf{b}]_2\}}$ $D_2 = \left(\frac{\text{Re}\{[\mathbf{b}]_1\}}{\text{Re}\{[\mathbf{b}]_2\}} - D_1\right)\tan\hat{\gamma}\cos\hat{\eta}$	$\theta \in [0, \frac{\pi}{2}]$ or $\theta \in (\frac{\pi}{2}, \pi]$
2.2	$\{e_y, e_z, h_z\}$	$\hat{\theta} = \begin{cases} \tan^{-1}\left\{\frac{\sqrt{1-D_1^2-D_2^2+\sqrt{D_1^4+(D_2^2-1)^2+2D_1^2(1+D_2^2)}}}{\sqrt{2}\lvert D_1\rvert}\right\}, & \text{if } \theta \in [0,\pi/2]. \\ \pi - \tan^{-1}\left\{\frac{\sqrt{1-D_1^2-D_2^2+\sqrt{D_1^4+(D_2^2-1)^2+2D_1^2(1+D_2^2)}}}{\sqrt{2}\lvert D_1\rvert}\right\}, & \text{if } \theta \in (\pi/2,\pi]. \end{cases}$ $\hat{\phi} = \begin{cases} \tan^{-1}\left\{\frac{D_1}{D_2\cos\hat{\theta}}\right\}, & \text{if } D_2 < 0, \\ \tan^{-1}\left\{\frac{D_1}{D_2\cos\hat{\theta}}\right\}+\pi, & \text{if } D_2 \geq 0. \end{cases}$ $\hat{\gamma} = \arctan\left\lvert\frac{[\hat{\mathbf{a}}]_2}{[\hat{\mathbf{a}}]_3}\right\rvert$ $\hat{\eta} = \angle\left\{\frac{[\hat{\mathbf{a}}]_2}{[\hat{\mathbf{a}}]_3}\right\} - \pi$	$\mathbf{b} \stackrel{\text{def}}{=} \hat{\mathbf{a}}e^{-j\angle[\hat{\mathbf{a}}]_3}$ $D_1 = \frac{\text{Im}\{[\mathbf{b}]_1\}}{\text{Im}\{[\mathbf{b}]_2\}}$ $D_2 = \left(\frac{\text{Re}\{[\mathbf{b}]_1\}}{\text{Re}\{[\mathbf{b}]_2\}} - D_1\right)\tan\hat{\gamma}\cos\hat{\eta}$	$\theta \in [0, \frac{\pi}{2}]$ or $\theta \in (\frac{\pi}{2}, \pi]$
2.3	$\{e_z, h_x, h_z\}$	$\hat{\theta} = \begin{cases} \tan^{-1}\left\{\frac{\sqrt{1-D_1^2-D_2^2+\sqrt{D_1^4+(D_2^2+1)^2+2D_1^2(-1+D_2^2)}}}{\sqrt{2}\lvert D_2\rvert}\right\}, & \text{if } \theta \in [0,\pi/2]. \\ \pi - \tan^{-1}\left\{\frac{\sqrt{1-D_1^2-D_2^2+\sqrt{D_1^4+(D_2^2+1)^2+2D_1^2(-1+D_2^2)}}}{\sqrt{2}\lvert D_2\rvert}\right\}, & \text{if } \theta \in (\pi/2,\pi]. \end{cases}$ $\hat{\phi} = \begin{cases} \tan^{-1}\left\{\frac{D_1\cos\hat{\theta}}{D_2}\right\}, & \text{if } D_2\tan\hat{\theta} \geq 0, \\ \tan^{-1}\left\{\frac{D_1\cos\hat{\theta}}{D_2}\right\}+\pi, & \text{if } D_2\tan\hat{\theta} < 0. \end{cases}$ $\hat{\gamma} = \arctan\left\lvert\frac{[\hat{\mathbf{a}}]_1}{[\hat{\mathbf{a}}]_3}\right\rvert$ $\hat{\eta} = \angle\left\{\frac{[\hat{\mathbf{a}}]_1}{[\hat{\mathbf{a}}]_3}\right\} - \pi$	$\mathbf{b} \stackrel{\text{def}}{=} \hat{\mathbf{a}}e^{-j\angle[\hat{\mathbf{a}}]_3}$ $D_1 = \frac{\text{Im}\{[\mathbf{b}]_2\}}{\text{Im}\{[\mathbf{b}]_1\}}$ $D_2 = \left(\frac{\text{Re}\{[\mathbf{b}]_2\}}{\text{Re}\{[\mathbf{b}]_1\}} - D_1\right)\tan\hat{\gamma}\cos\hat{\eta}$	$\theta \in [0, \frac{\pi}{2}]$ or $\theta \in (\frac{\pi}{2}, \pi]$
2.4	$\{e_z, h_y, h_z\}$	$\hat{\theta} = \begin{cases} \tan^{-1}\left\{\frac{\sqrt{1-D_1^2-D_2^2+\sqrt{D_1^4+(D_2^2+1)^2+2D_1^2(-1+D_2^2)}}}{\sqrt{2}\lvert D_2\rvert}\right\}, & \text{if } \theta \in [0,\pi/2]. \\ \pi - \tan^{-1}\left\{\frac{\sqrt{1-D_1^2-D_2^2+\sqrt{D_1^4+(D_2^2+1)^2+2D_1^2(-1+D_2^2)}}}{\sqrt{2}\lvert D_2\rvert}\right\}, & \text{if } \theta \in (\pi/2,\pi]. \end{cases}$ $\hat{\phi} = \begin{cases} \tan^{-1}\left\{\frac{-D_2}{D_1\cos\hat{\theta}}\right\}, & \text{if } D_1 < 0, \\ \tan^{-1}\left\{\frac{-D_2}{D_1\cos\hat{\theta}}\right\}+\pi, & \text{if } D_1 \geq 0. \end{cases}$ $\hat{\gamma} = \arctan\left\lvert\frac{[\hat{\mathbf{a}}]_1}{[\hat{\mathbf{a}}]_3}\right\rvert$ $\hat{\eta} = \angle\left\{\frac{[\hat{\mathbf{a}}]_1}{[\hat{\mathbf{a}}]_3}\right\} - \pi$	$\mathbf{b} \stackrel{\text{def}}{=} \hat{\mathbf{a}}e^{-j\angle[\hat{\mathbf{a}}]_3}$ $D_1 = \frac{\text{Im}\{[\mathbf{b}]_2\}}{\text{Im}\{[\mathbf{b}]_1\}}$ $D_2 = \left(\frac{\text{Re}\{[\mathbf{b}]_2\}}{\text{Re}\{[\mathbf{b}]_1\}} - D_1\right)\tan\hat{\gamma}\cos\hat{\eta}$	$\theta \in [0, \frac{\pi}{2}]$ or $\theta \in (\frac{\pi}{2}, \pi]$

Table 3.3: Formulas for Direction Finding & Polarization Estimation, for Other Triads with a Component-Antenna Along Each Cartesian Axis.

Composition	Antennas	Estimation Formulas	Intermediate Variables	Prior Info. Required
3.1	$\{e_x, e_z, h_y\}$	$\hat{\theta} = \cos^{-1}\left\{\frac{\mathrm{Im}\{[\mathbf{c}]_3\}}{\mathrm{Im}\{[\mathbf{c}]_1\}}\right\}$ $\hat{\phi} = \begin{cases} \cos^{-1}\left\{\frac{\mathrm{Re}\{[\mathbf{c}]_1\}\cos\hat{\theta}-\mathrm{Re}\{[\mathbf{c}]_3\}}{\mathrm{Re}\{[\mathbf{c}]_2\}\sin\hat{\theta}}\right\}, & \text{if} \quad \sin\phi \geq 0, \\ -\cos^{-1}\left\{\frac{\mathrm{Re}\{[\mathbf{c}]_1\}\cos\hat{\theta}-\mathrm{Re}\{[\mathbf{c}]_3\}}{\mathrm{Re}\{[\mathbf{c}]_2\}\sin\hat{\theta}}\right\}, & \text{if} \quad \sin\phi < 0. \end{cases}$ $\hat{\gamma} = \tan^{-1}\left\{\left\lvert\frac{[\mathbf{c}]_2\sin\hat{\phi}}{[\mathbf{c}]_1\sin\hat{\theta}+[\mathbf{b}]_2\cos\hat{\phi}\cos\hat{\theta}}\right\rvert\right\}$ $\hat{\eta} = \angle\left\{\frac{[\mathbf{c}]_2\sin\hat{\phi}}{[\mathbf{c}]_1\sin\hat{\theta}+[\mathbf{c}]_2\cos\hat{\phi}\cos\hat{\theta}}\right\}$	$\mathbf{c} \overset{\text{def}}{=} \hat{\mathbf{a}}e^{-j\angle[\hat{\mathbf{a}}]_2}$	$\phi \in [0,\pi)$ or $\phi \in [\pi, 2\pi)$
3.2	$\{e_x, h_y, h_z\}$	$\hat{\theta} = \cos^{-1}\left\{\frac{\mathrm{Im}\{[\mathbf{b}]_1\}}{\mathrm{Im}\{[\mathbf{b}]_2\}}\right\}$ $\hat{\phi} = \begin{cases} \sin^{-1}\left\{\frac{\mathrm{Re}\{[\mathbf{b}]_2\}\cos\hat{\theta}-\mathrm{Re}\{[\mathbf{b}]_1\}}{\mathrm{Re}\{[\mathbf{b}]_3\}\sin\hat{\theta}}\right\}, & \text{if} \quad \cos\phi \geq 0, \\ \pi - \sin^{-1}\left\{\frac{\mathrm{Re}\{[\mathbf{b}]_2\}\cos\hat{\theta}-\mathrm{Re}\{[\mathbf{b}]_1\}}{\mathrm{Re}\{[\mathbf{b}]_3\}\sin\hat{\theta}}\right\}, & \text{if} \quad \cos\phi < 0. \end{cases}$ $\hat{\gamma} = \tan^{-1}\left\{\left\lvert\frac{[\mathbf{b}]_2\sin\hat{\theta}+[\mathbf{b}]_3\sin\hat{\phi}\cos\hat{\theta}}{[\mathbf{b}]_3\cos\hat{\phi}}\right\rvert\right\}$ $\hat{\eta} = \angle\left\{\frac{[\mathbf{b}]_2\sin\hat{\theta}+[\mathbf{b}]_3\sin\hat{\phi}\cos\hat{\theta}}{[\mathbf{b}]_3\cos\hat{\phi}}\right\}$	$\mathbf{b} \overset{\text{def}}{=} \hat{\mathbf{a}}e^{-j\angle[\hat{\mathbf{a}}]_3}$	$\phi \in [-\frac{\pi}{2}, \frac{\pi}{2})$ or $\phi \in [\frac{\pi}{2}, \frac{3\pi}{2})$
3.3	$\{e_y, e_z, h_x\}$	$\hat{\theta} = \cos^{-1}\left\{\frac{-\mathrm{Im}\{[\mathbf{c}]_3\}}{\mathrm{Im}\{[\mathbf{c}]_1\}}\right\}$ $\hat{\phi} = \begin{cases} \sin^{-1}\left\{\frac{\mathrm{Re}\{[\mathbf{c}]_3\}+\mathrm{Re}\{[\mathbf{c}]_1\}\cos\hat{\theta}}{\mathrm{Re}\{[\mathbf{c}]_2\}\sin\hat{\theta}}\right\}, & \text{if} \quad \cos\phi \geq 0, \\ \pi - \sin^{-1}\left\{\frac{\mathrm{Re}\{[\mathbf{c}]_3\}+\mathrm{Re}\{[\mathbf{c}]_1\}\cos\hat{\theta}}{\mathrm{Re}\{[\mathbf{c}]_2\}\sin\hat{\theta}}\right\}, & \text{if} \quad \cos\phi < 0. \end{cases}$ $\hat{\gamma} = \tan^{-1}\left\{\left\lvert\frac{-[\mathbf{c}]_2\cos\hat{\phi}}{[\mathbf{c}]_1\sin\hat{\theta}+[\mathbf{c}]_2\sin\hat{\phi}\cos\hat{\theta}}\right\rvert\right\}$ $\hat{\eta} = \angle\left\{\frac{-[\mathbf{c}]_2\cos\hat{\phi}}{[\mathbf{c}]_1\sin\hat{\theta}+[\mathbf{c}]_2\sin\hat{\phi}\cos\hat{\theta}}\right\}$	$\mathbf{c} \overset{\text{def}}{=} \hat{\mathbf{a}}e^{-j\angle[\hat{\mathbf{a}}]_2}$	$\phi \in [-\frac{\pi}{2}, \frac{\pi}{2})$ or $\phi \in [\frac{\pi}{2}, \frac{3\pi}{2})$
3.4	$\{e_y, h_x, h_z\}$	$\hat{\theta} = \cos^{-1}\left\{\frac{-\mathrm{Im}\{[\mathbf{b}]_1\}}{\mathrm{Im}\{[\mathbf{b}]_2\}}\right\}$ $\hat{\phi} = \begin{cases} \cos^{-1}\left\{\frac{\mathrm{Re}\{[\mathbf{b}]_1\}+\mathrm{Re}\{[\mathbf{b}]_2\}\cos\hat{\theta}}{\mathrm{Re}\{[\mathbf{b}]_3\}\sin\hat{\theta}}\right\}, & \text{if} \quad \sin\phi \geq 0, \\ -\cos^{-1}\left\{\frac{\mathrm{Re}\{[\mathbf{b}]_1\}+\mathrm{Re}\{[\mathbf{b}]_2\}\cos\hat{\theta}}{\mathrm{Re}\{[\mathbf{b}]_3\}\sin\hat{\theta}}\right\}, & \text{if} \quad \sin\phi < 0. \end{cases}$ $\hat{\gamma} = \tan^{-1}\left\{\left\lvert\frac{[\mathbf{b}]_2\sin\hat{\theta}+[\mathbf{b}]_3\cos\hat{\phi}\cos\hat{\theta}}{-[\mathbf{b}]_3\sin\hat{\phi}}\right\rvert\right\}$ $\hat{\eta} = \angle\left\{\frac{[\mathbf{b}]_2\sin\hat{\theta}+[\mathbf{b}]_3\cos\hat{\phi}\cos\hat{\theta}}{-[\mathbf{b}]_3\sin\hat{\phi}}\right\}$	$\mathbf{b} \overset{\text{def}}{=} \hat{\mathbf{a}}e^{-j\angle[\hat{\mathbf{a}}]_3}$	$\phi \in [0,\pi)$ or $\phi \in [\pi, 2\pi)$

Table 3.4: Formulas for Direction Finding & Polarization Estimation, for Other Triads with a z-Axis Dipole or Loop.

Composition	Antennas	Estimation Formulas	Intermediate Variables	Prior Info. Required
4.1	$\{e_x, e_z, h_x\}$	$\hat{\theta} = \begin{cases} \tan^{-1}\left\{\frac{\sqrt{1-D_3^2-D_4^2+\sqrt{D_3^4+(D_4^2+1)^2+2D_3^2(-1+D_4^2)}}}{\sqrt{2}\lvert D_4\rvert}\right\}, & \text{if } \theta \in [0,\pi/2]. \\ \pi - \tan^{-1}\left\{\frac{\sqrt{1-D_3^2-D_4^2+\sqrt{D_3^4+(D_4^2+1)^2+2D_3^2(-1+D_4^2)}}}{\sqrt{2}\lvert D_4\rvert}\right\}, & \text{if } \theta \in (\pi/2,\pi]. \end{cases}$ $\hat{\phi} = \begin{cases} \tan^{-1}\left\{\frac{D_3\cos\hat{\theta}}{D_4}\right\}, & \text{if } D_4\tan\hat{\theta} \geq 0. \\ \tan^{-1}\left\{\frac{D_3\cos\hat{\theta}}{D_4}\right\}+\pi, & \text{if } D_4\tan\hat{\theta} < 0. \end{cases}$ $\hat{\gamma} = \tan^{-1}\left\{\frac{\lvert \mathrm{Re}\{[\mathbf{c}]_1\}\mathrm{Im}\{[\mathbf{c}]_3\} - \mathrm{Re}\{[\mathbf{c}]_3\}\mathrm{Im}\{[\mathbf{c}]_1\}\rvert}{\sqrt{(\mathrm{Im}\{[\mathbf{c}]_3\}^2+\mathrm{Im}\{[\mathbf{c}]_1\}^2)^2+(\mathrm{Re}\{[\mathbf{c}]_1\}\mathrm{Im}\{[\mathbf{c}]_1\}+\mathrm{Re}\{[\mathbf{c}]_3\}\mathrm{Im}\{[\mathbf{c}]_3\})^2}}\right\}$ $\hat{\eta} = \begin{cases} \angle\left\{\begin{array}{l} -(\mathrm{Im}\{[\mathbf{c}]_3\}\mathrm{Re}\{[\mathbf{c}]_3\}+\mathrm{Im}\{[\mathbf{c}]_1\}\mathrm{Re}\{[\mathbf{c}]_1\}) \\ +j(\mathrm{Im}\{[\mathbf{c}]_3\}^2+\mathrm{Im}\{[\mathbf{c}]_1\}^2)\end{array}\right\}, & \text{if } \sin\eta \geq 0, \\ \angle\left\{\begin{array}{l} -(\mathrm{Im}\{[\mathbf{c}]_3\}\mathrm{Re}\{[\mathbf{c}]_3\}+\mathrm{Im}\{[\mathbf{c}]_1\}\mathrm{Re}\{[\mathbf{c}]_1\}) \\ +j(\mathrm{Im}\{[\mathbf{c}]_3\}^2+\mathrm{Im}\{[\mathbf{c}]_1\}^2)\end{array}\right\}+\pi, & \text{if } \sin\eta < 0. \end{cases}$	$\mathbf{c} \stackrel{\text{def}}{=} \hat{\mathbf{a}}e^{-j\angle[\hat{\mathbf{a}}]_2}$ $D_3 = \frac{-\mathrm{Im}\{[\mathbf{c}]_1\}\sin\hat{\gamma}}{\mathrm{Re}\{[\mathbf{c}]_2\}\cos\hat{\gamma}\sin\hat{\eta}}$ $D_4 = \frac{-\mathrm{Im}\{[\mathbf{c}]_3\}\sin\hat{\gamma}}{\mathrm{Re}\{[\mathbf{c}]_2\}\cos\hat{\gamma}\sin\hat{\eta}}$	$\theta \in [0,\frac{\pi}{2}]$ or $\theta \in (\frac{\pi}{2},\pi]$ $\eta \in [0,\pi)$ or $\eta \in [-\pi,0)$
4.2	$\{e_x, h_x, h_z\}$	$\hat{\theta} = \begin{cases} \tan^{-1}\left\{\frac{\sqrt{1-D_5^2-D_6^2+\sqrt{D_5^4+(D_6^2+1)^2+2D_5^2(-1+D_6^2)}}}{\sqrt{2}\lvert D_6\rvert}\right\}, & \text{if } \theta \in [0,\pi/2]. \\ \pi - \tan^{-1}\left\{\frac{\sqrt{1-D_5^2-D_6^2+\sqrt{D_5^4+(D_6^2+1)^2+2D_5^2(-1+D_6^2)}}}{\sqrt{2}\lvert D_6\rvert}\right\}, & \text{if } \theta \in (\pi/2,\pi]. \end{cases}$ $\hat{\phi} = \begin{cases} \tan^{-1}\left\{\frac{D_5\cos\hat{\theta}}{D_6}\right\}, & \text{if } D_6\tan\hat{\theta} \geq 0. \\ \tan^{-1}\left\{\frac{D_5\cos\hat{\theta}}{D_6}\right\}+\pi, & \text{if } D_6\tan\hat{\theta} < 0. \end{cases}$ $\hat{\gamma} = \tan^{-1}\left\{\frac{\sqrt{(\mathrm{Im}\{[\mathbf{b}]_1\}^2+\mathrm{Im}\{[\mathbf{b}]_2\}^2)^2+(\mathrm{Re}\{[\mathbf{b}]_1\}\mathrm{Im}\{[\mathbf{b}]_1\}+\mathrm{Re}\{[\mathbf{b}]_2\}\mathrm{Im}\{[\mathbf{b}]_2\})^2}}{\lvert \mathrm{Re}\{[\mathbf{b}]_1\}\mathrm{Im}\{[\mathbf{b}]_2\}-\mathrm{Re}\{[\mathbf{b}]_2\}\mathrm{Im}\{[\mathbf{b}]_1\}\rvert}\right\}$ $\hat{\eta} = \begin{cases} \angle\left\{\begin{array}{l} (\mathrm{Re}\{[\mathbf{b}]_1\}\mathrm{Im}\{[\mathbf{b}]_1\}+\mathrm{Re}\{[\mathbf{b}]_2\}\mathrm{Im}\{[\mathbf{b}]_2\}) \\ +j(\mathrm{Im}\{[\mathbf{b}]_1\}^2+\mathrm{Im}\{[\mathbf{b}]_2\}^2)\end{array}\right\}, & \text{if } \sin\eta \geq 0, \\ \angle\left\{\begin{array}{l} (\mathrm{Re}\{[\mathbf{b}]_1\}\mathrm{Im}\{[\mathbf{b}]_1\}+\mathrm{Re}\{[\mathbf{b}]_2\}\mathrm{Im}\{[\mathbf{b}]_2\}) \\ +j(\mathrm{Im}\{[\mathbf{b}]_1\}^2+\mathrm{Im}\{[\mathbf{b}]_2\}^2)\end{array}\right\}+\pi, & \text{if } \sin\eta < 0. \end{cases}$	$\mathbf{b} \stackrel{\text{def}}{=} \hat{\mathbf{a}}e^{-j\angle[\hat{\mathbf{a}}]_3}$ $D_5 = \frac{-\mathrm{Im}\{[\mathbf{b}]_2\}\cos\hat{\gamma}}{\mathrm{Re}\{[\mathbf{b}]_3\}\sin\hat{\gamma}\sin\hat{\eta}}$ $D_6 = \frac{\mathrm{Im}\{[\mathbf{b}]_1\}\cos\hat{\gamma}}{\mathrm{Re}\{[\mathbf{b}]_3\}\sin\hat{\gamma}\sin\hat{\eta}}$	$\theta \in [0,\frac{\pi}{2}]$ or $\theta \in (\frac{\pi}{2},\pi]$ $\eta \in [0,\pi)$ or $\eta \in [-\pi,0)$

Table 3.5: Formulas for Direction Finding & Polarization Estimation, for Other Triads with a z-Axis Dipole or Loop.

Composition	Antennas	Estimation Formulas	Intermediate Variables	Prior Info. Required
4.3	$\{e_y, e_z, h_y\}$	$\hat{\theta} = \begin{cases} \tan^{-1}\left\{\frac{\sqrt{1-D_7^2-D_8^2+\sqrt{D_7^4+(D_8^2+1)^2+2D_7^2(-1+D_8^2)}}}{\sqrt{2}\lvert D_8\rvert}\right\}, & \text{if } \theta \in [0,\pi/2]. \\ \pi - \tan^{-1}\left\{\frac{\sqrt{1-D_7^2-D_8^2+\sqrt{D_7^4+(D_8^2+1)^2+2D_7^2(-1+D_8^2)}}}{\sqrt{2}\lvert D_8\rvert}\right\}, & \text{if } \theta \in (\pi/2,\pi]. \end{cases}$ $\hat{\phi} = \begin{cases} \tan^{-1}\left\{\frac{D_8}{D_7\cos\hat{\theta}}\right\}, & \text{if } D_7 \geq 0. \\ \tan^{-1}\left\{\frac{D_8}{D_7\cos\hat{\theta}}\right\}+\pi, & \text{if } D_7 < 0. \end{cases}$ $\hat{\gamma} = \tan^{-1}\left\{\frac{\lvert\mathrm{Re}\{[\mathbf{c}]_1\}\mathrm{Im}\{[\mathbf{c}]_3\}-\mathrm{Re}\{[\mathbf{c}]_3\}\mathrm{Im}\{[\mathbf{c}]_1\}\rvert}{\sqrt{(\mathrm{Im}\{[\mathbf{c}]_3\}^2+\mathrm{Im}\{[\mathbf{c}]_1\}^2)^2+(\mathrm{Re}\{[\mathbf{c}]_1\}\mathrm{Im}\{[\mathbf{c}]_1\}+\mathrm{Re}\{[\mathbf{c}]_3\}\mathrm{Im}\{[\mathbf{c}]_3\})^2}}\right\}$ $\hat{\eta} = \begin{cases} \angle\left\{\begin{matrix} -(\mathrm{Im}\{[\mathbf{c}]_3\}\mathrm{Re}\{[\mathbf{c}]_3\}+\mathrm{Im}\{[\mathbf{c}]_1\}\mathrm{Re}\{[\mathbf{c}]_1\}) \\ +j(\mathrm{Im}\{[\mathbf{c}]_3\}^2+\mathrm{Im}\{[\mathbf{c}]_1\}^2)\end{matrix}\right\}, & \text{if } \sin\eta \geq 0, \\ \angle\left\{\begin{matrix} -(\mathrm{Im}\{[\mathbf{c}]_3\}\mathrm{Re}\{[\mathbf{c}]_3\}+\mathrm{Im}\{[\mathbf{c}]_1\}\mathrm{Re}\{[\mathbf{c}]_1\}) \\ +j(\mathrm{Im}\{[\mathbf{c}]_3\}^2+\mathrm{Im}\{[\mathbf{c}]_1\}^2)\end{matrix}\right\}+\pi, & \text{if } \sin\eta < 0. \end{cases}$	$\mathbf{c} \stackrel{\text{def}}{=} \hat{\mathbf{a}}e^{-j\angle[\hat{\mathbf{a}}]_2}$ $D_7 = \frac{\mathrm{Im}\{[\mathbf{c}]_1\}\sin\hat{\gamma}}{\mathrm{Re}\{[\mathbf{c}]_2\}\cos\hat{\gamma}\sin\hat{\eta}} = \frac{\cos\phi}{\sin\theta}$ $D_8 = \frac{-\mathrm{Im}\{[\mathbf{c}]_3\}\sin\hat{\gamma}}{\mathrm{Re}\{[\mathbf{c}]_2\}\cos\hat{\gamma}\sin\hat{\eta}} = \frac{\sin\phi\cos\theta}{\sin\theta}$	$\theta \in [0, \frac{\pi}{2}]$ or $\theta \in (\frac{\pi}{2}, \pi]$ $\eta \in [0, \pi)$ or $\eta \in [-\pi, 0)$
4.4	$\{e_y, h_y, h_z\}$	$\hat{\theta} = \begin{cases} \tan^{-1}\left\{\frac{\sqrt{1-D_9^2-D_{10}^2+\sqrt{D_9^4+(D_{10}^2+1)^2+2D_9^2(-1+D_{10}^2)}}}{\sqrt{2}\lvert D_{10}\rvert}\right\}, & \text{if } \theta \in [0,\pi/2]. \\ \pi - \tan^{-1}\left\{\frac{\sqrt{1-D_9^2-D_{10}^2+\sqrt{D_9^4+(D_{10}^2+1)^2+2D_9^2(-1+D_{10}^2)}}}{\sqrt{2}\lvert D_{10}\rvert}\right\}, & \text{if } \theta \in (\pi/2,\pi]. \end{cases}$ $\hat{\phi} = \begin{cases} \tan^{-1}\left\{\frac{D_{10}}{D_9\cos\hat{\theta}}\right\}, & \text{if } D_9 \geq 0. \\ \tan^{-1}\left\{\frac{D_{10}}{D_9\cos\hat{\theta}}\right\}+\pi, & \text{if } D_9 < 0. \end{cases}$ $\hat{\gamma} = \tan^{-1}\left\{\frac{\sqrt{(\mathrm{Im}\{[\mathbf{b}]_1\}^2+\mathrm{Im}\{[\mathbf{b}]_2\}^2)^2+(\mathrm{Re}\{[\mathbf{b}]_1\}\mathrm{Im}\{[\mathbf{b}]_1\}+\mathrm{Re}\{[\mathbf{b}]_2\}\mathrm{Im}\{[\mathbf{b}]_2\})^2}}{\lvert\mathrm{Re}\{[\mathbf{b}]_1\}\mathrm{Im}\{[\mathbf{b}]_2\}-\mathrm{Re}\{[\mathbf{b}]_2\}\mathrm{Im}\{[\mathbf{b}]_1\}\rvert}\right\}$ $\hat{\eta} = \begin{cases} \angle\left\{\begin{matrix} (\mathrm{Re}\{[\mathbf{b}]_1\}\mathrm{Im}\{[\mathbf{b}]_1\}+\mathrm{Re}\{[\mathbf{b}]_2\}\mathrm{Im}\{[\mathbf{b}]_2\}) \\ +j(\mathrm{Im}\{[\mathbf{b}]_1\}^2+\mathrm{Im}\{[\mathbf{b}]_2\}^2)\end{matrix}\right\}, & \text{if } \sin\eta \geq 0, \\ \angle\left\{\begin{matrix} (\mathrm{Re}\{[\mathbf{b}]_1\}\mathrm{Im}\{[\mathbf{b}]_1\}+\mathrm{Re}\{[\mathbf{b}]_2\}\mathrm{Im}\{[\mathbf{b}]_2\}) \\ +j(\mathrm{Im}\{[\mathbf{b}]_1\}^2+\mathrm{Im}\{[\mathbf{b}]_2\}^2)\end{matrix}\right\}+\pi, & \text{if } \sin\eta < 0. \end{cases}$	$\mathbf{b} \stackrel{\text{def}}{=} \hat{\mathbf{a}}e^{-j\angle[\hat{\mathbf{a}}]_3}$ $D_9 = \frac{\mathrm{Im}\{[\mathbf{b}]_2\}\cos\hat{\gamma}}{\mathrm{Re}\{[\mathbf{b}]_3\}\sin\hat{\gamma}\sin\hat{\eta}} = \frac{\cos\phi}{\sin\theta}$ $D_{10} = \frac{\mathrm{Im}\{[\mathbf{b}]_1\}\cos\hat{\gamma}}{\mathrm{Re}\{[\mathbf{b}]_3\}\sin\hat{\gamma}\sin\hat{\eta}} = \frac{\sin\phi\cos\theta}{\sin\theta}$	$\theta \in [0, \frac{\pi}{2}]$ or $\theta \in (\frac{\pi}{2}, \pi]$ $\eta \in [0, \pi)$ or $\eta \in [-\pi, 0)$

Below are some qualitative observations on the above formulas:

{1} The various compositions are organized into the five tables, according to the prior knowledge needed in these closed-form estimation-formulas: Based on the prior requirement knowledge, the 16 configurations can be classified into 4 different groups:

(1a) The all-dipole or all-loop triads (i.e. compositions 1.1 and 1.2): Some prior knowledge of only η is required, to resolve a π-ambiguity in $\hat{\phi}$ as shown in Table 3.1.

(1b) Triads with both the z-oriented dipole *and* the z-oriented loop (i.e. compositions 2.1 to 2.4): Some prior knowledge of only θ is required, to resolve a π-ambiguity in $\hat{\phi}$ as shown in Table 3.2.

(1c) Other triads that have exactly one component-antenna along each of the three Cartesian axes (i.e. compositions 3.1 to 3.4): Some prior knowledge of only ϕ is required, to resolve a π-ambiguity in $\hat{\phi}$ as shown in Table 3.3.

(1d) The remaining 6 compositions: Some prior knowledge of both θ and η is required, to resolve π-ambiguities in $\hat{\phi}$, $\hat{\theta}$, $\hat{\phi}$ and $\hat{\eta}$.

{2} (2a) The dipole-triad $\{e_x, e_y, e_z\}$ and the loop-triad $\{h_x, h_y, h_z\}$ each has a validity region for (θ, ϕ) covering the entire sphere, if the sign of $\sin\eta$ is known a priori. This is because the dipole-triad $\{e_x, e_y, e_z\}$ and the loop-triad $\{h_x, h_y, h_z\}$, but no other composition, enjoys one additional constraint from the normalization $\|\mathbf{e}\| = 1$ or $\|\mathbf{h}\| = 1$.

(2b) For the four compositions of $\{e_x, e_z, h_y\}$, $\{e_x, h_y, h_z\}$, $\{e_y, e_z, h_x\}$, $\{e_y, h_x, h_z\}$, the $\hat{\phi}$ suffers ambiguity due to the presence of the $\cos^{-1}$ or $\sin^{-1}$ functions.

(2c) For the four compositions with the z-oriented dipole and the z-oriented loop, the azimuth-elevation direction-of-arrival estimate has (θ, ϕ) validity region over only an hemisphere. This is because $\hat{\theta}$ can be estimated only to $\tan^2\hat{\theta}$, hence there is ambiguity between $\theta \in [0, \frac{\pi}{2}]$ or $\theta \in (\frac{\pi}{2}, \pi]$.

(2d) Similarly for the six remaining compositions, $\hat{\phi}$ can be estimated only to within an hemisphere, and requires $\sin\eta$. The parameter η refers to the phase by which the electric field's y-axis component leads the x-axis component.

{3} (3a) For those compositions with exactly one component-antenna along each of x-, y-, and z-axis, the azimuth-elevation direction-of-arrival needs be estimated before the polarization parameters. There, the resulting array manifold's x-component and y-component would have imaginary parts interrelated by either

$\tan\phi$ or $\cos\theta$. For example, the composition $\{e_x, e_y, e_z\}$ has an x-component with an imaginary part of $\mathrm{Im}\{-\cos(\theta)\cos(\phi)\sin(\gamma) + \cos(\gamma)\sin(\phi)\cos(\eta) - j\cos(\gamma)\sin(\phi)\sin(\eta)\}$, and a y-component with an imaginary part of $\mathrm{Im}\{-\cos(\theta)\sin(\phi)\sin(\gamma) - \cos(\gamma)\cos(\phi)\cos(\eta) + j\cos(\gamma)\cos(\phi)\sin(\eta)\}$. They are interrelated by $-\tan\phi$.

(3b) For all other compositions, the polarization parameters need to be estimated before the azimuth-elevation direction-of-arrival. For example, for compositions with both the z-axis dipole and the z-axis loop, their array manifolds have entries $e^{j\eta}\sin(\theta)\sin(\gamma)$ and $\sin(\theta)\cos(\gamma)$, interrelated by a ratio of $-e^{j\eta}\tan(\gamma)$, which depends on only the polarization parameters.

3.3 Why Closed-Form Estimation-Formula *Un*available for the Other Four Compositions

Closed-form estimation-formulas are given in Section 3.2 for 16 compositions (out of 20 possible compositions) of a triad of orthogonally oriented dipole(s) and/or loop(s). The commonality among those 16 compositions are their inclusion of a z-axis dipole and/or a z-axis loop. With either, no closed-form estimation-formula is possible, due to the under-determined condition explained below.

Recall that each triad provides six real-value equations, from which the six real-value scalar unknowns of $\theta, \phi, \gamma, \eta, \mathrm{Re}\{\alpha\}, \mathrm{Im}\{\alpha\}$ are to be determined. However, these six equations would be linearly dependent for any of the four compositions without a z-axis dipole and without z-axis loop. Hence, the six unknowns would be under-determined.

For example, the triad $\{e_x, e_y, h_x\}$ has these six linearly dependent equations:

$$\mathrm{Re}\{\alpha\}(\cos\phi\cos\theta\sin\gamma\cos\eta - \sin\phi\cos\gamma) - \mathrm{Im}\{\alpha\}(\cos\phi\cos\theta\sin\gamma\sin\eta) = \mathrm{Re}\{[\hat{\mathbf{a}}]_1\} \quad (3.4)$$

$$\mathrm{Re}\{\alpha\}(\sin\phi\cos\theta\sin\gamma\cos\eta + \cos\phi\cos\gamma) - \mathrm{Im}\{\alpha\}(\sin\phi\cos\theta\sin\gamma\sin\eta) = \mathrm{Re}\{[\hat{\mathbf{a}}]_2\} \quad (3.5)$$

$$\mathrm{Re}\{\alpha\}(-\sin\phi\sin\gamma\cos\eta - \cos\phi\cos\theta\cos\gamma) - \mathrm{Im}\{\alpha\}(-\sin\phi\sin\gamma\sin\eta) = \mathrm{Re}\{[\hat{\mathbf{a}}]_3\} \quad (3.6)$$

$$\mathrm{Re}\{\alpha\}(\cos\phi\cos\theta\sin\gamma\sin\eta) + \mathrm{Im}\{\alpha\}(\cos\phi\cos\theta\sin\gamma\cos\eta - \sin\phi\cos\gamma) = \mathrm{Im}\{[\hat{\mathbf{a}}]_1\} \quad (3.7)$$

$$\mathrm{Re}\{\alpha\}(\sin\phi\cos\theta\sin\gamma\sin\eta) + \mathrm{Im}\{\alpha\}(\sin\phi\cos\theta\sin\gamma\cos\eta + \cos\phi\cos\gamma) = \mathrm{Im}\{[\hat{\mathbf{a}}]_2\} \quad (3.8)$$

$$\mathrm{Re}\{\alpha\}(-\sin\phi\sin\gamma\sin\eta) + \mathrm{Im}\{\alpha\}(-\sin\phi\sin\gamma\cos\eta - \cos\phi\cos\theta\cos\gamma) = \mathrm{Im}\{[\hat{\mathbf{a}}]_3\} \quad (3.9)$$

These six equations are linearly dependent, as

$$(\mathrm{Im}\{\alpha\}) \times (3.5) = (\mathrm{Re}\{\alpha\}) \times (3.8) - (\mathrm{Re}\{\alpha\})(\tan\phi) \times (3.7) + (\mathrm{Im}\{\alpha\})(\tan\phi) \times (3.4)$$

$$(\mathrm{Im}\{\alpha\}) \times (3.5) = (\mathrm{Re}\{\alpha\}) \times (3.8) + (\mathrm{Re}\{\alpha\})(\cos\theta) \times (3.9) - (\mathrm{Im}\{\alpha\})(\cos\theta) \times (3.6)$$

$$(\mathrm{Im}\{\alpha\})(\tan\phi) \times (3.4) = (\mathrm{Re}\{\alpha\})(\cos\theta) \times (3.9) - (\mathrm{Im}\{\alpha\})(\cos\theta) \times (3.6) + (\mathrm{Re}\{\alpha\})(\tan\phi) \times (3.7).$$

3.4 Monte Carlo Simulation

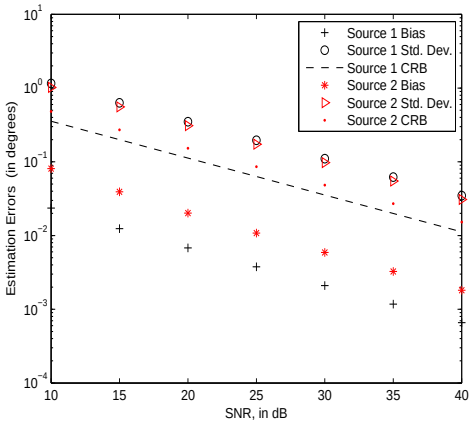

Figure 3.1a: Estimation errors in $\hat{\theta}$ for Composition 2.1: $\{e_x, e_z, h_z\}$.

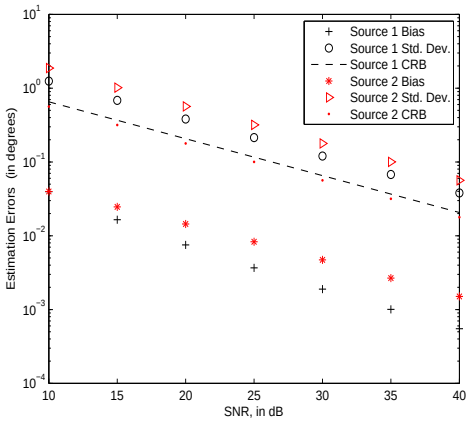

Figure 3.1b: Estimation errors in $\hat{\phi}$ for Composition 2.1: $\{e_x, e_z, h_z\}$.

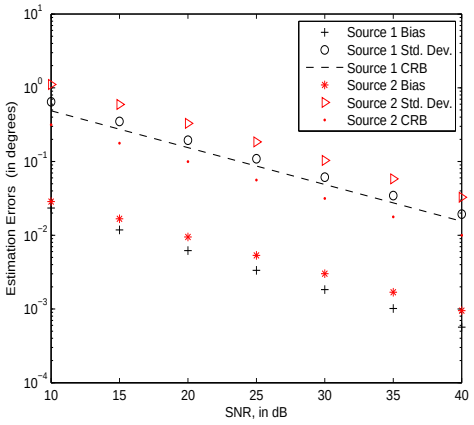

Figure 3.1c: Estimation errors in $\hat{\gamma}$ for Composition 2.1: $\{e_x, e_z, h_z\}$.

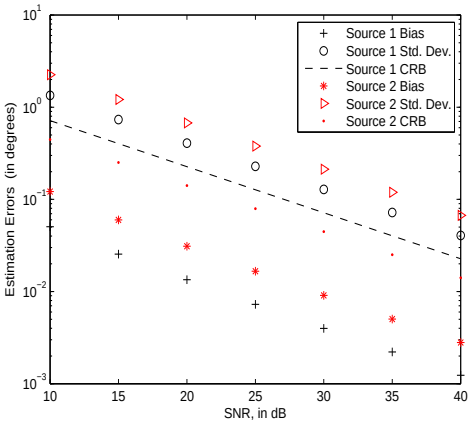

Figure 3.1d: Estimation errors in $\hat{\eta}$ for Composition 2.1: $\{e_x, e_z, h_z\}$.

To demonstrate the efficacy of the closed-form estimation-formulas with eigen-based parameter-estimation algorithms, Monte Carlo simulations are conducted here. The eigen-based parameter-estimation method used here is the *uni-vector-senor ESPRIT* method of [32]. The six-component vector-sensor in [32] is substituted by the triad.

Two pure-tone sources impinge upon the triad. Their digital frequencies are $f_1' = 0.0685$ and $f_2' = 0.2685\}$. Their elevation-azimuth angles-of-arrival are $(\theta_1, \phi_1) = (32°, 62°)$ and $(\theta_2, \phi_2) = (73°, 147°)$, with polarization states $(\gamma_1, \eta_1) = (45°, 90°)$ (left circularly polarized) and $(\gamma_2, \eta_2) = (45°, -90°)$ (right circularly polarized). Both sources have unity power. These signals are corrupted by additive noise, modeled as white complex complex Gaussian distributed (WGN). The estimates are based on 900 temporal snapshots. Each data-point on each graph consists of 2000 statistically independent Monte Carlo trials. The

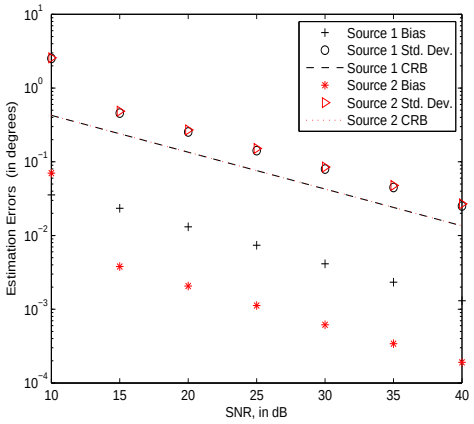

Figure 3.2a: Estimation errors in θ for Composition 1.2: $\{h_x, h_y, h_z\}$.

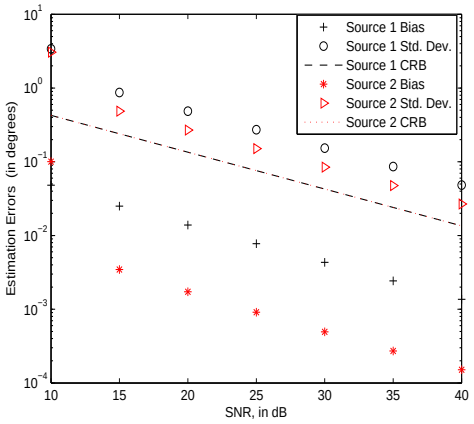

Figure 3.2b: Estimation errors in ϕ for Composition 1.2: $\{h_x, h_y, h_z\}$.

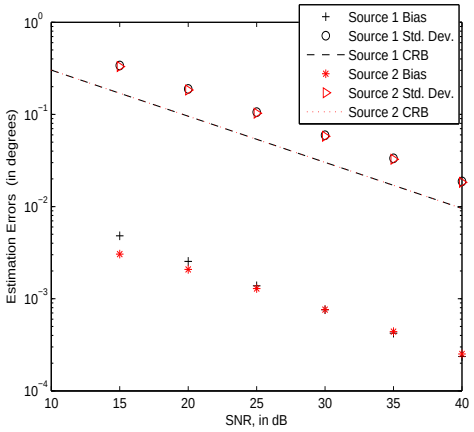

Figure 3.2c: Estimation errors in γ for Composition 1.2: $\{h_x, h_y, h_z\}$.

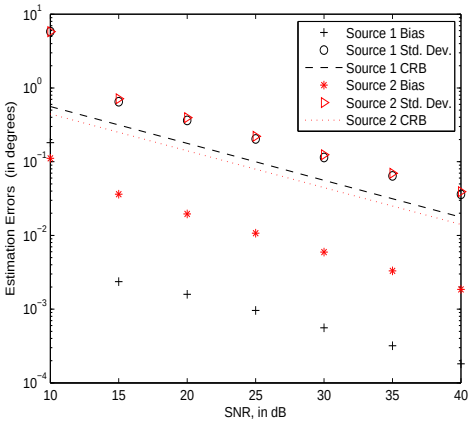

Figure 3.2d: Estimation errors in η for Composition 1.2: $\{h_x, h_y, h_z\}$.

following graphs clearly show the efficacy of the derived closed-form estimation-formula.

Figure 3.1 plots the bias and standard deviations of $(\theta, \phi, \gamma, \eta)$ for the triad $\{e_x, e_z, h_z\}$. Figure 3.2 plots the bias and standard deviations of $(\theta, \phi, \gamma, \eta)$ for the triad $\{h_x, h_y, h_z\}$. Figure 3.3 plots the bias and standard deviations of $(\theta, \phi, \gamma, \eta)$ for the triad $\{e_y, h_y, h_z\}$.

3.5 Summary

Azimuth-elevation direction finding and polarization estimation are investigated for all 20 possible different compositions of a collocated triad of orthogonally oriented dipole(s) and/or loop(s). For the 4 compositions without any dipole and any loop oriented along the z-axis, closed-form estimation is not viable. Closed-form estimation-formulas are derived for 16 compositions, 14 of these were previously *un*available in the open literature. The dipole-triad and the loop-triad alone (among all 20 compositions) allow unambiguous

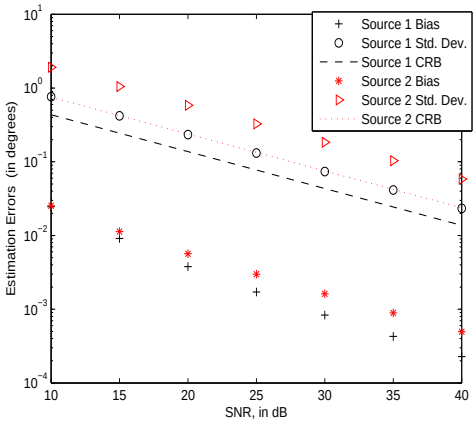

Figure 3.3a: Estimation errors in θ for Composition 4.4: $\{e_y, h_y, h_z\}$.

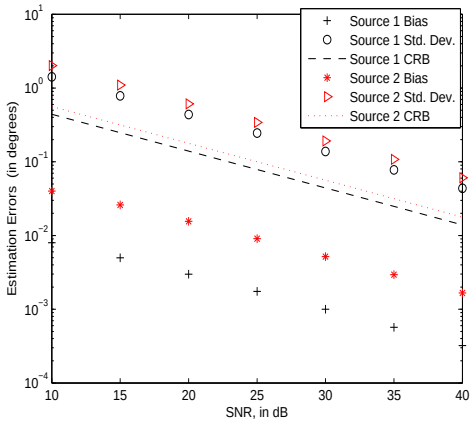

Figure 3.3b: Estimation errors in ϕ for Composition 4.4: $\{e_y, h_y, h_z\}$.

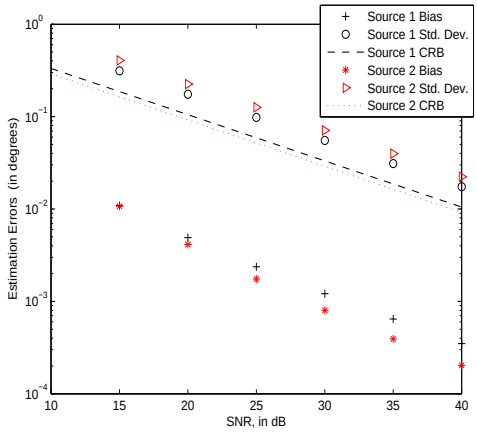

Figure 3.3c: Estimation errors in γ for Composition 4.4: $\{e_y, h_y, h_z\}$.

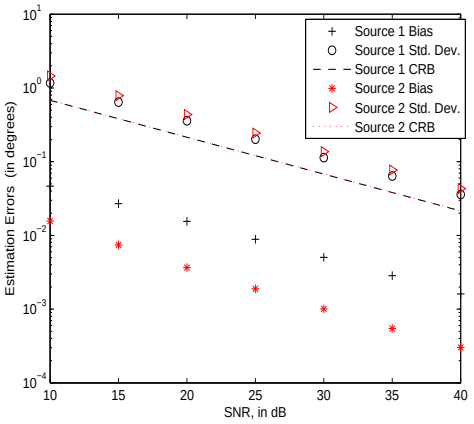

Figure 3.3d: Estimation errors in η for Composition 4.4: $\{e_y, h_y, h_z\}$.

direction-of-arrival estimation over the entire sphere. The other 14 compositions have azimuth-elevation arrival-angles estimates with only an hemispherical (not spherical) validity region, due to the hemispherical ambiguity in the trigonometric functions.

3.6 Appendix: The Detailed Derivation for Composition 1.3: $\{e_x, e_y, h_z\}$

To demonstrate detailed algebraic and trigonometric manipulations leading to the estimation-formulas in Tables 3.1-3.5, this appendix will use Composition 1.3: $\{e_x, e_y, h_z\}$ as an illustrative example.

The derivation here will start from the left-hand side of

$$\hat{\mathbf{a}} = \alpha \begin{bmatrix} e_x \\ e_y \\ h_z \end{bmatrix} = \alpha \begin{bmatrix} \cos\phi\cos\theta\sin\gamma e^{j\eta} - \sin\phi\cos\gamma \\ \sin\phi\cos\theta\sin\gamma e^{j\eta} + \cos\phi\cos\gamma \\ \sin\theta\cos\gamma \end{bmatrix}, \tag{3.10}$$

where α represents an unknown complex-value number that may have arisen from eigen-based data-processing as discussed in footnote 4.

As $\theta \in [0, \pi]$ and $\gamma \in [0, \pi/2)$, it is true that $\sin\theta\cos\gamma \geq 0$. Define

$$\begin{aligned} \mathbf{b} &\stackrel{\text{def}}{=} \hat{\mathbf{a}} e^{-j\angle[\hat{\mathbf{a}}]_3} \\ &= |\alpha| \begin{bmatrix} \cos\phi\cos\theta\sin\gamma\cos\eta - \sin\phi\cos\gamma \\ \sin\phi\cos\theta\sin\gamma\cos\eta + \cos\phi\cos\gamma \\ \sin\theta\cos\gamma \end{bmatrix} + j|\alpha| \begin{bmatrix} \cos\phi\cos\theta\sin\gamma\sin\eta \\ \sin\phi\cos\theta\sin\gamma\sin\eta \\ 0 \end{bmatrix} \end{aligned} \tag{3.11}$$

From (3.11),

$$\mathrm{Re}\{[\mathbf{b}]_1\} = |\alpha|(\cos\phi\cos\theta\sin\gamma\cos\eta - \sin\phi\cos\gamma), \tag{3.12}$$

$$\mathrm{Re}\{[\mathbf{b}]_2\} = |\alpha|(\sin\phi\cos\theta\sin\gamma\cos\eta + \cos\phi\cos\gamma), \tag{3.13}$$

$$\mathrm{Re}\{[\mathbf{b}]_3\} = |\alpha|(\sin\theta\cos\gamma), \tag{3.14}$$

$$\mathrm{Im}\{[\mathbf{b}]_1\} = |\alpha|(\cos\phi\cos\theta\sin\gamma\sin\eta), \tag{3.15}$$

$$\mathrm{Im}\{[\mathbf{b}]_2\} = |\alpha|(\sin\phi\cos\theta\sin\gamma\sin\eta). \tag{3.16}$$

3.6.1 To Derive $\hat{\phi}$

From (3.15)-(3.16),

$$\tan\phi = \frac{\mathrm{Im}\{[\mathbf{b}]_2\}}{\mathrm{Im}\{[\mathbf{b}]_1\}}. \tag{3.17}$$

As $\tan\phi = \tan(\phi + \pi)$,

$$\hat{\phi} = \begin{cases} \tan^{-1}\left(\frac{\mathrm{Im}\{[\mathbf{b}]_2\}}{\mathrm{Im}\{[\mathbf{b}]_1\}}\right), & \text{if} \quad (\cos\theta\sin\eta)\mathrm{Im}\{[\mathbf{b}]_1\} \geq 0 \\ \tan^{-1}\left(\frac{\mathrm{Im}\{[\mathbf{b}]_2\}}{\mathrm{Im}\{[\mathbf{b}]_1\}}\right) + \pi, & \text{if} \quad (\cos\theta\sin\eta)\mathrm{Im}\{[\mathbf{b}]_1\} < 0. \end{cases} \tag{3.18}$$

The above conditions arise from the following consideration:

$$\begin{aligned} (\cos\theta\sin\eta)\mathrm{Im}\{[\mathbf{b}]_1\} \geq 0 &\Rightarrow \cos\phi \geq 0 \Rightarrow \phi \in [-\pi/2, \pi/2] \\ (\cos\theta\sin\eta)\mathrm{Im}\{[\mathbf{b}]_1\} < 0 &\Rightarrow \cos\phi < 0 \Rightarrow \phi \in (\pi/2, 3\pi/2), \end{aligned}$$

which help to determine whether $\phi \in [-\pi/2, \pi/2]$ or $\phi \in (\pi/2, 3\pi/2)$. The inequalities in (3.18) require prior knowledge which of cases (i) or (ii) holds:

$$\begin{aligned} (i) \quad & \theta \in [0, \pi/2] \cap \eta \in [-\pi, 0) \Rightarrow \cos\theta\sin\eta \leq 0, \\ & \theta \in (\pi/2, \pi] \cap \eta \in [0, \pi) \Rightarrow \cos\theta\sin\eta \leq 0, \\ (ii) \quad & \theta \in [0, \pi/2] \cap \eta \in [0, \pi) \Rightarrow \cos\theta\sin\eta \geq 0, \\ & \theta \in (\pi/2, \pi] \cap \eta \in [-\pi, 0) \Rightarrow \cos\theta\sin\eta \geq 0. \end{aligned}$$

3.6.2 To Derive $\hat{\theta}$

From (3.12)-(3.13),

$$\mathrm{Re}\{[\mathbf{b}]_2\}\cos\hat{\phi} - \mathrm{Re}\{[\mathbf{b}]_1\}\sin\hat{\phi} \;=\; |\alpha|\cos\gamma. \tag{3.19}$$

Together with (3.14),

$$\sin\theta \;=\; \frac{\mathrm{Re}\,\{[\mathbf{b}]_3\}}{\mathrm{Re}\,\{[\mathbf{b}]_2\}\cos\hat{\phi} - \mathrm{Re}\,\{[\mathbf{b}]_1\}\sin\hat{\phi}}. \tag{3.20}$$

As $\sin\theta = \sin(\pi-\theta)$ for $\theta \in [0,\pi]$,

$$\hat{\theta} \;=\; \begin{cases} \sin^{-1}\left\{\left|\frac{\mathrm{Re}\{[\mathbf{b}]_3\}}{\mathrm{Re}\{[\mathbf{b}]_2\}\cos\hat{\phi}-\mathrm{Re}\{[\mathbf{b}]_1\}\sin\hat{\phi}}\right|\right\}, & \text{if} \quad \theta\in[0,\pi/2]; \\ \pi - \sin^{-1}\left\{\left|\frac{\mathrm{Re}\{[\mathbf{b}]_3\}}{\mathrm{Re}\{[\mathbf{b}]_2\}\cos\hat{\phi}-\mathrm{Re}\{[\mathbf{b}]_1\}\sin\hat{\phi}}\right|\right\}, & \text{if} \quad \theta\in(\pi/2,\pi]. \end{cases} \tag{3.21}$$

The above requires prior knowledge of whether $\theta \in [0,\pi/2]$ holds or $\theta \in (\pi/2,\pi]$ holds.

3.6.3 To Derive $\hat{\eta}$

From (3.12)-(3.13),

$$\begin{aligned} [\mathbf{b}]_1\cos\hat{\phi} + [\mathbf{b}]_2\sin\hat{\phi} &= |\alpha|\cos\theta\sin\gamma\cos\eta + j|\alpha|\cos\theta\sin\gamma\sin\eta \\ &= |\alpha|\cos\theta\sin\gamma(\cos\eta + j\sin\eta) \\ &= |\alpha|\cos\theta\sin\gamma e^{j\eta}. \end{aligned} \tag{3.22}$$

As $|\alpha|\sin\gamma \geq 0$,

$$\hat{\eta} \;=\; \angle\left\{\frac{[\mathbf{b}]_1\cos\hat{\phi} + [\mathbf{b}]_2\sin\hat{\phi}}{\cos\hat{\theta}}\right\}. \tag{3.23}$$

3.6.4 To Derive $\hat{\gamma}$

From (3.14) and (3.15),

$$\begin{aligned} \frac{\mathrm{Im}\{[\mathbf{b}]_1\}}{\mathrm{Re}\{[\mathbf{b}]_3\}} &= \tan\gamma(\cos\phi\cot\theta\sin\eta), \\ \tan\gamma &= \frac{\mathrm{Im}\{[\mathbf{b}]_1\}\tan\theta}{\mathrm{Re}\{[\mathbf{b}]_3\}\cos\phi\sin\eta}. \end{aligned} \tag{3.24}$$

As $\sin\gamma \geq 0$,

$$\hat{\gamma} \;=\; \tan^{-1}\left\{\left|\frac{\mathrm{Im}\{[\mathbf{b}]_1\}\tan\hat{\theta}}{\mathrm{Re}\{[\mathbf{b}]_3\}\cos\hat{\phi}\sin\hat{\eta}}\right|\right\}. \tag{3.25}$$

3.6.5 The Validity Region

Examining the prior knowledge required by the four estimation-formulas of (3.18), (3.21), (3.23) and (3.25), those estimation-formulas' validity region equals $\{\theta \in [0,\frac{\pi}{2}] \text{ or } \theta \in (\frac{\pi}{2},\pi]\} \cap \{\phi\in[0,2\pi)\} \cap \{\gamma\in[0,\frac{\pi}{2})\} \cap \{\eta \in [-\pi,0) \text{ or } \eta\in[0,\pi)\}$.

Chapter 4

Polarization Estimation with a Dipole-Dipole Pair, a Dipole-Loop Pair, or a Loop-Loop Pair of Various Orientations

Polarization is bivariate; hence, a minimum of two diversely polarized antennas are needed for polarimetry of a fully polarized wavefield. If limiting the choice of antennas to linearly polarized antennas (i.e. dipole(s) or/and loop(s)) aligned along some Cartesian axes, there exist $\begin{pmatrix} 6 \\ 2 \end{pmatrix} = 15$ possible antenna/orientation configurations, because two components are here chosen, out of a total of six electromagnetic components. The open literature presently offers no comprehensive comparison among these 15 configurations, even though the effectiveness of polarimetry depends critically on what and how the antennas are employed. This literature gap is filled by this chapter.

As reviewed in Section 1.2.3, closed-form estimation formulas are available in the open literature for polarization-parameters (with the incident source's direction-of-arrival is already known) for three out of fifteen possible antenna/orientation configurations. In this Chapter, Section 4.2 will provide closed-form estimation formulas for the other twelve. Section 4.3 will derive and will compare the corresponding Cramér-Rao lower bounds in polarization-estimation for these fifteen antenna/orientation configurations. Lastly, Section 4.4 will contrast these fifteen configurations' intrinsic numerical stability, with respect to the matrix-inversion implicitly involved in the polarization estimation, given prior knowledge of the direction-of-arrival. [1]

[1] Much of this chapter appears in [168].

4.1 The Antenna-Pair's Array Manifold

A fully polarized transverse electromagnetic wave is characterized by its six-component electromagnetic-field vector (equations (2.5)-(2.8) and (2.11)-(2.12) in [20] with the noise there set to zero),

$$\begin{bmatrix} \mathbf{e} \\ \mathbf{h} \end{bmatrix} = \begin{bmatrix} e_x \\ e_y \\ e_z \\ h_x \\ h_y \\ h_z \end{bmatrix} \stackrel{\text{def}}{=} \begin{bmatrix} e^{j\eta}\cos\phi\cos\theta\sin\gamma - \sin\phi\cos\gamma \\ e^{j\eta}\sin\phi\cos\theta\sin\gamma + \cos\phi\cos\gamma \\ -e^{j\eta}\sin\theta\sin\gamma \\ -e^{j\eta}\sin\phi\sin\gamma - \cos\phi\cos\theta\cos\gamma \\ e^{j\eta}\cos\phi\sin\gamma - \sin\phi\cos\theta\cos\gamma \\ \sin\theta\cos\gamma \end{bmatrix} = \underbrace{\begin{bmatrix} \mathbf{v}_1 & \mathbf{v}_2 \\ \mathbf{v}_2 & -\mathbf{v}_1 \end{bmatrix}}_{\stackrel{\text{def}}{=}\boldsymbol{\Theta}} \underbrace{\begin{bmatrix} \sin\gamma\, e^{j\eta} \\ \cos\gamma \end{bmatrix}}_{\stackrel{\text{def}}{=}\mathbf{g}} \quad (4.1)$$

where $\theta \in [0, \pi]$ signifies the emitter's elevation-angle measured from the positive z-axis, $\phi \in [0, 2\pi)$ denotes the corresponding azimuth-angle measured from the positive x-axis, $\gamma \in [0, \pi/2)$ refers to the auxiliary polarization angle, $\eta \in [-\pi, \pi)$ symbolizes the polarization phase difference, $\mathbf{v}_1 = [\cos\phi\cos\theta, \sin\phi\cos\theta, -\sin\theta]^T$, $\mathbf{v}_2 = [-\sin\phi, \cos\phi, 0]^T$. Note that $\boldsymbol{\Theta}$ depends on only the incident source's direction-of-arrival (DOA) and enjoys a block-radialoid structure, whereas $\mathbf{g}$ depends on only the sources' polarization state.

If the receive-antennas are either dipoles and/or loops, and if these receive-antennas orient along some Cartesian axes, then the array manifold would equal the two corresponding components of the six-element vector in (4.1). Thus, $\frac{6!}{2!4!} = 15$ different antenna/orientation configurations are possible for such an antenna-pair. For this selection of 2 out of 6 elements, it may be represented by a 2×6 selection-matrix $\mathbf{S}$, which has a "1" on each row, but zeroes elsewhere.

All subsequent analysis will allow these two receive-antennas to be spatially separated or collocated – the latter obviously represents a degenerate case of the former. More mathematically, let one antenna be located at the Cartesian origin, with the other antenna at a known location $(\Delta_x, \Delta_y, \Delta_z)$, without loss of generality. Then, a spatial phase-factor of $\exp\{-j\frac{2\pi}{\lambda}(\Delta_x \sin\theta\sin\phi + \Delta_y \sin\theta\cos\phi + \Delta_z\cos\theta)\}$ would exist between these two antennas. Each of these 15 configurations would have a 2×1 array-manifold,

$$\mathbf{a} = \underbrace{\begin{bmatrix} 1 & 0 \\ 0 & \exp\{-j\frac{2\pi}{\lambda}(\Delta_x \sin\theta\sin\phi + \Delta_y \sin\theta\cos\phi + \Delta_z\cos\theta)\} \end{bmatrix}}_{\stackrel{\text{def}}{=}\mathbf{D}} \mathbf{S} \begin{bmatrix} \mathbf{e} \\ \mathbf{h} \end{bmatrix}. \quad (4.2)$$

The question is: Which of these fifteen antenna-pair options would be "best", to estimate γ and η unambiguously. This work will investigate this issue, with regard to the numerical stability, the estimation accuracy, and the estimation validity-region of each antenna/orientation configuration.

Note that a number of relationships exist among the array manifolds of these 15 configurations:

$$\begin{aligned}
\mathbf{a}_{\{e_y,h_y\}}(\theta,\phi,\gamma,\eta) &= \mathbf{a}_{\{e_x,h_x\}}\left(\theta,\phi-\frac{\pi}{2},\gamma,\eta\right),\\
\mathbf{a}_{\{e_y,e_z\}}(\theta,\phi,\gamma,\eta) &= \mathbf{a}_{\{e_x,e_z\}}\left(\theta,\phi-\frac{\pi}{2},\gamma,\eta\right),\\
\mathbf{a}_{\{h_y,h_z\}}(\theta,\phi,\gamma,\eta) &= \mathbf{a}_{\{h_x,h_z\}}\left(\theta,\phi-\frac{\pi}{2},\gamma,\eta\right),\\
\mathbf{a}_{\{h_x,h_y\}}(\theta,\phi,\gamma,\eta) &= \mathbf{a}_{\{e_x,e_y\}}\left(\theta,\phi,\gamma-\frac{\pi}{2},-\eta\right)e^{j\eta},\\
\mathbf{a}_{\{h_x,h_z\}}(\theta,\phi,\gamma,\eta) &= \mathbf{a}_{\{e_x,e_z\}}\left(\theta,\phi,\gamma-\frac{\pi}{2},-\eta\right)e^{j\eta},\\
\mathbf{a}_{\{h_y,h_z\}}(\theta,\phi,\gamma,\eta) &= \mathbf{a}_{\{e_y,e_z\}}\left(\theta,\phi,\gamma-\frac{\pi}{2},-\eta\right)e^{j\eta}\\
&= \mathbf{a}_{\{e_x,e_z\}}\left(\theta,\phi-\frac{\pi}{2},\gamma-\frac{\pi}{2},-\eta\right)e^{j\eta},\\
\mathbf{a}_{\{e_y,h_z\}}(\theta,\phi,\gamma,\eta) &= \mathbf{a}_{\{e_x,h_z\}}\left(\theta,\phi-\frac{\pi}{2},\gamma,\eta\right),\\
\mathbf{a}_{\{h_y,e_z\}}(\theta,\phi,\gamma,\eta) &= \mathbf{a}_{\{h_x,e_z\}}\left(\theta,\phi-\frac{\pi}{2},\gamma,\eta\right).
\end{aligned}$$

4.2 The Polarization-Estimation Formulas for All 15 Antenna/Orientation Configurations

Eigen-based parameter-estimation algorithms typically involve an intermediate step, that estimates each incident source's steering vector, correct to within an *unknown* complex-value scalar c. That is, available (for each incident source)[2] is the estimate $\hat{\mathbf{a}} \approx c\mathbf{a}$, from which γ and η are to be estimated. (This approximation becomes equality in noiseless or asymptotic cases.) Hence, there exist two equations and two unknowns. Algebraic manipulation of the two equations yields the estimation formulas of $\hat{\gamma}$ and $\hat{\eta}$. For example, consider the $\{e_x, h_x\}$ pair (i.e. configuration 1A of Table 4.1). The two equations are the two rows of

$$c\mathbf{a} = c\begin{bmatrix} 1 & 0 \\ 0 & e^{-j\frac{2\pi}{\lambda}(\Delta_x \sin\theta\sin\phi+\Delta_y\sin\theta\cos\phi+\Delta_z\cos\theta)} \end{bmatrix}\begin{bmatrix} 1 & 0 & 0 & 0 & 0 & 0 \\ 0 & 0 & 0 & 1 & 0 & 0 \end{bmatrix}\mathbf{\Theta}\begin{bmatrix} \sin\gamma\, e^{j\eta} \\ \cos\gamma \end{bmatrix}. \tag{4.3}$$

The two unknowns are γ and η, with $\Delta_x, \Delta_y, \Delta_z, \theta, \phi$, and λ (thus $\mathbf{\Theta}$) already known.[3]

Table 4.1 lists the estimation formulas of $\hat{\gamma}$ and $\hat{\eta}$, for each of the 15 antenna/orientation configurations. [4]There, $B = \frac{2\pi}{\lambda}(\Delta_x \sin\theta\sin\phi+\Delta_y\sin\theta\cos\phi+\Delta_z\cos\theta)$. These estimation-formulas are applicable for the entire validity-region of $\gamma \in [0, \frac{\pi}{2})$ and $\eta \in [-\pi, \pi)$. These

[2]This does NOT presume only a single source impinging upon the receiver. There could be multiple sources. Moreover, these several sources could possibly be cross-correlated, broadband, and/or time-varying.

[3] If $\Delta_x = \Delta_y = \Delta_z = 0$ here, (4.3) gives the "COLD" array oriented along the x-axis.

[4]To facilitate the subsequent exposition, the orthogonal-loop-and-dipole (OLD) configurations of 1A, 1B and 1C in Table 4.1 will be identified as the "OLD array".

estimation-formulas are new to the open literature, to the best knowledge of the present authors, except those few antenna/orientation configurations with references cited in Table 4.1.

It is noteworthy that the vertically oriented "OLD array" (i.e. the $\{e_z, h_z\}$ configuration) has estimation-formulas independent of the source's direction-of-arrival; hence, $\hat{\gamma}$ and $\hat{\eta}$ there require no prior information of θ and ϕ. This independence applies to no other antenna/orientation configuration. This vertically oriented "OLD array" is unique in this regard, because

(i) Its array manifold is independent of the azimuth-angle ϕ.

(ii) Though its array manifold depends on the elevation-angle θ through (and only through) $\sin\theta$, this $\sin\theta$ factor is common to both entries in the array manifold. Hence, the ratio between these two entries would be independent of θ.

Table 4.1: Polarization-Estimation Formulas of the 15 Antenna/Orientation Configurations

Configuration	Antenna-Pair	$\hat{\gamma} =$	$\hat{\eta} =$
1A	$\{e_x, h_x\}$	$\tan^{-1}\left\{\sqrt{\frac{([\hat{\mathbf{a}}]_2)^2\sin^2\phi+([\hat{\mathbf{a}}]_1)^2(\cos\phi\cos\theta)^2-[\hat{\mathbf{a}}]_1[\hat{\mathbf{a}}]_2\sin(2\phi)\cos\theta\cos B}{([\hat{\mathbf{a}}]_1)^2\sin^2\phi+([\hat{\mathbf{a}}]_2)^2(\cos\phi\cos\theta)^2+[\hat{\mathbf{a}}]_1[\hat{\mathbf{a}}]_2\sin(2\phi)\cos\theta\cos B}}\right\}$	$\angle\left\{\frac{[\hat{\mathbf{a}}]_2\sin\phi-[\hat{\mathbf{a}}]_1\cos\phi\cos\theta\cos B+j[\hat{\mathbf{a}}]_1\cos\phi\cos\theta\sin B}{[\hat{\mathbf{a}}]_1\sin\phi\cos B+[\hat{\mathbf{a}}]_2\cos\phi\cos\theta-j[\hat{\mathbf{a}}]_1\sin\phi\sin B}\right\}$
1B	$\{e_y, h_y\}$	$\tan^{-1}\left\{\sqrt{\frac{([\hat{\mathbf{a}}]_1)^2(\sin\phi\cos\theta)^2+([\hat{\mathbf{a}}]_2)^2\cos^2\phi+[\hat{\mathbf{a}}]_1[\hat{\mathbf{a}}]_2\sin(2\phi)\cos\theta\cos B}{([\hat{\mathbf{a}}]_2)^2(\sin\phi\cos\theta)^2+([\hat{\mathbf{a}}]_1)^2\cos^2\phi-[\hat{\mathbf{a}}]_1[\hat{\mathbf{a}}]_2\sin(2\phi)\cos\theta\cos B}}\right\}$	$\angle\left\{\frac{-[\hat{\mathbf{a}}]_1\sin\phi\cos\theta\cos B-[\hat{\mathbf{a}}]_2\cos\phi+j[\hat{\mathbf{a}}]_1\sin\phi\cos\theta\sin B}{-[\hat{\mathbf{a}}]_1\cos\phi\cos B+[\hat{\mathbf{a}}]_2\sin\phi\cos\theta+j[\hat{\mathbf{a}}]_1\cos\phi\sin B}\right\}$
1C	$\{e_z, h_z\}$	$\tan^{-1}\left\{\left\lvert\frac{[\hat{\mathbf{a}}]_1}{[\hat{\mathbf{a}}]_2}\right\rvert\right\}$ [29, 88, 127, 153]	$\angle\left\{\frac{[\hat{\mathbf{a}}]_1\cos B-j[\hat{\mathbf{a}}]_1\sin B}{-[\hat{\mathbf{a}}]_2}\right\}$ [29, 88, 127, 153]
2A	$\{e_x, e_y\}$	$\tan^{-1}\left\{\frac{1}{\lvert\cos\theta\rvert}\sqrt{\frac{([\hat{\mathbf{a}}]_1)^2\cos^2\phi+([\hat{\mathbf{a}}]_2)^2\sin^2\phi+[\hat{\mathbf{a}}]_1[\hat{\mathbf{a}}]_2\sin(2\phi)\cos B}{[\hat{\mathbf{a}}]_2)^2\cos^2\phi+([\hat{\mathbf{a}}]_1)^2\sin^2\phi-[\hat{\mathbf{a}}]_1[\hat{\mathbf{a}}]_2\sin(2\phi)\cos B}}\right\}$ [11, 13, 31, 108, 138, 152, 157, 159]	$\angle\left\{\frac{[\hat{\mathbf{a}}]_1\cos\phi\cos B+[\hat{\mathbf{a}}]_2\sin\phi-j[\hat{\mathbf{a}}]_1\cos\phi\sin B}{\cos\theta([\hat{\mathbf{a}}]_2\cos\phi-[\hat{\mathbf{a}}]_1\sin\phi\cos B+j[\hat{\mathbf{a}}]_1\sin\phi\sin B)}\right\}$ [11, 13, 31, 108, 138, 152, 157, 159]
2B	$\{h_x, h_y\}$	$\tan^{-1}\left\{\lvert\cos\theta\rvert\sqrt{\frac{([\hat{\mathbf{a}}]_1)^2\sin^2\phi+([\hat{\mathbf{a}}]_2)^2\cos^2\phi-[\hat{\mathbf{a}}]_1[\hat{\mathbf{a}}]_2\sin(2\phi)\cos B}{([\hat{\mathbf{a}}]_1)^2\cos^2\phi+([\hat{\mathbf{a}}]_2)^2\sin^2\phi+[\hat{\mathbf{a}}]_1[\hat{\mathbf{a}}]_2\sin(2\phi)\cos B}}\right\}$	$\angle\left\{\frac{\cos\theta([\hat{\mathbf{a}}]_2\cos\phi-[\hat{\mathbf{a}}]_1\sin\phi\cos B+j[\hat{\mathbf{a}}]_1\sin\phi\sin B)}{-[\hat{\mathbf{a}}]_2\sin\phi-[\hat{\mathbf{a}}]_1\cos\phi\cos B+j[\hat{\mathbf{a}}]_1\cos\phi\sin B}\right\}$
3A	$\{e_x, e_z\}$	$\tan^{-1}\left\{\sqrt{\frac{([\hat{\mathbf{a}}]_2)^2\sin^2\phi}{([\hat{\mathbf{a}}]_1)^2\sin^2\theta+([\hat{\mathbf{a}}]_2)^2(\cos\phi\cos\theta)^2+[\hat{\mathbf{a}}]_1[\hat{\mathbf{a}}]_2\sin(2\theta)\cos\phi\cos B}}\right\}$ [70]	$\angle\left\{\frac{[\hat{\mathbf{a}}]_2\sin\phi}{[\hat{\mathbf{a}}]_1\sin\theta\cos B+[\hat{\mathbf{a}}]_2\cos\phi\cos\theta-j[\hat{\mathbf{a}}]_1\sin\theta\sin B}\right\}$ [70]
3B	$\{h_x, h_z\}$	$\tan^{-1}\left\{\sqrt{\frac{([\hat{\mathbf{a}}]_1)^2\sin^2\theta+([\hat{\mathbf{a}}]_2)^2(\cos\phi\cos\theta)^2+[\hat{\mathbf{a}}]_1[\hat{\mathbf{a}}]_2\sin(2\theta)\cos\phi\cos B}{([\hat{\mathbf{a}}]_2)^2\sin^2\phi}}\right\}$	$\angle\left\{\frac{[\hat{\mathbf{a}}]_1\sin\theta\cos B+[\hat{\mathbf{a}}]_2\cos\phi\cos\theta-j[\hat{\mathbf{a}}]_1\sin\theta\sin B}{-[\hat{\mathbf{a}}]_2\sin\phi}\right\}$
4A	$\{e_y, e_z\}$	$\tan^{-1}\left\{\sqrt{\frac{([\hat{\mathbf{a}}]_2)^2\cos^2\phi}{([\hat{\mathbf{a}}]_1)^2\sin^2\theta+([\hat{\mathbf{a}}]_2)^2(\sin\phi\cos\theta)^2+[\hat{\mathbf{a}}]_1[\hat{\mathbf{a}}]_2\sin(2\theta)\sin\phi\cos B}}\right\}$	$\angle\left\{\frac{-[\hat{\mathbf{a}}]_2\cos\phi}{[\hat{\mathbf{a}}]_1\sin\theta\cos B+[\hat{\mathbf{a}}]_2\sin\phi\cos\theta-j[\hat{\mathbf{a}}]_1\sin\theta\sin B}\right\}$
4B	$\{h_y, h_z\}$	$\tan^{-1}\left\{\sqrt{\frac{([\hat{\mathbf{a}}]_1)^2\sin^2\theta+([\hat{\mathbf{a}}]_2)^2(\sin\phi\cos\theta)^2+[\hat{\mathbf{a}}]_1[\hat{\mathbf{a}}]_2\sin(2\theta)\sin\phi\cos B}{([\hat{\mathbf{a}}]_2)^2\cos^2\phi}}\right\}$	$\angle\left\{\frac{[\hat{\mathbf{a}}]_1\sin\theta\cos B+[\hat{\mathbf{a}}]_2\sin\phi\cos\theta-j[\hat{\mathbf{a}}]_1\sin\theta\sin B}{[\hat{\mathbf{a}}]_2\cos\phi}\right\}$
5A	$\{e_x, h_y\}$	$\tan^{-1}\left\{\sqrt{\frac{([\hat{\mathbf{a}}]_1)^2(\sin\phi\cos\theta)^2+([\hat{\mathbf{a}}]_2)^2\sin^2\phi-2[\hat{\mathbf{a}}]_1[\hat{\mathbf{a}}]_2\sin^2\phi\cos\theta\cos B}{([\hat{\mathbf{a}}]_2)^2(\cos\phi\cos\theta)^2+([\hat{\mathbf{a}}]_1)^2\cos^2\phi-2[\hat{\mathbf{a}}]_1[\hat{\mathbf{a}}]_2\cos^2\phi\cos\theta\cos B}}\right\}$	$\angle\left\{\frac{[\hat{\mathbf{a}}]_2\sin\phi-[\hat{\mathbf{a}}]_1\sin\phi\cos\theta\cos B+j[\hat{\mathbf{a}}]_1\sin\phi\cos\theta\sin B}{[\hat{\mathbf{a}}]_2\cos\phi\cos\theta-[\hat{\mathbf{a}}]_1\cos\phi\cos B+j[\hat{\mathbf{a}}]_1\cos\phi\sin B}\right\}$
5B	$\{h_x, e_y\}$	$\tan^{-1}\left\{\sqrt{\frac{\cos^2\phi\left\{([\hat{\mathbf{a}}]_1)^2+([\hat{\mathbf{a}}]_2)^2\cos^2\theta+2[\hat{\mathbf{a}}]_1[\hat{\mathbf{a}}]_2\cos\theta\cos B\right\}}{\sin^2\phi\left\{([\hat{\mathbf{a}}]_1)^2\cos^2\theta+([\hat{\mathbf{a}}]_2)^2+2[\hat{\mathbf{a}}]_1[\hat{\mathbf{a}}]_2\cos\theta\cos B\right\}}}\right\}$	$\angle\left\{\frac{\cos\phi([\hat{\mathbf{a}}]_1\cos B+[\hat{\mathbf{a}}]_2\cos\theta-j[\hat{\mathbf{a}}]_1\sin B)}{-\sin\phi([\hat{\mathbf{a}}]_1\cos\theta\cos B+[\hat{\mathbf{a}}]_2-j[\hat{\mathbf{a}}]_1\cos\theta\sin B)}\right\}$
6A	$\{e_x, h_z\}$	$\tan^{-1}\left\{\sqrt{\frac{([\hat{\mathbf{a}}]_1)^2\sin^2\theta+([\hat{\mathbf{a}}]_2)^2\sin^2\phi+2[\hat{\mathbf{a}}]_1[\hat{\mathbf{a}}]_2\sin\theta\sin\phi\cos B}{([\hat{\mathbf{a}}]_2)^2(\cos\phi\cos\theta)^2}}\right\}$	$\angle\left\{\frac{[\hat{\mathbf{a}}]_1\sin\theta\cos B+[\hat{\mathbf{a}}]_2\sin\phi-j[\hat{\mathbf{a}}]_1\sin\theta\sin B}{[\hat{\mathbf{a}}]_2\cos\phi\cos\theta}\right\}$
6B	$\{h_x, e_z\}$	$\tan^{-1}\left\{\sqrt{\frac{([\hat{\mathbf{a}}]_2)^2(\cos\phi\cos\theta)^2}{([\hat{\mathbf{a}}]_1)^2\sin^2\theta+([\hat{\mathbf{a}}]_2)^2\sin^2\phi-2[\hat{\mathbf{a}}]_1[\hat{\mathbf{a}}]_2\sin\theta\sin\phi\cos B}}\right\}$	$\angle\left\{\frac{[\hat{\mathbf{a}}]_2\cos\phi\cos\theta}{[\hat{\mathbf{a}}]_1\sin\theta\cos B-[\hat{\mathbf{a}}]_2\sin\phi-j[\hat{\mathbf{a}}]_1\sin\theta\sin B}\right\}$
7A	$\{e_y, h_z\}$	$\tan^{-1}\left\{\sqrt{\frac{([\hat{\mathbf{a}}]_1)^2\sin^2\theta+([\hat{\mathbf{a}}]_2)^2\cos^2\phi-2[\hat{\mathbf{a}}]_1[\hat{\mathbf{a}}]_2\sin\theta\cos\phi\cos B}{([\hat{\mathbf{a}}]_2)^2(\sin\phi\cos\theta)^2}}\right\}$	$\angle\left\{\frac{[\hat{\mathbf{a}}]_1\sin\theta\cos B-[\hat{\mathbf{a}}]_2\cos\phi-j[\hat{\mathbf{a}}]_1\sin\theta\sin B}{[\hat{\mathbf{a}}]_2\sin\phi\cos\theta}\right\}$
7B	$\{h_y, e_z\}$	$\tan^{-1}\left\{\sqrt{\frac{([\hat{\mathbf{a}}]_2)^2(\sin\phi\cos\theta)^2}{([\hat{\mathbf{a}}]_1)^2\sin^2\theta+([\hat{\mathbf{a}}]_2)^2\cos^2\phi+2[\hat{\mathbf{a}}]_1[\hat{\mathbf{a}}]_2\sin\theta\cos\phi\cos B}}\right\}$	$\angle\left\{\frac{[\hat{\mathbf{a}}]_2\sin\phi\cos\theta}{[\hat{\mathbf{a}}]_1\sin\theta\cos B+[\hat{\mathbf{a}}]_2\cos\phi-j[\hat{\mathbf{a}}]_1\sin\theta\sin B}\right\}$

4.3 Cramér-Rao Bounds, CRB(γ) and CRB(η), for All 15 Antenna/Orientation Configurations of Section 4.2

To avoid unnecessary distraction from the present objective to compare among the fifteen antenna/orientation configurations, a very simple statistical data model will be used here for the Cramér-Rao bound derivation: The received signal $s(t) = e^{j(2\pi f_o + \epsilon)}$ is a pure tone at unity-power, a known frequency of f_o, and a known initial phase of ϵ. At the mth time-instant of $t = mT_s$, the antenna-pair collects the 2×1 data-vector,

$$\mathbf{z}(mT_s) \quad = \quad \mathbf{a}s(mT_s) + \mathbf{n}(mT_s), \tag{4.4}$$

where T_s refers to the time-sampling period, $\mathbf{n}(t)$ denotes a 2×1 vector of spatio-temporally uncorrelated zero-mean complex Gaussian additive noise, with an unknown deterministic covariance-matrix of $\mathbf{\Gamma}_0 = \text{diag}\left(\sigma^2, \sigma^2\right)$, where σ^2 representing the known noise-variance at each antenna.

With M number of time-samples, the $2M \times 1$ collected data-set equals

$$\boldsymbol{\zeta} \quad = \quad \left[(\mathbf{z}(T_s))^T, \cdots, (\mathbf{z}(MT_s))^T\right]^T \quad = \quad \underbrace{\mathbf{s} \otimes \mathbf{a}}_{=\boldsymbol{\mu}} + \underbrace{\left[(\mathbf{n}(T_s))^T, \cdots, (\mathbf{n}(MT_s))^T\right]^T}_{=\boldsymbol{\nu}}, \tag{4.5}$$

where $\mathbf{s} = e^{j\epsilon}\left[e^{jT_s\omega}, e^{j2T_s\omega}, \cdots, e^{jMT_s\omega}\right]^T$, $\boldsymbol{\nu}$ represents a $2M \times 1$ noise vector with a spatio-temporal covariance matrix of $\mathbf{\Gamma} = \mathbf{I}_M \otimes \mathbf{\Gamma}_0$, and $\mathbf{I}_M$ denotes an $M \times M$ identity matrix. Therefore, $\boldsymbol{\zeta} \sim \mathcal{N}(\boldsymbol{\mu}, \mathbf{\Gamma})$, i.e. a Gaussian vector with mean $\boldsymbol{\mu}$ and covariance $\mathbf{\Gamma}$.

The to-be-estimated γ and η are modeled as deterministic. Collect all deterministic unknown entities into the 2×1 vector of $\boldsymbol{\psi} = [\gamma, \eta]^T$. The resulting 2×2 Fisher Information Matrix (FIM)

$$\mathbf{J} \quad = \quad \begin{bmatrix} J_{\gamma,\gamma} & J_{\gamma,\eta} \\ J_{\eta,\gamma} & J_{\eta,\eta} \end{bmatrix} \tag{4.6}$$

has its (i,j)th entry equal to (please see equation (8.34) in [62]):

$$[\mathbf{J}]_{i,j} \quad = \quad 2\text{Re}\left[\left(\frac{\partial \boldsymbol{\mu}}{\partial [\boldsymbol{\psi}]_i}\right)^H \mathbf{\Gamma}^{-1} \left(\frac{\partial \boldsymbol{\mu}}{\partial [\boldsymbol{\psi}]_j}\right)\right] + \text{Tr}\left[\mathbf{\Gamma}^{-1}\frac{\partial \mathbf{\Gamma}}{\partial [\boldsymbol{\psi}]_i}\mathbf{\Gamma}^{-1}\frac{\partial \mathbf{\Gamma}}{\partial [\boldsymbol{\psi}]_j}\right], \tag{4.7}$$

where Re[.] denotes the real-value part of the entity inside [.], Tr[.] represents the trace

operator, and

$$\frac{\partial \boldsymbol{\mu}}{\partial \gamma} = \frac{\partial \mathbf{a}}{\partial \gamma} \otimes \mathbf{s}, \tag{4.8}$$

$$\frac{\partial \boldsymbol{\mu}}{\partial \eta} = \frac{\partial \mathbf{a}}{\partial \eta} \otimes \mathbf{s}, \tag{4.9}$$

$$\frac{\partial \mathbf{a}}{\partial \gamma} = \boldsymbol{\Omega} \begin{bmatrix} \cos\gamma e^{j\eta} \\ -\sin\gamma \end{bmatrix}, \tag{4.10}$$

$$\frac{\partial \mathbf{a}}{\partial \eta} = \boldsymbol{\Omega} \begin{bmatrix} j\sin\gamma e^{j\eta} \\ 0 \end{bmatrix}. \tag{4.11}$$

where $\boldsymbol{\Omega} \stackrel{\text{def}}{=} \mathbf{DS\Theta}$.

The elements of the Fisher Information Matrix equal:

$$\begin{aligned} J_{\gamma,\gamma} &= \frac{2M}{\sigma^2}\Big\{[([\mathbf{S\Theta}]_{1,1})^2 + ([\mathbf{S\Theta}]_{2,1})^2](\cos\gamma)^2 + [([\mathbf{S\Theta}]_{1,2})^2 + ([\mathbf{S\Theta}]_{2,2})^2](\sin\gamma)^2 \\ &\qquad -([\mathbf{S\Theta}]_{1,1}[\mathbf{S\Theta}]_{1,2} + [\mathbf{S\Theta}]_{2,1}[\mathbf{S\Theta}]_{2,2})\sin(2\gamma)(\cos\eta)\Big\} \qquad (4.12) \\ &= \frac{2M}{\sigma^2}\left[c_1(\cos\gamma)^2 + c_2(\sin\gamma)^2 - c_3\sin(2\gamma)(\cos\eta)\right], \qquad (4.13) \\ J_{\eta,\eta} &= \frac{2M}{\sigma^2}\left[([\mathbf{S\Theta}]_{1,1})^2 + ([\mathbf{S\Theta}]_{2,1})^2\right](\sin\gamma)^2 = \frac{2M}{\sigma^2}c_1(\sin\gamma)^2, \qquad (4.14) \\ J_{\gamma,\eta} &= \frac{2M}{\sigma^2}\Big[([\mathbf{S\Theta}]_{1,1}[\mathbf{S\Theta}]_{1,2} + [\mathbf{S\Theta}]_{2,1}[\mathbf{S\Theta}]_{2,2})(\sin\gamma)(\sin\eta)\Big] \\ &= \frac{2M}{\sigma^2}c_3(\sin\gamma)^2(\sin\eta), \qquad (4.15) \end{aligned}$$

where $c_1 = ([\mathbf{S\Theta}]_{1,1})^2 + ([\mathbf{S\Theta}]_{2,1})^2$, $c_2 = ([\mathbf{S\Theta}]_{1,2})^2 + ([\mathbf{S\Theta}]_{2,2})^2$, and $c_3 = [\mathbf{S\Theta}]_{1,1}[\mathbf{S\Theta}]_{1,2} + [\mathbf{S\Theta}]_{2,1}[\mathbf{S\Theta}]_{2,2}$, with $[\cdot]_{i,j}$ symbolizing the (i,j)th entry of the matrix in $[\cdot]$.

The polarization-estimation Cramér-Rao bounds equal

$$\begin{aligned} \mathrm{CRB}(\gamma) &= \left[\mathbf{J}^{-1}\right]_{1,1} \\ &= \frac{J_{\eta,\eta}}{J_{\gamma,\gamma}J_{\eta,\eta} - (J_{\gamma,\eta})^2} \\ &= \frac{\sigma^2}{2M}\frac{c_1}{[c_1^2(\cos\gamma)^2 + c_1c_2(\sin\gamma)^2 - c_3c_1\sin(2\gamma)(\cos\eta) - c_3^2(\sin\gamma)^2(\sin\eta)^2]}, \qquad (4.16) \\ \mathrm{CRB}(\eta) &= \left[\mathbf{J}^{-1}\right]_{2,2} \\ &= \frac{J_{\gamma,\gamma}}{J_{\gamma,\gamma}J_{\eta,\eta} - (J_{\gamma,\eta})^2} \\ &= \frac{\sigma^2}{2M}\frac{1}{(\sin\gamma)^2}\frac{[c_1(\cos\gamma)^2 + c_2(\sin\gamma)^2 - c_3\sin(2\gamma)(\cos\eta)]}{[c_1^2(\cos\gamma)^2 + c_1c_2(\sin\gamma)^2 - c_3c_1\sin(2\gamma)(\cos\eta) - c_3^2(\sin\gamma)^2(\sin\eta)^2]}. \qquad (4.17) \end{aligned}$$

Tables 4.2-4.3 [5] list the closed-form formulas for CRB(γ) and CRB(η), explicitly in terms of the data-model parameters. These Cramér-Rao bounds would be *un*changed by

[5] In these tables, $c_4 = (\cos\eta)(\cos\phi)(\sin\phi)(\cos\theta)\sin(2\gamma)$, $c_5 = 1 + 2(\cos\eta)^2(\cos\theta)^2 + (\cos\theta)^4$, $c_6 = 1 + 2\cos(2\eta)(\cos\theta)^2 + (\cos\theta)^4$.

any prior known spatial separation between the two receive-antennas, and these Cramér-Rao bounds are independent also of the value of the frequency, if prior known. This is because the values of the spatial separation and of the frequency would affect only B in $\mathbf{D}$, which is cancelled in the course of calculating the Fisher Information Matrix.

Figures 4.1a to 4.1c plot $\frac{2M}{\sigma^2}\text{CRB}(\gamma) = \frac{2M}{\sigma^2}(\sin\gamma)^2\text{CRB}(\eta)$ for the three "OLD arrays" of configurations 1A-1C of Table 4.1. Figures 4.2a to 4.2b plot CRB(γ) and CRB(η) of the horizontally oriented dipole-pair (i.e. configuration 2A). Figures 4.2c to 4.2d do the same for the horizontally loop-pair (i.e. configuration 2B). Each remaining configuration has CRB(γ) and CRB(η) dependent on three or more independent variables, thus not fully representable by any three-dimensional graph.

Below are some qualitative observations on these derived Cramér-Rao bounds.

{1} The *horizontally* oriented "OLD arrays" ($\{e_x, h_x\}$ of configuration 1A, and $\{e_y, h_y\}$ of configuration 1B) offer finite Cramér-Rao bounds for sources impinging *not horizontally*. Please see Figures 4.1a and 4.1b. In contrast, the *vertically* oriented "OLD array" ($\{e_z, h_z\}$ of configuration 1C) offers finite Cramér-Rao bounds for sources impinging *horizontally*. Please see Figure 4.1c.

{2} The *horizontally* oriented "OLD arrays" ($\{e_x, h_x\}$ of configuration 1A, and $\{e_y, h_y\}$ of configuration 1B) has a CRB(γ) independent of the polarization parameters of γ and η. The *vertically* oriented "OLD array" ($\{e_z, h_z\}$ of configuration 1C) has both CRB(γ) and CRB(η) independent of the azimuth-angle ϕ.

{3} The Cramér-Rao bounds of the $\{e_x, h_x\}$ "OLD array" are related to the Cramér-Rao bounds of the other horizontally oriented "OLD array" of $\{e_y, h_y\}$, by substituting ϕ by $\phi + \frac{\pi}{2}$. This is because $\mathbf{a}_{1A}(\theta, \phi, \gamma, \eta) = \mathbf{a}_{1B}(\theta, \phi + \frac{\pi}{2}, \gamma, \eta)$. Similar relationships exist between configurations 3A and 4A, between configurations 3B and 4B, between configurations 6A and 7A, and between configurations 6B and 7B.

{4} For configurations 3A-7B, both CRB(γ) and CRB(η) depend on the direction-of-arrival (i.e. θ and ϕ) and the polarization (i.e. γ and η). Other dependencies are listed in Table 4.4.

{5} CRB(η) $\to \infty$ as $\gamma \to 0$ for all 15 configurations.

Table 4.2: Cramér-Rao Bounds for Polarization-Estimates for the 15 Antenna/Orientation Configurations – a

Configuration	Receive-Antennas	CRB's
1A	$\{e_x, h_x\}$	$\mathrm{CRB}(\gamma) = \frac{\sigma^2}{2M}\frac{1}{\left[(\sin\phi)^2+(\cos\phi)^2(\cos\theta)^2\right]} = (\sin\gamma)^2\mathrm{CRB}(\eta)$
1B	$\{e_y, h_y\}$	$\mathrm{CRB}(\gamma) = \frac{\sigma^2}{2M}\frac{1}{\left[(\cos\phi)^2+(\sin\phi)^2(\cos\theta)^2\right]} = (\sin\gamma)^2\mathrm{CRB}(\eta)$
1C	$\{e_z, h_z\}$	$\mathrm{CRB}(\gamma) = \frac{\sigma^2}{2M}\frac{1}{(\sin\theta)^2} = (\sin\gamma)^2\mathrm{CRB}(\eta)$ [145]
2A	$\{e_x, e_y\}$	$\mathrm{CRB}(\gamma) = \frac{\sigma^2}{2M}\frac{1}{\left[(\sin\gamma)^2+(\cos\theta)^2(\cos\gamma)^2\right]}$ $\mathrm{CRB}(\eta) = \frac{\sigma^2}{2M}\frac{1}{(\sin\gamma)^2}\frac{1}{(\cos\theta)^2}$
2B	$\{h_x, h_y\}$	$\mathrm{CRB}(\gamma) = \frac{\sigma^2}{2M}\frac{1}{\left[(\cos\gamma)^2+(\cos\theta)^2(\sin\gamma)^2\right]}$ $\mathrm{CRB}(\eta) = \frac{\sigma^2}{2M}\frac{1}{(\sin\gamma)^2}$
3A	$\{e_x, e_z\}$	$\mathrm{CRB}(\gamma) = \frac{\sigma^2}{2M}\frac{\left[1-(\cos\theta)^2(\sin\phi)^2\right]}{c_{3A}}$ $\mathrm{CRB}(\eta) = \frac{\sigma^2}{2M}\frac{1}{(\sin\gamma)^2}\frac{\left\{\begin{array}{c}(\sin\phi)^2+(\cos\gamma)^2[(\cos\phi)^2\\ -(\cos\theta)^2(\sin\phi)^2]+c_4\end{array}\right\}}{c_{3A}}$ $c_{3A} = \left\{\begin{array}{c}(\cos\phi)^2[(\cos\eta)^2(\cos\theta)^2\\ +(\cos\gamma)^2(1-2\cos^4\theta+\cos^2\theta\sin^2\eta)\\ -(\sin\theta)^2]+(\cos\phi)^4[(\cos\gamma)^2(\cos\theta)^4\\ -(\cos\eta)^2(\cos\theta)^2(\sin\gamma)^2]\\ +c_4[(\cos\phi)^2(\cos\theta)^2+(\sin\theta)^2]\\ +(\sin\theta)^2[1-(\cos\gamma)^2(\cos\theta)^2]\end{array}\right\}$
3B	$\{h_x, h_z\}$	$\mathrm{CRB}(\gamma) = \frac{\sigma^2}{2M}\frac{1}{c_{3B}}$ $\mathrm{CRB}(\eta) = \frac{\sigma^2}{2M}\frac{1}{(\sin\gamma)^2}\frac{\left\{\begin{array}{c}(\csc\phi)^2[1-(\cos\gamma)^2(\cos\phi)^2\\ -(\cos\theta)^2(\sin\phi)^2(\sin\gamma)^2-c_4]\end{array}\right\}}{c_{3B}}$ $c_{3B} = \left\{\begin{array}{c}(\sin\theta)^2+(\cos\phi)^2(\cos\theta)^2(\sin\gamma)^2(\cos\eta)^2\\ +(\cos\gamma)^2[(\cos\theta)^2-(\cos\phi)^2]-c_4\end{array}\right\}$
4A	$\{e_y, e_z\}$	$\mathrm{CRB}(\gamma) = \frac{\sigma^2}{2M}\frac{\left[1-(\cos\theta)^2(\cos\phi)^2\right]}{c_{4A}}$ $\mathrm{CRB}(\eta) = \frac{\sigma^2}{2M}\frac{1}{(\sin\gamma)^2}\frac{\left\{(\cos\phi)^2+(\cos\gamma)^2[(\sin\phi)^2-(\cos\theta)^2(\cos\phi)^2]-c_4\right\}}{c_{4A}}$ $c_{4A} = \left\{\begin{array}{c}(\cos\phi)^2[1+(\cos\theta)^2(\sin\phi)^2(\cos\eta)^2-(\cos\theta)^2\\ -(\cos\gamma)^2(1+(\cos\theta)^2(1+\cos^2\eta))]\\ +(\cos\phi)^4(\cos\gamma)^2(\cos\theta)^2[(\cos\eta)^2+(\cos\theta)^2]\\ +(\cos\gamma)^2-c_4[1-(\cos\phi)^2(\cos\theta)^2]\end{array}\right\}$
4B	$\{h_y, h_z\}$	$\mathrm{CRB}(\gamma) = \frac{\sigma^2}{2M}\frac{1}{c_{4B}}$ $\mathrm{CRB}(\eta) = \frac{\sigma^2}{2M}\frac{1}{(\sin\gamma)^2}\frac{\left\{\begin{array}{c}-(\cos\theta)^2(\sin\gamma)\\ -(\cos\gamma)^2(\tan\phi)^2+(\sec\phi)^2(1+c_4)\end{array}\right\}}{c_{4B}}$ $c_{4B} = \left\{\begin{array}{c}(\sin\theta)^2+(\cos\gamma)^2[(\cos\theta)^2(\sin^2\eta\\ +\cos^2\eta\cos^2\phi)-(\sin\phi)^2]\\ +(\cos\theta)^2(\cos\eta)^2(\sin\phi)^2+c_4\end{array}\right\}$

Table 4.3: Cramér-Rao Bounds for Polarization-Estimates for the 15 Antenna/Orientation Configurations – b

Configuration	Receive-Antennas	CRB's
5A	$\{e_x, h_y\}$	$\mathrm{CRB}(\gamma) = \frac{\sigma^2}{2M}\frac{\left[1+(\cos\theta)^2\right]}{c_{5A}}$ $\mathrm{CRB}(\eta) = \frac{\sigma^2}{2M}\frac{1}{(\sin\gamma)^2}\frac{(\sec\phi)^2\{[3+\cos(2\theta)][(\cos\gamma)^2\cos(2\phi) + (\sin\phi)^2] + 4c_4\}}{2c_{5A}}$ $c_{5A} = \left\{\begin{array}{c} -2(\cos\theta)^2(\sin\eta)^2 + c_5[1+2(\cos\gamma)^2(\cos\phi)^2] \\ -c_6[(\cos\phi)^2 + (\cos\gamma)^2] + 2c_4[1+(\cos\theta)^2] \end{array}\right\}$
5B	$\{e_y, h_x\}$	$\mathrm{CRB}(\gamma) = \frac{\sigma^2}{2M}\frac{\left[-1-(\cos\theta)^2\right]}{c_{5B}}$ $\mathrm{CRB}(\eta) = \frac{\sigma^2}{2M}\frac{1}{(\sin\gamma)^2}\frac{(\csc\phi)^2\{-(\cos\phi)^2\left[1+(\cos\theta)^2\right] + \frac{1}{2}(\cos\gamma)^2\cos(2\phi)\,[3+\cos(2\theta)] + 2c_4\}}{c_{5B}}$ $c_{5B} = \left\{\begin{array}{c} 2c_4[1+(\cos\theta)^2] + 2c_5(\cos\gamma)^2(\cos\phi)^2 \\ -c_6(\cos\phi)^2 - (\cos\gamma)^2[1+(\cos\theta)^2]^2 \end{array}\right\}$
6A	$\{e_x, h_z\}$	$\mathrm{CRB}(\gamma) = \frac{\sigma^2}{2M}\frac{1}{c_{6A}}$ $\mathrm{CRB}(\eta) = \frac{\sigma^2}{2M}\frac{1}{(\sin\gamma)^2}\frac{\left\{\begin{array}{c}(\sec\phi)^2(\sec\theta)^2[2(\sin\gamma)^2 + c_4] \\ -(\sin\gamma)^2[(\sec\theta)^2 + (\sec\phi)^2] + (\cos\gamma)^2\end{array}\right\}}{c_{6A}}$ $c_{6A} = \left\{\begin{array}{c}(\sin\gamma)^2[(\sin\theta)^2 + (\sin\phi)^2(\cos\eta)^2] \\ +(\cos\gamma)^2(\cos\phi)^2(\cos\theta)^2 + c_4\end{array}\right\}$
6B	$\{e_z, h_x\}$	$\mathrm{CRB}(\gamma) = \frac{\sigma^2}{2M}\frac{\{2[2-\cos(2\phi)-\cos(2\theta)]\}}{c_{6B}}$ $\mathrm{CRB}(\eta) = \frac{\sigma^2}{2M}\frac{4}{(\sin\gamma)^2}\frac{\left\{\begin{array}{c}(\cos\phi)^2(\cos\theta)^2(\sin\gamma)^2 \\ +(\cos\gamma)^2[(\sin\theta)^2 + (\sin\phi)^2] - c_4\end{array}\right\}}{c_{6B}}$ $c_{6B} = \left\{\begin{array}{c}4(\cos\gamma)^2[(\cos^2\theta - 2)^2 \\ +(\cos\phi)^4(1+\cos^2\eta\cos^2\theta) \\ +(\cos\phi)^2(-4+(\cos\theta)^4 + \cos^2\theta\sin^2\eta)] \\ +4(\cos\phi)^2(\cos\theta)^2(\sin\theta)^2 \\ +2c_4[\csc(2\gamma)\sin(2\phi)(\cos\eta)(\cos\theta) \\ +\cos(2\theta) + \cos(2\phi) - 2]\end{array}\right\}$
7A	$\{e_y, h_z\}$	$\mathrm{CRB}(\gamma) = \frac{\sigma^2}{2M}\frac{1}{c_{7A}}$ $\mathrm{CRB}(\eta) = \frac{\sigma^2}{2M}\frac{1}{(\sin\gamma)^2}\frac{(\csc\phi)^2(\sec\theta)^2\{(\cos\phi)^2[(\sin\gamma)^2 - (\cos\gamma)^2(\cos\theta)^2] + (\sin\theta)^2 + (\cos\gamma)^2\cos(2\theta) - c_4\}}{c_{7A}}$ $c_{7A} = \left\{\begin{array}{c}(\cos\eta)^2(\cos\phi)^2(\sin\gamma)^2 - c_4 + (\sin\theta)^2 \\ -(\cos\gamma)^2[1-2(\cos\theta)^2 + (\cos\theta)^2(\cos\phi)^2]\end{array}\right\}$
7B	$\{e_z, h_y\}$	$\mathrm{CRB}(\gamma) = \frac{\sigma^2}{2M}\frac{\left[(\cos\phi)^2+(\sin\theta)^2\right]}{c_{7B}}$ $\mathrm{CRB}(\eta) = \frac{\sigma^2}{2M}\frac{1}{(\sin\gamma)^2}\frac{\left\{\begin{array}{c}(\cos\gamma)^2[\frac{3}{2}(\cos\phi)^2 + \frac{1}{2}(\cos\phi)^2\cos(2\theta) \\ -\cos(2\theta)] + (\cos\theta)^2(\sin\phi)^2 + c_4\end{array}\right\}}{c_{7B}}$ $c_{7B} = \left\{\begin{array}{c}(\cos\gamma)^2\{(\cos\phi)^4[1+(\cos\eta)^2(\cos\theta)^2] \\ -(\cos\phi)^2[-2+(1+(\cos\eta)^2)(\cos\theta)^2 \\ +(\cos\theta)^4] - \cos(2\theta)(\sin\theta)^2\} \\ +c_4[(\sin\theta)^2 + (\cos\phi)^2] \\ +(\cos\theta)^2(\sin\phi)^2[(\cos\eta)^2(\cos\phi)^2 + (\sin\theta)^2]\end{array}\right\}$

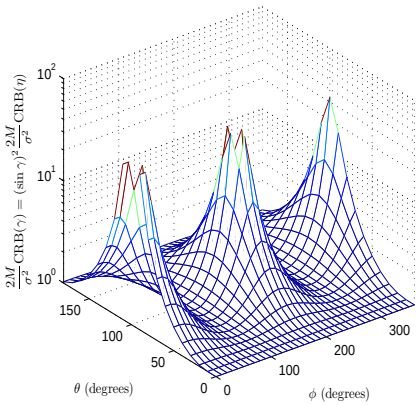

Figure 4.1a: $\frac{2M}{\sigma^2}\mathrm{CRB}(\gamma) = (\sin\gamma)^2\frac{2M}{\sigma^2}\mathrm{CRB}(\eta)$ plotted versus θ and ϕ, for configuration 1A (i.e. the horizontally oriented "OLD" array, $\{e_x, h_x\}$).

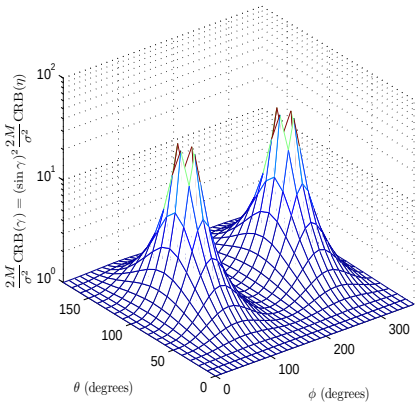

Figure 4.1b: $\frac{2M}{\sigma^2}\mathrm{CRB}(\gamma) = (\sin\gamma)^2\frac{2M}{\sigma^2}\mathrm{CRB}(\eta)$ plotted versus θ and ϕ, for configuration 1B (i.e. the horizontally oriented "OLD" array, $\{e_y, h_y\}$).

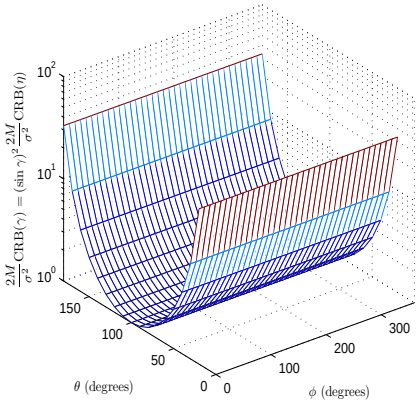

Figure 4.1c: $\frac{2M}{\sigma^2}\mathrm{CRB}(\gamma) = (\sin\gamma)^2\frac{2M}{\sigma^2}\mathrm{CRB}(\eta)$ plotted versus θ and ϕ, for configuration 1C (i.e. the vertically oriented "OLD" array, $\{e_z, h_z\}$).

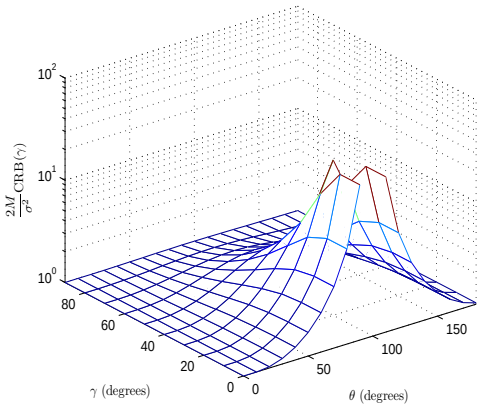

Figure 4.2a: $\frac{2M}{\sigma^2}\text{CRB}(\gamma)$ plotted versus θ and γ, for configuration 2A (i.e. $\{e_x, e_y\}$).

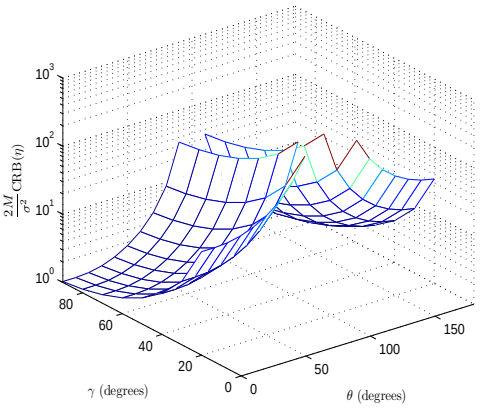

Figure 4.2b: $\frac{2M}{\sigma^2}\text{CRB}(\eta)$ plotted versus θ and γ, for configuration 2A (i.e. $\{e_x, e_y\}$).

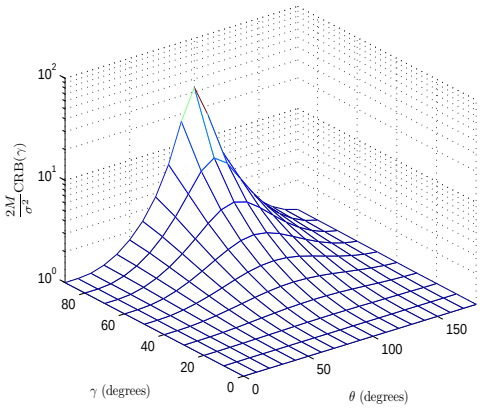

Figure 4.2c: $\frac{2M}{\sigma^2}\text{CRB}(\gamma)$ plotted versus θ and γ, for configuration 2B (i.e. $\{h_x, h_y\}$).

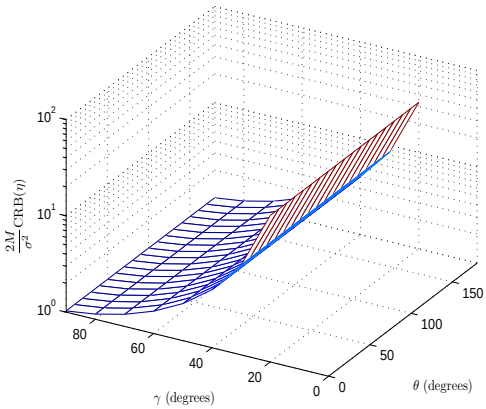

Figure 4.2d: $\frac{2M}{\sigma^2}\text{CRB}(\eta)$ plotted versus θ and γ, for configuration 2B (i.e. $\{h_x, h_y\}$).

Table 4.4: Characteristics of CRB(γ) and CRB(η).

Configuration	Receive-Antennas	CRB(γ) $\to \infty$ at	CRB(η) $\to \infty$ at	CRB(γ) Independent of	CRB(η) Independent of
1A	$\{e_x, h_x\}$	$(\theta, \phi) = (\frac{\pi}{2}, 0), (\frac{\pi}{2}, \pi)$	$\{(\theta, \phi) = (\frac{\pi}{2}, 0), (\frac{\pi}{2}, \pi)\} \cup \{\gamma = 0\}$	γ, η	η
1B	$\{e_y, h_y\}$	$(\theta, \phi) = (\frac{\pi}{2}, \frac{\pi}{2}), (\frac{\pi}{2}, \frac{3\pi}{2})$	$\{(\theta, \phi) = (\frac{\pi}{2}, \frac{\pi}{2}), (\frac{\pi}{2}, \frac{3\pi}{2})\} \cup \{\gamma = 0\}$	γ, η	η
1C	$\{e_z, h_z\}$	$\theta = 0, \pi$	$\{\theta = 0, \pi\} \cup \{\gamma = 0\}$	ϕ, γ, η	ϕ, η
2A	$\{e_x, e_y\}$	$(\theta, \gamma) = (\frac{\pi}{2}, 0)$	$\{\theta = \frac{\pi}{2}\} \cup \{\gamma = 0\}$	ϕ, η	ϕ, η
2B	$\{h_x, h_y\}$	$(\theta, \gamma) = (\frac{\pi}{2}, \frac{\pi}{2})$	$\gamma = 0$	ϕ, η	θ, ϕ, η
3A	$\{e_x, e_z\}$	$(\phi, \gamma) = (0, \frac{\pi}{2}), (\pi, \frac{\pi}{2})$	$\{(\theta, \phi) = (0, \frac{\pi}{2}), (0, \frac{3\pi}{2}), (\pi, \frac{\pi}{2}), (\pi, \frac{3\pi}{2})\} \cup \{\gamma = 0\}$	-	-
3B	$\{h_x, h_z\}$	$(\theta, \phi, \gamma) = \left\{ \begin{array}{l} (0, \frac{\pi}{2}, \frac{\pi}{2}), (0, \frac{3\pi}{2}, \frac{\pi}{2}), \\ (\pi, \frac{\pi}{2}, \frac{\pi}{2}), (\pi, \frac{3\pi}{2}, \frac{\pi}{2}) \end{array} \right\}$	$\{\phi = 0, \pi\} \cup \{\gamma = 0\}$	-	-
4A	$\{e_y, e_z\}$	$(\phi, \gamma) = (\frac{\pi}{2}, \frac{\pi}{2}), (\frac{3\pi}{2}, \frac{\pi}{2})$	$\{(\theta, \phi) = (0, 0), (0, \pi), (\pi, 0), (\pi, \pi)\} \cup \{\gamma = 0\}$	-	-
4B	$\{h_y, h_z\}$	$(\theta, \phi, \gamma) = \left\{ \begin{array}{l} (0, 0, \frac{\pi}{2}), (0, \pi, \frac{\pi}{2}), \\ (\pi, 0, \frac{\pi}{2}), (\pi, \pi, \frac{\pi}{2}) \end{array} \right\}$	$\{\phi = \frac{\pi}{2}, \frac{3\pi}{2}\} \cup \{\gamma = 0\}$	-	-
5A	$\{e_x, h_y\}$	$(\phi, \gamma) = (0, \frac{\pi}{2}), (\pi, \frac{\pi}{2})$	$\{\phi = \frac{\pi}{2}, \frac{3\pi}{2}\} \cup \{\gamma = 0\}$	-	-
5B	$\{h_x, e_y\}$	$(\phi, \gamma) = (\frac{\pi}{2}, \frac{\pi}{2}), (\frac{3\pi}{2}, \frac{\pi}{2})$	$\{\phi = 0, \pi\} \cup \{\gamma = 0\}$	-	-
6A	$\{e_x, h_z\}$	$(\theta, \phi, \gamma) = \left\{ \begin{array}{l} (0, 0, \frac{\pi}{2}), (0, \pi, \frac{\pi}{2}), \\ (\pi, 0, \frac{\pi}{2}), (\pi, \pi, \frac{\pi}{2}) \end{array} \right\}$	$\{\phi = \frac{\pi}{2}, \frac{3\pi}{2}\} \cup \{\theta = \frac{\pi}{2}\} \cup \{\gamma = 0\}$	-	-
6B	$\{h_x, e_z\}$	$\{(\theta, \gamma) = (\frac{\pi}{2}, \frac{\pi}{2})\}$ $\cup\{(\phi, \gamma) = (\frac{\pi}{2}, \frac{\pi}{2}), (\frac{3\pi}{2}, \frac{\pi}{2})\}$	$\{(\theta, \phi) = (0, 0), (0, \pi), (\pi, 0), (\pi, \pi)\} \cup \{\gamma = 0\}$	-	-
7A	$\{e_y, h_z\}$	$(\theta, \phi, \gamma) = \left\{ \begin{array}{l} (0, \frac{\pi}{2}, \frac{\pi}{2}), (0, \frac{3\pi}{2}, \frac{\pi}{2}), \\ (\pi, \frac{\pi}{2}, \frac{\pi}{2}), (\pi, \frac{3\pi}{2}, \frac{\pi}{2}) \end{array} \right\}$	$\{\phi = 0, \pi\} \cup \{\theta = \frac{\pi}{2}\} \cup \{\gamma = 0\}$	-	-
7B	$\{h_y, e_z\}$	$\{(\theta, \gamma) = (\frac{\pi}{2}, \frac{\pi}{2})\}$ $\cup\{(\phi, \gamma) = (0, \frac{\pi}{2}), (\pi, \frac{\pi}{2})\}$	$\{(\theta, \phi) = (0, \frac{\pi}{2}), (0, \frac{3\pi}{2}), (\pi, \frac{\pi}{2}), (\pi, \frac{3\pi}{2})\} \cup \{\gamma = 0\}$	-	-

4.4 The Condition Numbers Associated with the Estimation-Formulas of Section 4.2

The estimate $\hat{\mathbf{g}}$ could be construed as

$$\hat{\mathbf{g}} \;=\; \left(\underbrace{\mathbf{DS\Theta}}_{=\mathbf{\Omega}}\right)^{-1} \underbrace{\mathbf{z}(t)}_{\approx c\mathbf{DS\Theta g}} \;\approx\; c\,(\mathbf{S\Theta})^{-1}\,\mathbf{S\Theta g}, \tag{4.18}$$

where $\mathbf{z}(t)$ denotes the 2×1 data collected at the time-instant t. The above requires an inversion of the 2×2 matrix $\mathbf{\Omega} = \mathbf{DS\Theta}$. [6]The numerical robustness in computing $\hat{\mathbf{g}}$ thus depends on the condition number $\mathcal{K}_2 = \frac{\lambda_{\max}}{\lambda_{\min}}$ of $\mathbf{\Omega}$, where $\lambda_{\max}$ denotes the largest-magnitude eigenvalue of the matrix $\mathbf{\Omega}$, and $\lambda_{\min}$ symbolizes the smallest-magnitude eigenvalue. If $\mathbf{\Omega}$ approaches singularity, $\mathcal{K}_2$ would approach infinity. The numerically most stable matrix-inversion corresponds to $\mathcal{K}_2 = 1$.

Table 4.5 lists the condition number for each of the 15 different composition/orientation configurations, derived by the present authors. Because $\mathcal{K}_2$ depends only on $\mathbf{\Omega}$, $\mathcal{K}_2$ is independent of γ and η, but depends only on θ and ϕ.

The ideal $\mathcal{K}_2 = 1$ is attained by only the three "OLD array" compositions/orientations of $\{e_x, h_x\}$, $\{e_y, h_y\}$, and $\{e_z, h_z\}$. For the other 12 configurations (i.e. configurations 2A-2B to 7A-7B), Figures 4.3a-4.3f plot their condition numbers versus $\theta \in [0, \pi]$ and versus $\phi \in [0, 2\pi)$. Each figure shows the values of θ and ϕ where $\mathcal{K}_2 \to \infty$. These are summarized in the two rightmost columns of Table 4.5.

Below are some qualitative observations:

{6} The condition numbers are all independent of the spatial separation between the two component-antennas, and independent of the frequency. This is because the matrix $\mathbf{D}$ always has a unity condition number, regardless of the aforementioned entities. Hence, $\mathcal{K}_2$ is unaffected by these entities.

{7} For and only for the three "OLD array" configurations (i.e. a dipole and a loop in an identical orientation), $\mathcal{K}_2 = 1, \forall\theta, \phi$. The reason is as follows: From (4.1),

$$\mathbf{DS\Theta} \;=\; \mathbf{D}\begin{bmatrix} [\mathbf{v}_1]_m & [\mathbf{v}_2]_m \\ [\mathbf{v}_2]_m & -[\mathbf{v}_1]_m \end{bmatrix} \;=\; \mathbf{\Omega}, \tag{4.19}$$

with $[.]_m$ referring to the mth entry of the vector inside the square brackets. The radialoid structure of $\mathbf{\Omega}$ gives $\mathbf{\Omega}^H\mathbf{\Omega} = \left([\mathbf{v}_1]_m^2 + [\mathbf{v}_2]_m^2\right)\mathbf{I}_2$, where $\mathbf{I}_2$ symbolizes a 2×2

[6] If $\mathbf{g}$ were estimated without the above matrix inversion, this condition-number analysis would be irrelevant.

identity matrix. Hence, the condition number equals 1. [7]

{8} For all the dipole-pair configurations and all the loop-pair configurations (i.e. configurations 2A-2B, 3A-3B, 4A-4B), each "A" configuration (such as 2A) can lead to the corresponding "B" configuration (such as 2B), by switching e with h. More precisely, with $\mathbf{\Omega} = \mathbf{\Omega}_A$ for the "A" configuration and with $\mathbf{\Omega} = \mathbf{\Omega}_B$ for the "B" configuration, then $\mathbf{\Omega}_B = \mathbf{\Omega}_A\mathbf{P}$, where $\mathbf{P} = \begin{bmatrix} 0 & -1 \\ 1 & 0 \end{bmatrix}$ denotes a 90°-rotation matrix. That is, $\mathbf{\Omega}_A$ and $\mathbf{\Omega}_B$ are similar matrices. Hence, configuration 2A must have the same condition number as configuration 2B. Similar reasoning applies between 3A and 3B, and between 4A and 4B.

{9} For non-identically oriented dipole/loop antenna-pairs (i.e. configurations 5A-5B to 7A-7B), each "A" configuration (such as 5A) can lead to the corresponding "B" configuration (such as 5B), also by switching e with h. Consider configurations 5A and 5B, $\mathbf{\Omega}_B = \mathbf{R}\mathbf{\Omega}_A\mathbf{P}$, where $\mathbf{R} = \begin{bmatrix} 1 & 0 \\ 0 & -1 \end{bmatrix}$ denotes a reflection matrix. Hence, $\mathbf{\Omega}_A$ and $\mathbf{\Omega}_B$ have the same condition number. Consequentially, configuration 5A must have the same condition number as configuration 5B, Similar reasoning applies between 6A and 6B, and between 7A and 7B.

{10} The condition number of configurations 3A-3B, with a $\frac{\pi}{2}$ shift in ϕ, leads to the condition number of configurations 4A-4B. This is because the x-axis in 3A-3B corresponds to the y-axis in 4A-4B. Similarly, this holds between configurations 6A-6B on one hand and configurations 7A-7B on the other hand.

{11} For each antenna/orientation configuration, the condition number is symmetric with respect to $\theta = \frac{\pi}{2}$ along the θ-axis, and with respect to $\phi = \pi$ along the ϕ-axis.

[7] Below is a more intuitive explanation: For a dipole and a loop, they would most "completely" measure the incident electromagnetic field, if the dipole and the loop are identically oriented. As an example, consider a vertically oriented dipole/loop pair, i.e. $\{e_z, h_z\}$. The vertically oriented loop h_z measures the z-axis magnetic field, which contains partial information of the x-axis and y-axis components of the electrical field, complementary to the vertical dipole's z-axis electric field measurement. This complementarity (between the dipole's measurement and the loop's measurement) would disappear for any of the twelve *non*-"OLD-array" configurations.

Table 4.5: Condition-Numbers For Table 4.1's Polarization-Estimation Formulas.

Configuration	Receive-Antennas	$\mathbf{DS\Theta} = \mathbf{\Omega} =$	Condition Number $\mathcal{K}_2$ of $\mathbf{DS\Theta}$	$\kappa_2 \to \infty$ $\forall\phi$, as $\theta \to$	$\kappa_2 \to \infty$ $\forall\theta$, as $\phi \to$
1A	$\{e_x, h_x\}$	$\begin{bmatrix} \cos\phi\cos\theta & -\sin\phi \\ -e^{-jB}\sin\phi & -e^{-jB}\cos\phi\cos\theta \end{bmatrix}$	1	-	-
1B	$\{e_y, h_y\}$	$\begin{bmatrix} \sin\phi\cos\theta & \cos\phi \\ e^{-jB}\cos\phi & -e^{-jB}\sin\phi\cos\theta \end{bmatrix}$	1	-	-
1C	$\{e_z, h_z\}$	$\begin{bmatrix} -\sin\theta & 0 \\ 0 & e^{-jB}\sin\theta \end{bmatrix}$	1	-	-
2A	$\{e_x, e_y\}$	$\begin{bmatrix} \cos\phi\cos\theta & -\sin\phi \\ e^{-jB}\sin\phi\cos\theta & e^{-jB}\cos\phi \end{bmatrix}$	$\frac{1}{\lvert\cos\theta\rvert}$	$\frac{\pi}{2}$	-
2B	$\{h_x, h_y\}$	$\begin{bmatrix} -\sin\phi & -\cos\phi\cos\theta \\ e^{-jB}\cos\phi & -e^{-jB}\sin\phi\cos\theta \end{bmatrix}$	$\frac{1}{\lvert\cos\theta\rvert}$	$\frac{\pi}{2}$	-
3A	$\{e_x, e_z\}$	$\begin{bmatrix} \cos\phi\cos\theta & -\sin\phi \\ -e^{-jB}\sin\theta & 0 \end{bmatrix}$	$\frac{1}{\lvert\sin\theta\sin\phi\rvert}$	$0, \pi$	$0, \pi$
3B	$\{h_x, h_z\}$	$\begin{bmatrix} -\sin\phi & -\cos\phi\cos\theta \\ 0 & e^{-jB}\sin\theta \end{bmatrix}$	$\frac{1}{\lvert\sin\theta\sin\phi\rvert}$	$0, \pi$	$0, \pi$
4A	$\{e_y, e_z\}$	$\begin{bmatrix} \sin\phi\cos\theta & \cos\phi \\ -e^{-jB}\sin\theta & 0 \end{bmatrix}$	$\frac{1}{\lvert\sin\theta\cos\phi\rvert}$	$0, \pi$	$\frac{\pi}{2}, \frac{3\pi}{2}$
4B	$\{h_y, h_z\}$	$\begin{bmatrix} \cos\phi & -\sin\phi\cos\theta \\ 0 & e^{-jB}\sin\theta \end{bmatrix}$	$\frac{1}{\lvert\sin\theta\cos\phi\rvert}$	$0, \pi$	$\frac{\pi}{2}, \frac{3\pi}{2}$
5A	$\{e_x, h_y\}$	$\begin{bmatrix} \cos\phi\cos\theta & -\sin\phi \\ e^{-jB}\cos\phi & -e^{-jB}\sin\phi\cos\theta \end{bmatrix}$	$\sqrt{\frac{\cos^2\theta+1+\sqrt{(\cos^2\theta+1)^2-4\sin^2\phi\cos^2\phi\sin^4\theta}}{\cos^2\theta+1-\sqrt{(\cos^2\theta+1)^2-4\sin^2\phi\cos^2\phi\sin^4\theta}}}$	$0, \pi$	$0, \frac{\pi}{2}, \pi, \frac{3\pi}{2}$
5B	$\{h_x, e_y\}$	$\begin{bmatrix} -\sin\phi & -\cos\phi\cos\theta \\ e^{-jB}\sin\phi\cos\theta & e^{-jB}\cos\phi \end{bmatrix}$	$\sqrt{\frac{\cos^2\theta+1+\sqrt{(\cos^2\theta+1)^2-4\sin^2\phi\cos^2\phi\sin^4\theta}}{\cos^2\theta+1-\sqrt{(\cos^2\theta+1)^2-4\sin^2\phi\cos^2\phi\sin^4\theta}}}$	$0, \pi$	$0, \frac{\pi}{2}, \pi, \frac{3\pi}{2}$
6A	$\{e_x, h_z\}$	$\begin{bmatrix} \cos\phi\cos\theta & -\sin\phi \\ 0 & e^{-jB}\sin\theta \end{bmatrix}$	$\sqrt{\frac{\sin^2\phi\sin^2\theta+1+\sqrt{(\sin^2\phi\sin^2\theta+1)^2-4\sin^2\theta\cos^2\theta\cos^2\phi}}{\sin^2\phi\sin^2\theta+1-\sqrt{(\sin^2\phi\sin^2\theta+1)^2-4\sin^2\theta\cos^2\theta\cos^2\phi}}}$	$0, \frac{\pi}{2}, \pi$	$\frac{\pi}{2}, \frac{3\pi}{2}$
6B	$\{h_x, e_z\}$	$\begin{bmatrix} -\sin\phi & -\cos\phi\cos\theta \\ -e^{-jB}\sin\theta & 0 \end{bmatrix}$	$\sqrt{\frac{\sin^2\phi\sin^2\theta+1+\sqrt{(\sin^2\phi\sin^2\theta+1)^2-4\sin^2\theta\cos^2\theta\cos^2\phi}}{\sin^2\phi\sin^2\theta+1-\sqrt{(\sin^2\phi\sin^2\theta+1)^2-4\sin^2\theta\cos^2\theta\cos^2\phi}}}$	$0, \frac{\pi}{2}, \pi$	$\frac{\pi}{2}, \frac{3\pi}{2}$
7A	$\{e_y, h_z\}$	$\begin{bmatrix} \sin\phi\cos\theta & \cos\phi \\ 0 & e^{-jB}\sin\theta \end{bmatrix}$	$\sqrt{\frac{\cos^2\phi\sin^2\theta+1+\sqrt{(\cos^2\phi\sin^2\theta+1)^2-4\sin^2\theta\cos^2\theta\sin^2\phi}}{\cos^2\phi\sin^2\theta+1-\sqrt{(\cos^2\phi\sin^2\theta+1)^2-4\sin^2\theta\cos^2\theta\sin^2\phi}}}$	$0, \frac{\pi}{2}, \pi$	$0, \pi$
7B	$\{h_y, e_z\}$	$\begin{bmatrix} \cos\phi & -\sin\phi\cos\theta \\ -e^{-jB}\sin\theta & 0 \end{bmatrix}$	$\sqrt{\frac{\cos^2\phi\sin^2\theta+1+\sqrt{(\cos^2\phi\sin^2\theta+1)^2-4\sin^2\theta\cos^2\theta\sin^2\phi}}{\cos^2\phi\sin^2\theta+1-\sqrt{(\cos^2\phi\sin^2\theta+1)^2-4\sin^2\theta\cos^2\theta\sin^2\phi}}}$	$0, \frac{\pi}{2}, \pi$	$0, \pi$

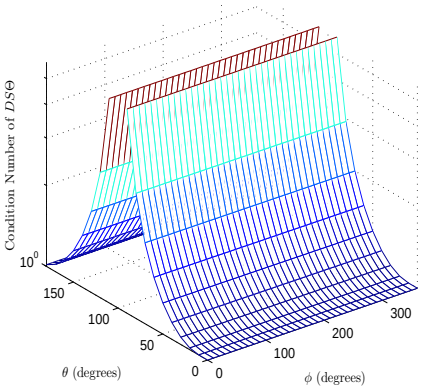

Figure 4.3a: The condition number of **DSΘ** for configuration 2A (i.e. $\{e_x, e_y\}$) and the configuration 2B (i.e. $\{h_x, h_y\}$).

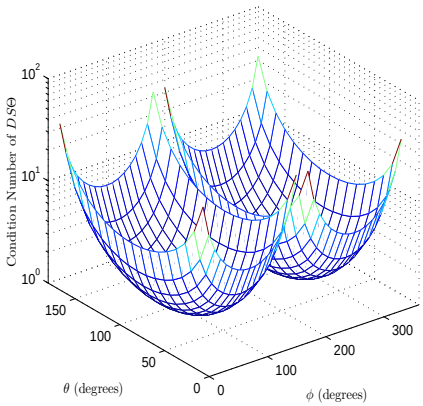

Figure 4.3b: The condition number of **DSΘ** for configuration 3A (i.e. $\{e_x, e_z\}$) and the configuration 3B (i.e. $\{h_x, h_z\}$).

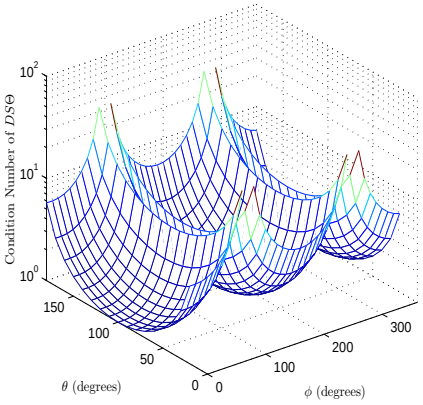

Figure 4.3c: The condition number of **DSΘ** for configuration 4A (i.e. $\{e_y, e_z\}$) and the configuration 4B (i.e. $\{h_y, h_z\}$).

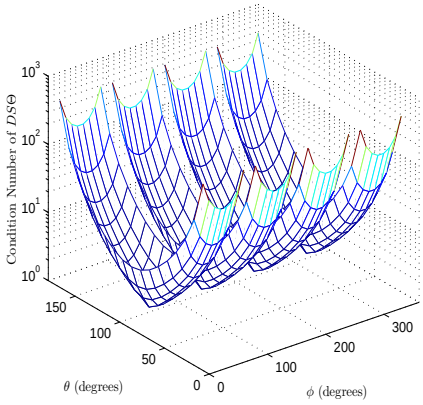

Figure 4.3d: The condition number of **DSΘ** for configuration 5A (i.e. $\{e_x, h_y\}$) and the configuration 5B (i.e. $\{h_x, e_y\}$).

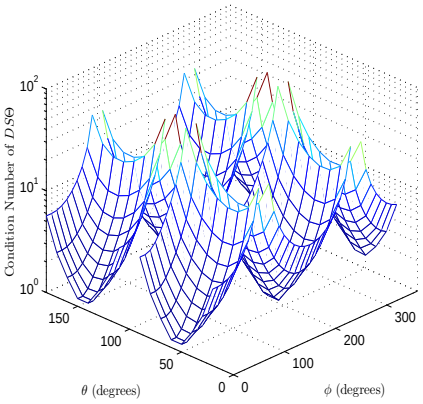

Figure 4.3e: The condition number of **DSΘ** for configuration 6A (i.e. $\{e_x, h_z\}$) and the configuration 6B (i.e. $\{e_z, h_x\}$).

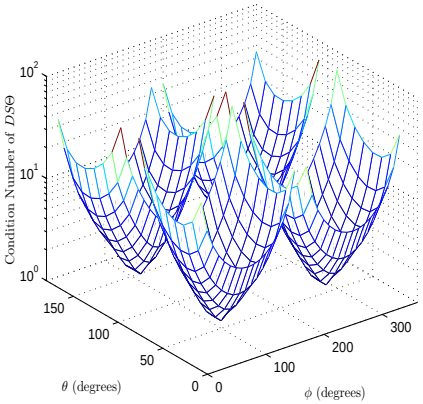

Figure 4.3f: The condition number of **DSΘ** for configuration 7A (i.e. $\{e_y, h_z\}$) and the configuration 7B (i.e. $\{e_z, h_y\}$).

4.5 Summary

Investigated herein are *all* 15 possible antenna/orientation configurations that measure any 2 of the 6 components of the electromagnetic-field vector. Obtained for each antenna/orientation configuration are the closed-form polarization-estimation formulas, the corresponding validity region for unambiguous estimation, the corresponding Cramér-Rao bounds, and the corresponding condition number as a function of the azimuth-elevation direction-of-arrival. The same derived results would apply, whether each pair is collocated or spatially separated. Among these 15 configurations, especially advantageous is the vertically oriented "OLD array" (i.e. the $\{e_z, h_z\}$ configuration), which requires *no prior* information of the source's direction-of-arrival for polarization, but offers an ideal condition number of unity, and has a finite Cramér-Rao bounds except for near-*vertically* incident sources. For the horizontally oriented "OLD arrays" (i.e. the $\{e_x, h_x\}$ configuration or the $\{e_y, h_y\}$ configuration), they also offer the ideal condition number of unity, and have finite Cramér-Rao bounds except for near-*horizontally* incident sources.

Chapter 5

Conclusion

This study investigates the direction-finding and/or polarization estimation with diversely polarized antenna-arrays, which include: a) a spatially spread electromagnetic vector sensor, b) various triad-compositions of collocated dipoles/loops, and c) a pair of diversely polarized antennas.

Chapter 2 has proposed a spatially spread electromagnetic vector sensor composed of six orthogonally oriented but spatially *non*-collocating dipoles / loops to advance the "vector cross-product" direction-of-arrival estimator. This new scheme has great practical value, in reducing mutual coupling, in simplifying the antennas hardware, and in extending the spatial aperture to refine the direction-finding accuracy by orders of magnitude.

Chapter 3 has investigated various triad-compositions of collocated dipoles/loops, for direction finding and polarization estimation. Among the 20 different compositions, closed-form formulas are produced for 16 compositions to estimate the azimuth-elevation direction-of-arrival and the polarization-parameters. The reason is given why such estimation is inviable for the remaining 4 compositions. The dipole-triad and the loop-triad are found to allow unambiguous direction-of-arrival estimation over the entire sphere.

Chapter 4 has developed the polarization estimation of fully polarized sources, given prior knowledge of the incident sources' azimuth-elevation directions-of-arrival, using a pair of diversely polarized antennas – two electrically small dipoles, or two small loops, or one each. The pair may be collocated or spatially separated by a known displacement. Each antenna may orient along any Cartesian coordinate. Among the 15 configurations, the "OLD arrays" are found to be advantageous.

Some future work may be conducted, such as:

1) In Chapter 2, to further study the geometry of the spatially-spread electromagnetic vector sensor, some generalized array configuration may be more efficient for direction finding and polarization estimation. In addition, the spatially-spread elec-

tromagnetic vector sensor used for coherent sources direction finding could be developed.

2) In Chapter 3, to further study the direction finding and polarization estimation with four collocated dipoles/loops, some compositions may have larger validity region for the direction-of-arrival and polarization parameters. In addition, comprehensive comparison among the 20 triad-compositions could be developed based on the associated Cramér-Rao bounds.

Bibliography

[1] J. Capon, "High-resolution frequency-wavenumber spectrum analysis," *Proceeding of the IEEE*, vol. 57, no. 8, pp. 1408-1418, August 1969.

[2] H. Goldstein, *Classical Mechanics*, 2nd edition, Addison-Wesley, 1980.

[3] V. Zieren & S. Middelhoek, "Magnetic-Field Vector Sensor Based on a Two-Collector Transistor Structure," *Sensors and Actuators*, vol. 2, pp. 251-261, 1982.

[4] R. Schmidt, "Multiple Emitter Location and Signal Parameter Estimation," *IEEE Transactions on Antennas and Propagation*, vol. 34, no. 3, pp. 276-280, March 1986.

[5] M. D. Zoltowski & D. Stavrinides, "Sensor Array Signal Processing Via a Procrustes Rotations Based Eigenanalysis of the ESPRIT Data Pencil," *IEEE Transactions on Acoustics, Speech and Signal Processing*, vol. 37, no. 6, pp. 832-861, June 1989.

[6] R. Roy & T. Kailath, "ESPRIT - Estimation of Signal Parameters Via Rotational Invariance Techniques," *IEEE Transactions on Acoustics, Speech and Signal Processing*, vol. 37, no. 7, pp. 984-995, July 1989.

[7] B. D. Rao & K. V. S. Hari, "Performance Analysis of Root-MUSIC," *IEEE Transactions on Acoustics, Speech and Signal Processing*, vol. 37, no. 12, pp. 1939-1949, December 1989.

[8] F. T. Ulaby & C. Elachi, *Radar Polarimetry for Geoscience Applications*, Boston, U.S.A.: Artech House Publishers, 1990.

[9] P. Stoica & K. C. Sharman, "Maximum Likelihood Methods for Direction-of-Arrival Estimation," *IEEE Transactions on Acoustics, Speech and Signal Processing*, vol. 38, no. 7, pp. 1132-1143, July 1990.

[10] M. Viberg & B. Ottersten, "Sensor Array processing Based on Subspace Fitting," *IEEE Transactions on Signal Processing*, vol. 39, no. 5, pp. 1110-1121, May 1991.

[11] J. Li & R. T. Compton, Jr., "Angle and Polarization Estimation Using ESPRIT with a Polarization Sensitive Array," *IEEE Transactions on Antennas and Propagation*, vol. 39, no. 9, pp. 1376-1383, September 1991.

[12] J. Li & R. T. Compton, Jr., "Angle Estimation Using Polarized Sensitive Array," *IEEE Transactions on Antennas and Propagation*, vol. 39, no. 10, pp. 1539-1543, October 1991.

[13] J. Li & R. T. Compton, Jr., "Two-Dimensional Angle and Polarization Estimation Using the ESPRIT Algorithm," *IEEE Transactions on Antennas and Propagation*, vol. 40, no. 5, pp. 550-555, May 1992.

[14] M. D. Zoltowski, G. M. Kautz & S. D. Silverstein, "Beamspace Root-MUSIC," *IEEE Transactions on Signal Processing*, vol. 41, no. 1, pp. 344-364, January 1993.

[15] J. Li, "Direction and Polarization Estimation Using Arrays with Small Loops and Short Dipoles," *IEEE Transactions on Antennas and Propagation*, vol. 41, no. 3, pp. 379-387, March 1993.

[16] Y. Hua, "A Pencil-MUSIC Algorithm for Finding Two-Dimensional Angles and Polarization Using Crossed Dipoles," *IEEE Transactions on Antennas and Propagation*, vol. 41, no. 3, pp. 370-376, March 1993.

[17] A. J. Weiss & B. Friedlander, "Direction Finding for Diversely Polarized Signals Using Polynomial Rooting," *IEEE Transactions on Signal Processing*, vol. 41, no. 5, pp. 1893-2021, May 1993.

[18] J. Li & R. T. Compton, Jr., "Angle and Polarization Estimation in a Coherent Signal Environment," *IEEE Transactions on Aerospace and Electronic Systems*, vol. 29, no. 3, pp. 706-716, July 1993.

[19] A. Swindlehurst & M. Viberg, "Subspace Fitting with Diversely Polarized Antenna Arrays," *IEEE Transactions on Antennas and Propagation*, vol. 41, no. 12, pp. 1687-1694, December 1993.

[20] A. Nehorai & E. Paldi, "Vector-Sensor Array Processing for Electromagnetic Source Localization," *IEEE Transactions on Signal Processing*, vol. 42, no. 2, pp. 376-398, February 1994.

[21] H. Lee & R. Stovall, "Maximum Likelihood Methods for Determining the Direction of Arrival for a Single Electromagnetic Source with Unknown Polarization," *IEEE Transactions on Signal Processing*, vol. 42, no. 2, pp. 474-479, February 1994.

[22] J. Li, "On Polarization Estimation Using a Crossed-Dipole Array," *IEEE Transactions on Signal Processing*, vol. 42, no. 4, pp. 977-980, April 1994.

[23] B. Friedlander & A. J. Weiss, "The Resolution Threshold of a Direction-Finding Algorithm for Diversely Polarized Arrays," *IEEE Transactions on Signal Processing*, vol. 42, no. 7, pp. 1719-1727, July 1994.

[24] M. D. Zoltowski & C. P. Mathews, "Real-Time Frequency and 2-D Angle Estimation with Sub-Nyquist Spatio-Temporal Sampling," *IEEE Transactions on Signal Processing*, vol. 42, no. 10, pp. 2781-2794, October 1994.

[25] J. Li, "Efficient Parameter Estimation of Partially Polarized Electromagnetic Waves," *IEEE Transactions on Signal Processing*, vol. 42, no. 11, pp. 3114-3125, November 1994.

[26] Q. Cheng & Y. Hua, "Performance Analysis of the MUSIC and Pencil-MUSIC Algorithms for Diversely Polarized Array," *IEEE Transactions on Signal Processing*, vol. 42, no. 11, pp. 3150-3165, November 1994.

[27] B. Hochwald & A. Nehorai, "Polarimetric Modeling and Parameter Estimation with Applications to Remote Sensing," *IEEE Transactions on Signal Processing*, vol. 43, no. 8, pp. 1923-1935, August 1995.

[28] Q. Cheng & Y. Hua, "Further Study of the Pencil-MUSIC Algorithm," *IEEE Transactions on Aerospace and Electronic Systems*, vol. 32, no. 1, pp. 284-299, January 1996.

[29] J. Li, P. Stoica & D. Zheng, "Efficient Direction and Polarization Estimation with a COLD Array," *IEEE Transactions on Antennas and Propagation*, vol. 44, no. 4, pp. 539-547, April 1996.

[30] H. Krim & M. Viberg, "Two Decades of Array Signal Processing Research: The Parametric Approach," *IEEE Signal Processing Magazine*, vol. 13, no. 4, pp. 67-94, July 1996.

[31] J. E. F. del Rio & M. F. Catedra-Perez, "The Matrix Pencil Method for Two-Dimensional Direction of Arrival Estimation Employing an L-Shaped Array," *IEEE Transactions on Antennas and Propagation*, vol. 45, no. 11, pp. 1693-1694, November 1997.

[32] K. T. Wong & M. D. Zoltowski, "Uni-Vector-Sensor ESPRIT for Multi-Source Azimuth, Elevation, and Polarization Estimation," *IEEE Transactions on Antennas and Propagation*, vol. 45, no. 10, pp. 1467-1474, October 1997.

[33] K.-C. Ho, K.-C. Tan & B. T. G. Tan, "Efficient Method for Estimating Directions-of-Arrival of Partially Polarized Signals with Electromagnetic Vector Sensors," *IEEE Transactions on Signal Processing*, vol. 45, no. 10, pp. 2485-2498, October 1997.

[34] M. Hirari & M. Hayakawa, "DOA Estimation Using Blind Separation of Sources," *IEEE Signal Processing Workshop on Higher-Order Statistics*, pp. 311-315, 1997.

[35] D. Lemur, Y. Erhel, F. Marie & L. Bertel, "Redundancy in the Measurement of HF Direction Finding," *IEE International Conference on HF Radio Systems and Techniques*, IEE conference publication no. 411, pp. 320-324, 1997.

[36] P. L. Overfelt, "Electric Lines of Force of an Electrically Small Dipole-Loop Antenna Array," *IEEE Transactions on Antennas and Propagation*, vol. 46, no. 3, pp. 451-456, March 1998.

[37] Q. Cheng & Y. Hua, "Comment on "Direction and Polarization Estimation Using Arrays with Small Loops and Short Dipoles" ," *IEEE Transactions on Antennas and Propagation*, vol. 46, no. 3, p. 461, March 1998.

[38] J. E. F. del Rio & M. F. Catedra, "Efficient Configurations of the Matrix Pencil with Data Provided by Two Orthogonal Linear Arrays of Electrically Small Dipoles," *Digital Signal Processing*, vol. 8, no. 2, pp. 103-113, April 1998.

[39] B. Lindmark, S. Lundgren, J. R. Sanford & C. Beckman, "Dual-Polarized Array for Signal-Processing Applications in Wireless Communications," *IEEE Transactions on Antennas and Propagation*, vol. 46, no. 6, pp. 758-763, June 1998.

[40] K.-C. Ho, K.-C. Tan & B. T. G. Tan, "Linear Dependence of Steering Vectors Associated with Tripole Arrays," *IEEE Transactions on Antennas and Propagation*, vol. 46, no. 11, pp. 1705-1711, November 1998.

[41] S.-H. Chang, T.-Y. Lee & W.-H. Fang, "High-Resolution Bearing Estimation via UNItary Decomposition Artificial Neural Network (UNIDANN)," *IEICE Transactions on Fundamentals*, vol. E81E-A, no. 11, pp. 2455-2462, 1998.

[42] T. Ratnarajah, "An H^{∞} Approach to Multi-Source Tracking," *IEEE International Conference on Acoustics, Speech and Signal Processing*, vol. 4, pp. 2205-2208, 1998.

[43] P.-H. Chua, C.-M. S. See, A. Nehorai, "Vector-Sensor Array Processing for Estimating Angles and Times of Arrival of Multipath Communication Signals," *IEEE International Conference on Acoustics, Speech and Signal Processing*, vol. 6, pp. 3325-3328, 1998.

[44] F. Tefiku & C. A. Grimes, "Coupling Between Elements of Electrically Small Compound Antennas," *Microwave and Optical Technology Letters*, vol. 22, no. 1, pp. 16-21, July 1999.

[45] P. Chevalier & A. Ferreol, "On the Virtual Array Concept for the Fourth-Order Direction Finding Problem," *IEEE Transactions on Signal Processing*, vol. 47, no. 9, pp. 2592-2595, September 1999.

[46] K.-C. Ho, K.-C. Tan & A. Nehorai, "Estimating Directions of Arrival of Completely and Incompletely Polarized Signals with Electromagnetic Vector Sensors," *IEEE Transactions on Signal Processing*, vol. 47, no. 10, pp. 2845-2852, October 1999.

[47] A. Nehorai & P. Tichavský, "Cross-Product Algorithms for Source Tracking Using an EM Vector Sensor," *IEEE Transactions on Signal Processing*, vol. 47, no. 10, pp. 2863-2867, October 1999.

[48] E. L. Afraimovich, V. V. Chernukhov, V. A. Kobzar & K. S. Palamartchouk, "Determining Polarization Parameters and Angles of Arrival of HF Radio Signals Using Three Mutually Orthogonal Antennas," *Radio Science*, vol. 34, no. 5, pp. 1217-1225, September-October 1999.

[49] E. N. Onggosanusi, B. D. Van Veen & A. M. Sayeed, "Space-Time Polarization Signaling for Wireless Communications," *IEEE Sensor Array and Multichannel Signal Processing Workshop*, pp. 188-192, 2000.

[50] K. T. Wong & M. D. Zoltowski, "Closed-Form Direction-Finding with Arbitrarily Spaced Electromagnetic Vector-Sensors at Unknown Locations," *IEEE Transactions on Antennas and Propagation*, vol. 48, no. 5, pp. 671-681, May 2000.

[51] M. D. Zoltowski & K. T. Wong, "ESPRIT-based 2D Direction Finding with a Sparse Array of Electromagnetic Vector-Sensors," *IEEE Transactions on Signal Processing*, vol. 48, no. 8, pp. 2195-2204, August 2000.

[52] M. D. Zoltowski & K. T. Wong, "Closed-Form Eigenstructure-Based Direction Finding Using Arbitrary but Identical Subarrays on a Sparse Uniform Rectangular Array Grid," *IEEE Transactions on Signal Processing*, vol. 48, no. 8, pp. 2205-2210, August 2000.

[53] K. T. Wong & M. D. Zoltowski, "Self-Initiating MUSIC Direction Finding & Polarization Estimation in Spatio-Polarizational Beamspace," *IEEE Transactions on Antennas and Propagation*, vol. 48, no. 8, pp. 1235-1245, August 2000.

[54] K. ALMidfa, E. Tameh & A. Nix, "Improved DOA Estimation Using Polarisation Diversity: Simulations Using a Wideband Propagation Model," *IEEE International Symposium on Personal, Indoor and Mobile Radio Communications*, vol. 1, pp. 539-543, 2000.

[55] D. H. Brandwood & D. J. Sadler, "Superresolution Direction Finding at HF for Signals of Unknown Polarization," *IEE International Conference on HF Radio Systems and Techniques*, IEE conference publication no. 474, pp. 133-137, 2000.

[56] K. T. Wong, "Geolocation/Beamforming for Multiple Wideband-FFH with Unknown Hop-Sequences," *IEEE Transactions on Aerospace and Electronic Systems*, vol. 37, no. 1, pp. 65-76, January 2001.

[57] Y.-Y. Wang, J.-T. Chen & W.-H. Fang, "Joint Estimation of DOA and Delay Using TST MUSIC in a Wireless Channel," *IEEE Signal Processing Letters*, vol.8, no.2, pp.58-60, February 2001.

[58] Y.-Y. Wang, J.-T. Chen & W.-H. Fang, "TST-MUSIC for Joint DOA-Delay Estimation," *IEEE Transactions on Signal Processing*, vol. 49, no. 4, pp. 721-729, April 2001.

[59] K. T. Wong, "Direction Finding / Polarization Estimation — Dipole and/or Loop Triad(s)," *IEEE Transactions on Aerospace and Electronic Systems*, vol. 37, no. 2, pp. 679-684, April 2001.

[60] R. C. Hansen, "The Electrically Small Dipole-Loop," *ACES Journal*, vol. 16, no. 3, pp. 228-229, November 2001.

[61] Y. Huang, G. Friedman & A. Nehorai, "Balancing Magnetic and Electric Responses of Vector-Sensing Antenna," *IEEE Antennas and Propagation Society International Symposium*, vol. 4, pp. 212-215, 2001.

[62] H. L. Van Trees, *Detection, Estimation, and Modulation Theory, Part IV: Optimum Array Processing*, New York, U.S.A.: Wiley, 2002.

[63] C. C. Ko, J. Zhang & A. Nehorai, "Separation and Tracking of Multiple Broadband Sources with One Electromagnetic Vector Sensor," *IEEE Transactions on Aerospace and Electronic Systems*, vol. 38, no. 3, pp. 1109-1116, July 2002.

[64] J. Wang & T. Chen, "Performance Analysis for Joint Estimation of Frequency, 2-D AOA And Polarization Under Array Error," *International Conference on Communications, Circuits and Systems*, vol. 2, pp. 1021-1024, 2002.

[65] Y. Huang, A. Nehorai & G. Friedman, "Mutual Coupling of Two Collocated Orthogonally Oriented Circular Thin-Wire Loops," *IEEE Transactions on Antennas and Propagation*, vol. 51, no. 6, pp. 1307-1314, June 2003.

[66] X. Zhenhai, W. Xuesong, X. Shunping & Z. Zhaowen, "Joint Spectrum Estimation of Polarization and Space," *IEEE International Conference on Neural Networks an Signal Processing*, vol. 2, pp. 1285-1289, 2003.

[67] B. A. Obeidat, Y. Zhang & M. G. Amin, "Polarimetric Time-Frequency ESPRIT," *Asilomar Conference on Signals, Systems and Computers*, vol. 1, pp. 1178-1182, 2003.

[68] J. Lundback & S. Nordebo, "On Polarization Estimation Using Tripole Arrays," *IEEE Antennas and Propagation Society International Symposium*, vol. 1, pp. 65-68, 2003.

[69] C.-M. S. See & A. Nehorai, "Source Localization with Distributed Electromagnetic Component Sensor Array Processing," *International Symposium on Signal Processing and Its Applications*, vol. 1, pp. 177-180, 2003.

[70] A. Manikas & J. W. P. Ng, "Crossed-Dipole Arrays for Asynchronous DS-CDMA Systems," *IEEE Transactions on Antennas and Propagation*, vol. 52, no. 1, pp. 122-131, January 2004.

[71] X. You-gen & L. Zhi-wen, "Simultaneous Estimation of 2-D DOA and Polarization of Multiple Coherent Sources Using an Electromagnetic Vector Sensor Array," *Journal of China Institute of Communications*, vol. 25, no. 5, pp. 28-38, May 2004.

[72] S. Krishnan, L.-W. Li & M.-S. Leong, "Comments on "Mutual Coupling of Two Collocated Orthogonally Oriented Circular Thin-Wire Loops"," *IEEE Transactions on Antennas and Propagation*, vol. 52, no. 6, pp. 1625-1626, June 2004.

[73] N. Le Bihan & J. Mars, "Singular Value Decomposition of Quaternion Matrices: a New Tool for Vector-Sensor Signal Processing," *Signal Processing*, pp. 1177-1199, July 2004.

[74] D. Rahamim, J. Tabrikian & R. Shavit, "Source Localization Using Vector Sensor Array in a Multipath Environment," *IEEE Transactions on Signal Processing*, vol. 52, no. 11, pp. 3096-3103, November 2004.

[75] K. T. Wong, L. Li & M. D. Zoltowski, "Root-MUSIC-Based Direction-Finding & Polarization-Estimation Using Diversely-Polarized Possibly-Collocated Antennas," *IEEE Antennas and Wireless Propagation Letters*, vol. 3, no. 8, pp. 129-132, 2004.

[76] Y. G. Xu & Z. W. Liu, "Regularized ESPRIT-Based Direction Finding and Polarization Estimation with One Electromagnetic Vector Sensor," *International Conference on Signal processing*, pp. 399-402, 2004.

[77] J. Lundback & S. Nordebo, "Analysis of a Tripole Array for Polarization and Direction of Arrival Estimation," *Sensor Array and Multichannel Signal Processing Workshop Proceedings*, pp. 284-288, 2004.

[78] B. A. Obeidat, Y. Zhang & M. G. Amin, "Range and DOA Estimation of Polarized Near-Field Signals Using Fourth-order Statistics," *IEEE International Conference on Acoustics, Speech and Signal Processing*, vol. 2, pp. II. 97-100, May 2004.

[79] J. Tinbergen, *Astronomical Polarimetry*, Cambridge, U.K.: Cambridge University Press, 2005.

[80] J.-D. Lin, W.-H. Fang & J.-T. Chen, "Constrained TST MUSIC for Joint Spatio-Temporal Channel Parameter Estimation in DS/CDMA Systems," *Journal of Wireless Communication and Mobile Computing, Special Issue on Emerging Multiple Access Technologies*, vol. 5, pp. 57-67, January 2005.

[81] K. T. Wong & A. K.-Y. Lai, "Inexpensive Upgrade of Base-Station Dumb-Antennas by Two Magnetic Loops for 'Blind' Adaptive Downlink Beamforming," *IEEE Antennas and Propagation Magazine*, vol. 47, no. 1, pp. 189-193, February 2005.

[82] D.-H. Kwon, "On the Radiation Q and the Gain of Crossed Electric and Magnetic Dipole Moments," *IEEE Transactions on Antennas and Propagation*, vol. 53, no. 5, pp. 1681-1687, May 2005.

[83] S. Krishnan, L.-W. Li & M.-S. Leong, "Entire-Domain MoM Analysis of an Array of Arbitrarily Oriented Circular Loop Antennas: A General Formulation," *IEEE Transactions on Antennas and Propagation*, vol. 53, no. 9, pp. 2961-2968, September 2005.

[84] D. Su, J. J. Qian, H. Yang & D. Fu, "A Novel Broadband Polarization Diversity Antenna Using a Cross-Pair of Folded Dipoles," *IEEE Antennas and Wireless Propagation Letters*, vol. 4, pp. 433-435, 2005.

[85] H. S. Mir, J. D. Sahr & C.M. Keller, "Source Location Using Airborne Vector Sensors," *IEEE International Conference on Acoustics, Speech and Signal Processing*, vol. 4, pp. 1033-1036, 2005.

[86] L. Wang, G. Liao & H. Wang, "A New Method for Estimation of Gain and Phase Uncertainty of an Electromagnetic Vector Sensor," *IEEE International Symposium on Microwave, Antenna, Propagation and EMC Technologies for Wireless Communications*, pp. 712-715, 2005.

[87] X. You-gen, L. Zhi-wen & Y. Guang-xiang, "Uni-Vector-Sensor SOS/HOS-CSS for Wide-band Non-Gaussian Source Direction Finding," *IEEE International Symposium on Microwave, Antenna, Propagation and EMC Technologies for Wireless Communications*, pp. 855-858, 2005.

[88] J.-C. Huang, Y.-W. Shi & J.-W. Tao, "Closed-Form Estimation of DOA and Polarization for Multisource with a Uniform Circular Array," *International Conference on Machine Learning and Cybernetics*, vol. 7, pp. 4469-4474, 2005.

[89] S. Miron, N. Le Bihan & J. I. Mars, "Quaternion-MUSIC for Vector-Sensor Array Processing," *IEEE Transactions on Signal Processing*, vol. 54, no. 4, pp. 1218-1229, April 2006.

[90] F. L. Lerma, G. Ruvio & M. J. Ammann, "A Microstrip-Fed Printed Crossed Dipole for Wireless Applications," *Microwave and Optical Technology Letters*, vol. 48, no. 4, pp. 751-753, April 2006.

[91] S. Nordebo, M. Gustafsson & J. Lundback, "Fundamental Limitations for DOA and Polarization Estimation with Applications in Array Signal Processing," *IEEE Transactions on Signal Processing*, vol. 54, no. 10, pp. 4055-4061, October 2006.

[92] S. Hwang, S. Burintramart, T. K. Sarkar & S. R. Best, "Direction of Arrival (DOA) Estimation Using Electrically Small Tuned Dipole Antennas," *IEEE Transactions on Antennas and Propagation*, vol. 54, no. 11, pp. 3292-3301, November 2006.

[93] J.-D. Lin, W.-H. Fang, Y.-Y. Wang & J.-T. Chen, "FSF MUSIC for Joint DOA-FOA Estimation and its Performance Analysis," *IEEE Transactions on Signal Processing*, vol. 54, no. 12, pp. 4529-4542, December 2006.

[94] F. Ji & S. Kwong, "Frequency and 2D Angle Estimation based on a Sparse Uniform Array of electromagnetic Vector Sensors," *EURASIP Journal on Applied Signal Processing* , vol. 2006, no. 13, 2006.

[95] Y. Xu & Z. Liu, "Adaptive Quasi-Cross-Product Algorithm for Uni-Tripole Tracking of Moving Source," *International Conference on Communication Technology*, pp. 1-4, 2006.

[96] S. Appadwedula & C. M. Keller, "Direction-Finding Results for a Vector Sensor Antenna on a Small UAV," *IEEE Sensor Array and Multichannel Signal Processing Workshop*, pp. 74-78, 2006.

[97] Y. Xu & Z. Liu, "On Single-Vector-Sensor Direction Finding for Linearly Polarized Sources Having Non-circular Constellations," *International Conference on Signal Processing*, 2006.

[98] L. Zhou & W. Li, "Partial Discharge Sources Detection and Location with an Electromagnetic Vector Sensor," *IEEE Conference on Industrial Electronics and Applications*, 2006.

[99] Q. Zhang, L. Wang, Y. Wang & J.-C. Huang, "Cyclostationarity-Based DOA and Polarization Estimation for Multipath Signals with a Uniform Linear Array of Electromagnetic Vector Sensors," *International Conference on Machine Learning and Cybernetics*, pp. 2047-2052, 2006.

[100] X. Gong, Y. Xu & Z. Liu, "On the Equivalence of Tensor-MUSIC and Matrix-MUSIC," *International Symposium on Antennas, Propagation and EM Theory*, pp. 26-29, 2006.

[101] H. S. Mir & J. D. Sahr, "Passive Direction Finding Using Airborne Vector Sensors in the Presence of Manifold Perturbations," *IEEE Transactions on Signal Processing*, vol. 55, no. 1, pp. 156-164, January 2007.

[102] M. Hurtado & A. Nehorai, "Performance Analysis of Passive Low-Grazing-Angle Source Localization in Maritime Environments Using Vector Sensors," *IEEE Transactions on Aerospace and Electronic Systems*, vol. 43, no. 2, pp. 780-789, April 2007.

[103] M. Tsutsui, S. Konagaya & T. Kagawa, "A Method of Direction Finding for Dispersive Electromagnetic Pulses," *Electronics and Communications in Japan*, part 1, vol. 90, no. 5, pp. 23-32, 2007.

[104] J. Kim & Y. Rahmat-Samii, "Integrated Low-Profile Dual Loop-Dipole Antennas Using an Embedded Electromagnetic Bandgap Structure," *Microwave and Optical Technology Letters*, vol. 49, no. 5, pp. 1085-1089, May 2007.

[105] Y. Xu & Z. Liu, "Polarimetric Angular Smoothing Algorithm for an Electromagnetic Vector-Sensor Array," *IET Radar, Sonar and Navigation*, vol. 1, no. 3, pp. 230-240, June 2007.

[106] A. Kisliansky, R. Shavit & J. Tabrikian, "Direction of Arrival Estimation in the Presence of Noise Coupling in Antenna Arrays," *IEEE Transactions on Antennas and Propagation*, vol. 55, no. 7, pp. 1940-1947, July 2007.

[107] D. Li, Z. Feng, J. She & Y. Cheng, "Unique Steering Vector Design of Cross-Dipole Array with Two Pairs," *Electronic Letters*, vol. 43, no. 15, pp. 796-797, 19th July 2007.

[108] Y. Wu, H. C. So, C. Hou & J. Li, "Passive Localization of Near-Field Sources With a Polarization Sensitive Array," *IEEE Transactions on Antennas and Propagation*, vol. 55, no. 8, pp. 2402-2408, August 2007.

[109] N. Le Bihan, S. Miron & J. Mars, "MUSIC Algorithm for Vector-Sensors Array Using Biquaternions," *IEEE Transactions on Signal Processing*, vol. 55, no. 9, pp. 4523-4533, September 2007.

[110] P. Chevalier, A. Ferreol, L. Albera & Gwenael Birot, "Higher Order Direction Finding From Arrays With Diversely Polarized Antennas: The PD-2q-MUSIC Algorithms," *IEEE Transactions on Signal Processing*, vol. 55, no. 11, pp. 5337-5350, November 2007.

[111] C.-Y. Chiu, J.-B. Yan & R. D. Murch, "Compact Three-Port Orthogonally Polarized MIMO Antennas," *IEEE Antennas and Wireless Propagation Letter*, vol. 6, pp. 619-622, 2007.

[112] P. W. Chan, H. Wong & E. K. N. Yung, "Printed Antenna Composed of a Bow-Tie Dipole and a Loop," *IEEE Antennas and Propagation Society International Symposium*, pp. 681-684, 2007.

[113] C.-H. Lin, W.-H. Fang, W.-S. Yang & J.-D. Lin, "SPS-ESPRIT for Joint DOA and Polarization Estimation with a COLD Array," *IEEE Antennas and Propagation Society International Symposium*, pp. 1136-1139, 2007.

[114] S. R. Best, "The Electrically Small Dipole-Loop Pair Revisited," *IEEE Antennas and Propagation Society International Symposium*, pp. 2265-2268, 2007.

[115] Y. Ravinder, V. M. Pandharipande, "Real Valued Minimum Mean Square Error Approach for Polarization Diversity Adaptive Arrays," *Asia-Pacific Conference on Applied Electromagnetics*, pp. 1-5, 2007.

[116] H. Kwak, E. Yang & J. Chun, "Vector Sensor Arrays in DOA Estimation for the Low Angle Tracking," *International Waveform Diversity and Design Conference*, pp. 183-187, 2007.

[117] L. Lo Monte, B. Elnour, D. Erricolo & A. Nehorai, "Design and Realization of a Distributed Vector Sensor for Polarization Diversity Applications," *International Waveform Diversity and Design Conference*, pp. 358-361, 2007.

[118] L. Lo Monte, B. Elnour & D. Erricolo, "Distributed 6D Vector Antennas Design for Direction of Arrival Application," *IEEE International Conference on Electromagnetic in Advanced Applications*, pp. 431-434, 2007.

[119] S. Hongyan, H. Hong & S. Yaowu, "Novel Solution of Direction Finding and Polarization Estimation of Multipath Cyclostationary Signals," *International Conference on Innovative Computing, Information and Control*, p. 564, 2007.

[120] N. Honma, R. Kudo, K. Nishimori, Y. Takatori, A. Ohta & S. Kubota, "Antenna Selection Method for Terminal Antennas Employing Orthogonal Polarizations and Patterns in Outdoor Multiuser MIMO System," *IEICE Transactions on Communications*, vol. E91-B, no. 6, pp. 1752-1759, June 2008.

[121] B. Li, K.-J. Lee, H.-T. Chou & W. Gu, "A Polarization Compensation Approach Utilizing a Paraboloid Photonic-Crystal Structure for Cross-Dipole Excited Reflector Antennas," *Progress In Electromagnetics Research*, vol. 85, pp. 393-408, 2008.

[122] Y. Shi & X. Zhang, "Quadrilinear Decomposition-Based Blind Signal Detection for Polarization Sensitive Uniform Square Array," *Progress In Electromagnetics Research*, vol. 87, pp. 263-278, 2008.

[123] C.-N. Chiu & Y.-F. Kuo, "Bandpass Shielding Enclosure Design for Modern Handheld Communication Devices with Internal Electric-Dipole and Magnetic-Loop Antennas," *Microwave and Optical Technology Letters*, vol. 50, no. 8, pp. 2223-2226, August 2008.

[124] S. Shastri, K. Shah & R. Shekhar, "Modified Circular Polarized Loop Antenna," *IEEE International Conference on Recent Advances in Microwave Theory and Applications*, pp. 934-936, 2008.

[125] L. Shuai, Q. Xiaolin & J. Ming, "Joint Polarization-DOA Estimation Using Sparse Antenna Array," *International Conference on Signal Processing*, pp. 353-357, 2008.

[126] X. Gong, Y. Xu & Z. Liu, "Quaternion ESPRIT for Direction Finding with a Polarization Sensitive Array," *International Conference on Signal Processing*, pp. 378-381, 2008.

[127] J. Tao, H. Xu & J.-W. Tao, "Closed-Form Direction Finding for Multiple Sources Based On Uniform Circular Arrays with Trimmed Vector Sensor," *World Congress on Intelligent Control and Automation*, pp. 2392-2395, 2008.

[128] X. Zhang, Y. Shi & D. Xu, "Novel Blind Joint Direction of Arrival and Polarization Estimation for Polarization-Sensitive Uniform Circular Array," *Progress In Electromagnetics Research*, vol. 86, pp. 19-37, 2008.

[129] Y. Xu, Z. Liu & S. Fu, "Polarimetric Smoothing Revisited: Applicability to Randomly Polarized Sources and to Incomplete Electromagnetic Vector-Sensors," *International Conference on Signal Processing*, pp. 328-331, 2008.

[130] S. H. Zainud-Deen, H. A. Malhat, K. H. Awadalla & E. S. El-Hadad, "Direction of Arrival and State of Polarization Estimation Using Radial Basis Function Neural Network (RBFNN)," *National Radio Science Conference*, pp. B10-1 to B10-8, 2008.

[131] X. Gong, Z. Liu & Y. Xu, "Quad-Quaternion MUSIC for DOA Estimation Using Electromagnetic Vector Sensors," *EURASIP Journal on Advances in Signal Processing*, Volume 2008, pp. 1-14, 2008.

[132] X. Shi & Y. Wang, "Parameter Estimation of Distributed Sources with Electromagnetic Vector Sensors," *International Conference on Signal Processing*, pp. 203-206, 2008.

[133] Z. Xin, S. Yaowu & Y. Wenhong, "2-D DOA and Polarization Estimation of LFM signals with One Electromagnetic Vector Sensor," *International Conference on Signal Processing*, pp. 386-389, 2008.

[134] Z. Xin, S. Yaowu, G. Hongzhi & L. Jun, "Parameter Estimation of Wideband Cyclostationary Sources Based on Uni-vector-sensor," *Chinese Control Conference*, pp. 298-302, 2008.

[135] F. Ji, C. C. Fung, S. Kwong & C.-W. Kok, "Joint Frequency and 2-D Angle Estimation Based on Vector Sensor Array with Sub-Nyquist Temporal Sampling," *European Signal Processing Conference*, 2008.

[136] C. K. Au Yeung & K. T. Wong, "CRB: Sinusoid-Sources' Estimation using Collocated Dipoles/Loops," *IEEE Transactions on Aerospace and Electronic Systems*, vol. 45, no. 1, pp. 94-109, January 2009.

[137] J. He & Z. Liu, "Computationally Efficient 2D Direction Finding and Polarization Estimation with Arbitrarily Spaced Electromagnetic Vector Sensors at Unknown Locations Using the Propagator Method," *Digital Signal Processing*, vol. 19, no. 3, pp. 491-503, May 2009.

[138] X. Gong, Z.-W. Liu, Y.-G. Xu & M. I. Ahmad, "Direction-of-Arrival Estimation via Twofold Mode-Projection," *Signal Processing*, vol. 89, no. 5, pp. 831-842, May 2009.

[139] H. D. Hristov, H. Carrasco, R. Feick & B. L. Ooi, "Low-Profile X Antenna with Flat Reflector for Polarization Diversity Applications," *Microwave and Optical Technology Letters*, vol. 51, no. 6, pp. 1508-1512, June 2009.

[140] W.-S. Yoon, S.-M. Han, J.-W. Baik, S. Pyo, J. Lee & Y.-S. Kim, "Crossed Dipole Antenna with Switchable Circular Polarisation Sense," *Electronics Letters*, vol. 45, no. 14, pp. 717-718, July 2, 2009.

[141] K.-H. Wu & W.-H. Fang, "A Low Complexity Adaptive Algorithm for Eigenspace-Based Two Dimensional Direction of Arrival Tracking," *IEICE Transactions on Fundamentals*, vol. E92-A, no. 8, pp. 2097-2106, August 2009.

[142] L. JunLi, L. Ding, & Z. JunYing, "Joint Frequency, 2-D DOA, and Polarization Estimation Using Parallel Factor Analysis," *Science in China, Series F - Information Sciences*, vol. 52, no. 10, pp. 1891-1904, October 2009.

[143] C.-Y. Chiu, J.-B. Yan, R. D. Murch, J. X. Yun & R. G. Vaughan, "Design and Implementation of a Compact 6-Port Antenna," *IEEE Antennas and Wireless Propagation Letters*, vol. 8, pp. 767-770, 2009.

[144] X. Gao, X. Zhang, Z. Sun, W. Chen & Y. Shi, "On Multilinear-based Approaches of Blind Receiver for Polarization Sensitive Uniform Square Array", *International Conference on Wireless Networks and Information Systems*, pp. 338-342, 2009.

[145] R. Boyer, "Analysis of the COLD Uniform Linear Array," *IEEE Workshop on Signal Processing Advances in Wireless Communications*, pp. 563-567, 2009.

[146] L. K. S. Daldorff, D. S. Turaga, O. Verscheure & A. Biem, "Direction of Arrival Estimation Using Single Tripole Radio Antenna," *IEEE International Conference on Acoustics, Speech and Signal Processing*, pp. 2149-2152, 2009.

[147] L. Liang, T. Jian-wu & C. Wei, "DOA Estimation Based on Sparse and Nonuniform COLD Array," *International Conference on Communications and Mobile Computing*, vol. 1, pp. 391-395, 2009.

[148] L. Shuai, J. Ming & Q. Xiaolin, "Joint Polarization-DOA Estimation Using Circle Array," *IET International Radar Conference*, 2009.

[149] D. M. Pozar, "New Results for Minimum Q, Maximum Gain, and Polarization Properties of Electrically Small Arbitrary Antennas," *European Conference on Antennas and Propagation*, pp. 1993-1996, 2009.

[150] J. He, S. Jiang, J. Wang & Z. Liu, "Polarization Difference Smoothing for Direction Finding of Coherent Signals," *IEEE Transactions on Aerospace and Electronic Systems*, vol. 46, no. 1, pp. 469-480, January 2010.

[151] J.-H. Lin, W.-H. Fang, K.-H. Wu & J.-D. Lin, "A Fast Algorithm for Joint Two-Dimensional Direction of Arrival and Frequency Estimation via Hierarchical Space-Time Decomposition," *Signal Processing*, vol. 90, no 1, pp. 207-216, January 2010.

[152] W. Li-guo, W. Ke & S. Xiao-ying, "Joint Estimation Method of Azimuth, Elevation, Range and Polarization for Near Field Sources Based on MP Algorithm," *Journal of Jilin University (Engineering and Technology Edition)*, vol. 40, no. 3, pp. 842-847, May 2010.

[153] T. Jun, T. Yantao, C. Wei & Y. Mao, "DOA Estimation Algorithm of Scattered Sources Based on Polarization Sensitive Sensor Array," *Chinese Journal of Scientific Instrument*, vol. 31, no. 6, pp. 1224-1233, June 2010.

[154] B. Elnour & D. Erricolo, "A Novel Colocated Cross-Polarized Two-Loop PCB Antenna in the ISM 2.4-GHz Band," *IEEE Antennas and Wireless Propagation Letters*, vol. 9, pp. 1237-1240, 2010.

[155] C. Wei, L. YunPeng & L. LuQin "A Novel Quaternion DOA Estimation Algorithm Based on Magnetic Loop Antenna," *International Conference on Wireless Communications Networking and Mobile Computing*, 2010.

[156] D. P. Atwater & M. L. Heron, "Temporal Error Analysis for Compact Cross-Loop Direction-Finding HF Radar," *IEEE OCEANS Conference*, 2010.

[157] L. Wang & K. Wang, "A Joint Estimation Method of Azimuth, Elevation, Range and Polarization for Near Field Sources without Pairing Parameters," *International Conference on Computer, Mechatronics, Control and Electronic Engineering*, vol. 3, pp. 325-328, 2010.

[158] V. Dehghanian, J. Nielsen & G. Lachapelle, "Merger of Polarization and Spatial Diversity by Moving a Pair of Orthogonally Polarized Dipoles," *IEEE Canadian Conference on Electrical and Computer Engineering*, 2010.

[159] H. Jiang, D.-F. Wang & C. Liu, "Estimation of DOD and 2D-DOA and Polarizations for Bistatic MIMO Radar," *Annual Wireless and Optical Communications Conference*, 2010.

[160] I. Seo, I. Cho, C. Lee, H. Jung, J. Oh, J. Jung, H. Lee, Y. Lim, "Design of Dual Polarized Antenna for DCS, UMTS, WiBro Base Stations," *IEEE International Conference on Wireless Information Technology and Systems*, 2010.

[161] K. T. Wong & X. Yuan, "Vector Cross-Product Direction-Finding with an Electromagnetic Vector-Sensor of Six Orthogonally Oriented but Spatially Non-Collocating Dipoles / Loops," *IEEE Transactions on Signal Processing*, vol. 59, no. 1, pp. 160-171, January 2011.

[162] M. N. El Korso, R. Boyer, A. Renaux & S. Marcos, "Statistical Resolution Limit of the Uniform Linear Cocentered Orthogonal Loop and Dipole Array," *IEEE Transactions on Signal Processing*, vol. 59, no. 1, pp. 425-431, January 2011.

[163] X. Gong, Z.-W. Liu & Y.-G. Xu, "Direction Finding via Biquaternion Matrix Diagonalization with Vector-Sensors," *Signal Processing*, vol. 91, no. 4, pp. 821-831, April 2011.

[164] A. Elsherbini & K. Sarabandi, "Dual-Polarized Coupled Sectorial Loop Antennas for UWB Applications," *IEEE Antennas and Wireless Propagation Letters*, vol. 10, pp. 75-78, 2011.

[165] D. T. Vu, A. Renaux, R. Boyer & S. Marcos, "Weiss-Weinstein Bound and SNR Threshold Analysis for DOA Estimation with a Cold Array," *IEEE Statistical Signal Processing Workshop*, pp. 13-16, 2011.

[166] W. Liguo & S. Xiaoying, "A New Joint Estimation Method of DOA and Polarization Based on MP," *International Conference on Intelligent Computation Technology and Automation*, vol. 2, pp. 358-361, 2011.

[167] X. Yuan, K. T. Wong, Z. Xu & K. Agrawal, "Various Compositions to Form a Triad of Collocated Dipoles/Loops, for Direction Finding and Polarization Estimation," accepted by the *IEEE Sensors Journal*.

[168] X. Yuan, K. T. Wong & K. Agrawal, "Polarization Estimation with a Dipole-Dipole Pair, a Dipole-Loop Pair, or a Loop-Loop Pair of Various Orientations," accepted by the *IEEE Transactions on Antennas and Propagation*.